Development of an Optimal Controller and Validation Test Stand for Fuel Efficient Engine Operation

Jack G. Rehn III
Marquette University

DEVELOPMENT OF AN OPTIMAL CONTROLLER AND VALIDATION TEST STAND FOR FUEL EFFICIENT ENGINE OPERATION

by

Jack G. Rehn III, B.S.

A Thesis submitted to the Faculty of the Graduate School,
Marquette University,
in Partial Fulfillment of the Requirements for
the Degree of Master of Science

Milwaukee, Wisconsin

August 2017

ABSTRACT
DEVELOPMENT OF AN OPTIMAL CONTROLLER AND VALIDATION TEST STAND
FOR FUEL EFFICIENT ENGINE OPERATION

Jack G. Rehn III, B.S.

Marquette University, 2017

There are numerous motivations for improvements in automotive fuel efficiency. As concerns over the environment grow at a rate unmatched by hybrid and electric automotive technologies, the need for reductions in fuel consumed by current road vehicles has never been more present. Studies have shown that a major cause of poor fuel consumption in automobiles is improper driving behavior, which cannot be mitigated by purely technological means. The emergence of autonomous driving technologies has provided an opportunity to alleviate this inefficiency by removing the necessity of a driver. Before autonomous technology can be relied upon to reduce gasoline consumption on a large scale, robust programming strategies must be designed and tested.

The goal of this thesis work was to design and deploy an autonomous control algorithm to navigate a four cylinder, gasoline combustion engine through a series of changing load profiles in a manner that prioritizes fuel efficiency. The experimental setup is analogous to a passenger vehicle driving over hilly terrain at highway speeds. The proposed approach accomplishes this using a model-predictive, real-time optimization algorithm that was calibrated to the engine.

Performance of the optimal control algorithm was tested on the engine against contemporary cruise control. Results indicate that the “efficient” strategy achieved one to two percent reductions in total fuel consumed for all load profiles tested. The consumption data gathered also suggests that further improvements could be realized on a different subject engine and using extended models and a slightly modified optimal control approach.

ACKNOWLEDGMENTS

Jack G. Rehn III, B.S.

Firstly, I would like to thank my advisor, Dr. Casey Allen, for allowing me the opportunity to pursue my graduate degree in your research department. Your knowledge and encouragement were integral to my success as a graduate student. Thank you for being an engaging mentor and for keeping your door open to me at all, and sometimes unreasonably late, hours. I would also like to thank the other members of my thesis committee, Doctors Mark Nagurka and Somesh Roy for agreeing to work with me. Your advice and insights at critical junctures during this research were invaluable.

This thesis study would not have been possible without the generosity of our partners in industry at PowerTest, Kubota, National Instruments, Grunau, Staff Electric, and Johnson Controls, among others. Thank you for your assistance in the construction and commissioning of the Engine Testing Facility. The quality of your handiwork and products is of the highest level.

I would also like to thank my research colleagues David Wilson, Jenna Ezzell, and Mark Carioscio as well as my friends in the Shock Physics Lab for sharing this journey with me, and making life as a graduate student more enjoyable than I could have hoped for. It has been my absolute honor to be counted among such kind and brilliant individuals. Each of you have the greatest potential and I wish you the best of luck in your future endeavors.

Finally, I wish to above all else thank my family for their unwavering love and support of my continued education. This project would not have been a success without the strength and guidance you have always given me. For all of the opportunities and experiences that you have made possible for me, I dedicate this work to you.

TABLE OF CONTENTS

LIST OF TABLES

LIST OF FIGURES

CHAPTER 1

INTRODUCTION

The modern combustion engine has been a cornerstone of the global economy for over 120 years. While the principal and primary components of a reciprocating, internal combustion engine have gone nearly unchanged since the development of the Otto engine in 1867, a vast amount of research and development has transformed the 19th century combustion engine into the industrial powerhouse it is today. The vast number of vehicles on roads worldwide has had a major impact on the global economic climate as well as the environment. Uncertainty in oil prices and growing concern over climate change has caused increased regulation of the transportation industry and has made fuel efficiency a top priority with auto-makers.

A major cause of poor fuel consumption in road vehicles is improper driving behavior, which technical improvements to engines and automotive subsystems cannot account for. Cruise control and driver heads up displays (HUDs) are two methods currently in production vehicles that attempt to increase fuel efficiency by promoting good driving practices. The recent emergence of autonomous control technology has provided an opportunity to significantly reduce fuel consumption due to inefficient driving techniques by removing the necessity of a driver. At the time of this writing, there have been some successful deployments of autonomous systems on projects run by major entities in both automotive and computing worlds like Ford and Google's Waymo Project.

For proprietary reasons, it is unclear as to whether or not fuel efficiency is prioritized in the operation of these vehicles but there have been academic studies into whether or not fuel efficient autonomous control strategies can be developed and implemented in consumer automobiles. These studies have shown that, in simulation, optimal control strategies are a viable approach. However, before any hard conclusions can be drawn, models and simulations need to be verified on real-life equipment. One route to doing so is by using an engine dynamometer test bench to validate models and control algorithms. Dynamometer platforms are well suited for controls testing in that they provide a wide range of precisely controlled experimental conditions and can readily accept adjustments to control strategies and test subjects.

In 2016 Marquette University finished construction of its Engine Testing Facility and installed a dynamometer, test engine, measurement and controls equipment to support combustion experiments. In addition to covering the construction of the test cell, this thesis

presents the design and verification of an engine controller that optimized engine fuel consumption in response to changing road conditions and given a desired operating speed. A controlled testing environment was set-up in the new facility using sophisticated control systems to perform a hardware-in-the-loop analysis of the proposed autonomous controller. This manuscript will detail the background, motivation, methods, experimental configurations, calibration tests performed, and the results of both simulation and physical deployment of the optimal control algorithm on a subject engine.

The remainder of this chapter will be a review of the background and potential of fuel efficiency techniques applied to passenger and light industrial automobiles on today's roads. The chapter will be structured as follows: first, a brief history of the innovations and events during the development of the modern automobile in the context of fuel and emissions efficiency will be presented, followed by an overview of the socio-economic and environmental impacts that further improvements in this sector can offer. Major factors governing fuel efficiency in todays automotive environment will be discussed as well as methods currently in practice for mitigating fuel inefficiencies. Finally, several academic studies into applying optimal control strategies to autonomous automobiles to improve fuel and emissions efficiency will be reviewed to establish the base of knowledge this work seeks to improve upon.

1.1 History of Innovation

1.1.1 Early Engines

Once the potential of combustion engines had been established, earliest efforts toward innovation were focused on broadening the range of applications suitable for combustion power as the prime mover. Technology soon improved to a point where it became practical as a consumer product. By the 1880s carburetors and ignition systems had progressed enough that combustion engines could be placed in both high-speed road automobiles and low-speed farming equipment. Around this time the conclusion was drawn that fuel efficiency was directly related to the amount of expansion that was allowed to take place during an engines power stroke and that the phenomenon of engine knock was the limiting factor to this "compression ratio" [28]. This fact became the basis for the first efforts to improve automotive fuel efficiency were focused. By increasing compression ratio, engine makers could draw more power for a given mass of fuel injected from an engine cycle. However, if the volatile fuel-air mixture is compressed too much,

auto-ignition, or engine knock, becomes likely which can damage the engine. Research became focused on how to design engines to take advantage of higher compression ratios while avoiding engine knock. Further motivation arose from a crude oil shortage in the early 1900s. This is attributed to the fivefold increase in gasoline demand due to the rapid influx of combustion engines into world markets [28]. Initially limited by the fuels available at the time, the first notable innovations to actual engine fuel were the invention of the diesel combustion system by German engineer Rudolf Diesel in 1892, and the 1923 discovery of tetraethyl lead by General Motors as an additive to gasoline, which greatly improved its knock behavior [8].

1.1.2 Post-War Era

The automotive sector saw rapid growth in consumer and light-industrial markets in the first half of the 20th century. By 1920 nearly all road vehicles and aircraft were powered by combustion engines. By 1950, an estimated 50 million vehicles were registered in the United States alone [3]. Innovations to the automotive engine during this time were primarily motivated by competition between auto manufacturers seeking to take advantage of an erupting consumer population. Advancements in electronics, suspension, and chassis design facilitated the transformation of the automobile into the form that we are familiar with today.

Engines grew bigger and stronger virtually unchecked until 1954 when a paper was published demonstrating that levels of smog in Los Angeles, California were a result of reactions between nitrogen oxides and hydrocarbons in the presence of sunlight [27]. It became clear that engine exhaust was a major source of these particulates and as a result, the first standards on emissions were introduced by the State of California in 1960 [38]. The rest of the nation soon adopted policies on vehicle emissions followed shortly by Europe and Japan. To combat these rising emissions, catalysts were introduced into exhaust systems of spark-ignited engines and restrictions on levels of toxic lead in gasoline were imposed [28]. This reduced automotive fuel efficiency because less volatile fuels and lower compression ratios had to be employed to meet increasing emissions standards.

Pushes for improved fuel efficiency became prominent again during the end of the 20th century when political instability and embargoes from OPEC nations caused crude oil prices to fluctuate sharply in the United States. This coupled with the growing concern over the dwindling supply of fossil fuels served to create a tense atmosphere around the energy debate in America. The first piece of federal legislation to regulate automotive fuel economy was the US Energy

Policy and Conservation Act of 1975. It created the Consumer Average Fuel Economy (CAFE) standards which set miles per gallon (mpg) of fuel consumed (or fuel mileage) requirements for all passenger cars and light trucks to have reached 27.5 mpg by the year 1990 [5]. By 1985, average fuel consumption of passenger cars had risen by 80% and trucks by 50% [32], therefore reducing national oil consumption by an estimated 55 billion gallons and saving consumers $70 billion in fuel costs [24].

1.1.3 Present Day

Between the year 1990 and present day, there have been conflicts, discoveries, and technological advancements that have drastically changed the world climate surrounding fossil fuel consumption. However, the need for more fuel efficient motor vehicles has not only remained a strong issue, but has grown into a top priority of U.S. energy and economic policy. "US Energy Independence" is a buzz-phrase that has held various meanings in legislation and economic conversation over the past decade, being heralded as both a critical national security goal and also an unachievable myth [25]. It inspired the Energy Independence and Security Act of 2007 which raised the CAFE standards to require consumer vehicles to reach an average fuel consumption of 35.5mpg by the year 2020 [4]. In 2012, the Obama Administration moved the deadline forward to 2016 and increased mandates to 54. 5mpg by the year 2025 [14]. Since 2012, the new mandates have received some resistance from lawmakers as well as members of the auto industry, claiming that the mpg standards are too costly and unachievable in the allotted time-frame.

The 2012 regulations also instructed the Environmental Protection Agency (EPA) and the Department of Transportation (DOT) to impose regulations on emissions levels of consumer and light-industrial vehicles in a similar format to the CAFE standards [14]. Since then, concerns over climate change and pollution have become increasingly grave and the auto industry is shouldering a large portion of the blame. In 2016 the annual minimum concentration of observed CO_2 in Earth's atmosphere, an important marker for global climate change, failed to dip below 400 parts per million for the first time since humanity began tracking its ability to change the global ecosystem. This event has been defined by scientists as the point at which we will lose the capability to keep global warming in check [20]. We are also drawing closer to the threshold of a global average temperature rise of 2 degrees Celsius above pre-industrial temperatures, the point at which scientists think we will be at risk of major global climate changes that would prove hazardous to humans. The Paris Agreements of 2015 set goals of limiting temperature rise to 1.5

degrees. However, experts think that this may no longer possible given the current state of our atmosphere [45]. Models run by the Intergovernmental Panel on Climate Change (IPCC) indicate that any proposed scenario that successfully limits global warming to the 2 degree threshold, the world needs to completely end positive net carbon emissions by the year 2100 through reductions to existing carbon producing industries and a major deployment of negative emissions technologies (NETs) [44]. Third party studies [9] [21] have concluded that this is an overly generous outlook, especially given the fact that NETs remain at best, mostly conceptual in the large scale and, at worst, an abstraction used in models to achieve an agreeable result. In the immediate-term, the impetus has fallen to the non-renewable electricity and automotive sectors, the two largest producers of carbon emissions worldwide, to take major steps in reducing their carbon footprints.

In addition to hazards on a planetary scale, vehicular emissions also directly threaten public safety through air pollution and smog formation due to emissions of carbon monoxide (CO), nitric oxides (NO_X), unburned hydrocarbons (UHCs), and soot. In urban cities and areas of dense traffic, air quality is measurably lower and has proven to be hazardous to health. Recent independent studies performed in various cities [47] [12] [26] have observed or predicted correlations between emissions concentration and hospital admissions for cardiovascular and respiratory health problems. These patterns become critical in extremely dense populations in industrialized countries such as China, India, and the US.

The EPA and the National Highway Traffic Safety Administration (NHTSA) have been very active in regulating combustion powered vehicles to combat automotive related detriments to both the environment and the health of US citizens. In August of 2016, the organizations finalized their “phase 2” regulations on fuel consumption and emissions of passenger, commercial, vocational, and recreational vehicles. Consumption targets as high as 12% reductions between model years 2010-2027 are required for certain vehicle classes as well as emissions reductions of up to 27% [51].

Better fuel economy has always been a primary motivation in engine research. Given the pressure currently placed on the auto industry from these economic and environmental sources, it is clear that innovation in fuel consumption technology remains a very high research priority.

1.2 Motivation

Improved automotive fuel consumption has positive implications on all scales. In 2014, global CO_2 emission levels reached an estimated 35.7 billion tons, 15% of which were produced by the United States [43]. The transportation sector can be attributed 31% of the nation's total carbon emissions, roughly 1.7 million tons of CO_2 for that year [49]. As a major global contributor to world greenhouse gas emissions, any amount of reduction in national fuel consumption would have huge impacts on climate change. Less fuel consumed by an engine results in less carbon emissions from the combustion process. Applied to every vehicle on the road today, improvements could significantly slow down global warming and provide flexibility in the models being used to budget the world's future carbon production.

Another important implication of reduced fuel consumption worldwide is the reduced demand for crude oil. In 2010, the Organization of Petroleum Exporting Countries (OPEC) held 79% of the worlds proven oil reserves. In recent years, the U.S. has increased its market share as an oil exporter through newly discovered reserves. However, OPEC still has great capacity to influence crude oil prices through embargoes and production curtailing. Reduced demand coupled with higher production from non-OPEC sources would promote sustained low oil prices and market stability [25]. The United States is in a prime position to be the catalyst for this market shift. Increased regulation and a large rise in oil production due to fracking and newly tapped reserves in Alaska and offshore sites have reduced our dependence on foreign oil imports. This has had a positive impact on national GDP through decreased spending and increased exports [25]. The benefits to the U.S. economy could be magnified through further reductions in oil demand freeing more supply for export.

In 2016, emissions reduction became a matter of foreign policy when the Paris Agreements were ratified. The U.S. has committed to further reducing its carbon footprint and aiding other nations to do the same. Automotive fuel technology will have a large role in achieving these commitments. Emissions are another economic drain. Levy et.al (2010) estimated that in 2000, the public health costs of deaths related to carbon emissions was $31 billion (2007 dollars) [36].

There is probably no greater motivation for consumption improvements than at the manufacturer level where fuel economy directly relates to increased profits. Pressure from government regulation falls directly on auto producers who are subject to hefty fines and other

penalties for non-compliance. These days, fuel economy is one of the top price points among consumers and often can be the factor car buyers use when deciding upon a specific model. This results in a good deal of competition between manufacturers to continue to reduce the fuel consumption of their products. This can be observed through the increasing production of hybrid and electric models as well, although they remain very expensive to produce. Finally, a great deal of profit stands to be made through the development and patenting of fuel efficiency technologies.

From a consumer perspective, historical precedent shows the reduction in crude oil prices from improvements in fuel consumption would result in lower gas prices. Continued innovation in fuel efficiency and hybrid technologies, which are already saving consumers money in the long term, would result in lower production costs of those efficient vehicles, further saving the car-buyer money. There have always been clear motivations to continue to improve the fuel efficiency of engines and there have been countless research efforts to do so. The next paragraphs will discuss the known influences on engine fuel consumption and what is currently being done to mitigate them.

1.3 Background and Previous Work

1.3.1 Fuel Consumption Factors

It is well known that at the fundamental level, the amount of fuel energy required by an engine scales with its desired power output. An ideal engine would consume only as much energy from fuel as is exactly required to propel whatever it is moving at some desired speed. However, real engines have internal losses due to friction, fluid dynamics, chemistry, and the energy required to sustain its own motion. The amount of usable power an engine can draw from a mass of consumed fuel is its efficiency, which is also a measure of these losses.

Inside an engine cylinder, the first opportunity for lost efficiency is from incomplete combustion. This happens when poor mixing or improper amounts of fuel injected causes some of the fuel to remain unburnt, thus no energy is released for that mass of fuel consumed. Modern engines are capable of 100% combustion efficiency if they do not run too rich [28]. The fuel that does combust in the cylinder produces energy in the form of either piston work due to gas expansion, or waste heat that increases temperatures of the gas mixture and engine. A large portion of chemical energy stored inside a mass of fuel gets wasted as heat. This phenomenon is very dependent on the temperature of the engine and the air being drawn into the cylinders [28].

Of the usable work that drives piston motion, a portion is required to overcome internal friction and inertia of the pistons and crankshaft. Further work is used to drive internal components such as the camshaft and oil pump, which are crucial to engine operation. Alternators, radiator fans, and air-conditionings also require some of the energy available in fuel to operate. Thus, only a fraction of the energy contained in the fuel consumed by an engine is available at the flywheel for use. A great deal of effort has gone into designing and tuning modern engines to maximize the amount of usable energy extracted from fuel to the point where variations in fuel economy are now much more sensitive to conditions outside the engine and how it is operated, rather than internally.

The two variables commonly used to describe the state of an engine are its rotational speed and the amount of "load" it is under. The term engine load can have many different meanings. In this study engine load is defined as the amount of effort, in terms of either torque or power, required from an engine to overcome some resistance being imparted upon it. Prediction and control of engines hinges on deriving this two-part state of the engine in real-time because many parameters such as temperature and various efficiencies are dependent on it. During engine calibration and tuning processes, contour maps such as the one in figure 1.1 are built using engine speed and load as independent variables. Many different engine performance metrics can be represented well by maps and are often used to program engine control units (ECUs).

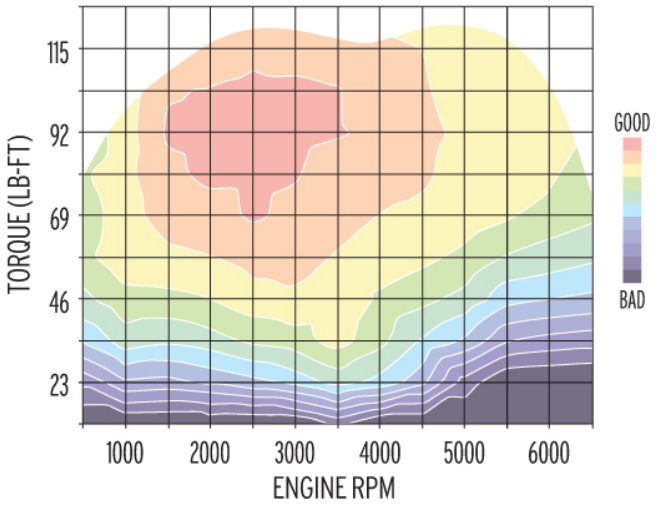

Figure 1.1: Example Contour Map of Brake Specific Fuel Consumption (BSFC)[17]

There are also many outside sources of load that an engine must overcome. The larger they are, the more fuel the engine consumes to maintain a desired speed or acceleration. Curb weight, the properties of its drive-train, and aerodynamics can greatly affect how fuel efficient a vehicle is. One clear example is a semi-truck and trailer versus a modern sports car. High performance car bodies are streamlined to keep drag coefficients as low as possible which keeps aerodynamic forces low. Semi-trucks are very square and have a great deal of surface area, which result in a great deal of wind resistance at higher speeds, thus requiring more fuel during operation. A great deal of research and development has gone into improving aerodynamics of commercial trucks to achieve savings in fuel costs [40].

Environmental factors such as weather, road shape, and density of traffic also have an effect on fuel efficiency. These factors constitute the resistance to motion an engine would encounter when driving at steady speed. When the engine is required to accelerate, added effort is required due to the change in momentum of the vehicle or equipment being driven. Studies [41] [18] have shown that primary indicators of automotive fuel consumption are the frequency and intensity of accelerations during engine operation. Most of these fuel inefficient accelerations can be directly correlated to the behavior of drivers.

1.3.2 Driving Behavior

Since the operator is the most uncertain variable in engine operation, many studies have been performed to quantify driver impact on automotive fuel economy. De Viegler et al. (1997) [18] conducted on-highway experiments to measure fuel consumption and emissions efficiency for a variety of variables. They concluded that highway motorists driving in a “calm” manner experienced on average 7% fuel savings over fast, aggressive drivers. Another study performed by Mierlo et al. (2004) [41] used both a chassis dynamometer and controlled, on-road tests to compare the fuel efficacy of different driving styles. In both settings, the study concluded that fuel consumption could vary by as much as 25% depending on how aggressive driver behavior was. The study also measured the effect of surrounding traffic on single-vehicle fuel consumption. Results showed that frequent stops and starts due to slow, congested traffic were very detrimental to fuel efficiency. From the studies on driver impact reviewed for this work, the general conclusion can be made that there stands to be a great amount of fuel savings made by employing a conscious effort to “drive efficiently.”

Eco-driving is defined in [31] as "the set of guidelines that should be followed by a human driver to minimize fuel consumption, while coping with varying and uncertain road traffic by operating in the most efficient zone of the engine wherever possible." Attempts have been made to formulate these guidelines into an education program that, if successfully disseminated to enough drivers, could significantly reduce the fuel consumption of a population. However, educators observed large variations in drivers' interpretation of the program which led them to view the guidelines as contradictory and undesirable. In some cases, a misinterpretation of eco-driving tips led to reduced efficiencies [41]. While there seems to be a consensus on the impact of driver behavior on fuel consumption, studies show that there is too much uncertainty in human factors to apply a systematic approach to reducing fuel consumption from it. Therefore, preferred methods have shifted to using technology to assist drivers in making fuel efficient decisions.

1.3.3 Driver Assist Technologies

Control technology has always had applications in the automotive sector. Starting with the implementation of simple feedback control in various subsystems, autonomous vehicular control has progressed over the last 50 years to being capable of taking control entirely away from a driver.

Electronic Cruise Control (ECC) was patented in 1979 as an improvement on the mechanical cruise control device invented much earlier, and can be found in some form on nearly every production car today. It was the first device to allow for a vehicle to function normally with reduced input from the driver by storing a desired speed value, set by the driver, to internal memory and using feedback from speed sensors to hold the desired speed automatically. Most ECC systems use proportional-integral (PI) control on the signal between the foot pedal and throttle actuator to regulate speed [11].

ECC proved to be much better at maintaining a fixed engine speed than a human driver and was quickly adopted by automakers worldwide as an accessory that allowed for increased driver comfort during long distance highway driving. It also had positive impacts on fuel economy by eliminating the small accelerations that occur from lag and overcompensation in human response when attempting to maintain a fixed speed under changing conditions. ECC capabilities are limited to maintaining a fixed speed with functionality to allow the driver to change the set-point incrementally in real time and temporarily accelerate or decelerate before returning to the cruising set-point. While these functions were necessary in order to avoid

dangerous driving events, they still required driver input, which is sub-optimal in the fuel consumption sense.

In 1995 Adaptive Cruise Control (ACC) was patented as an extension to contemporary cruise control that allowed deviations from cruising speed to automatically course-correct in certain situations, further removing driver involvement [34]. ACC functions very similarly to ECC but changes instantaneous cruising speed based on sensor information, primarily radar or LIDAR, to vary speed in order to maintain a specified following distance behind another vehicle.

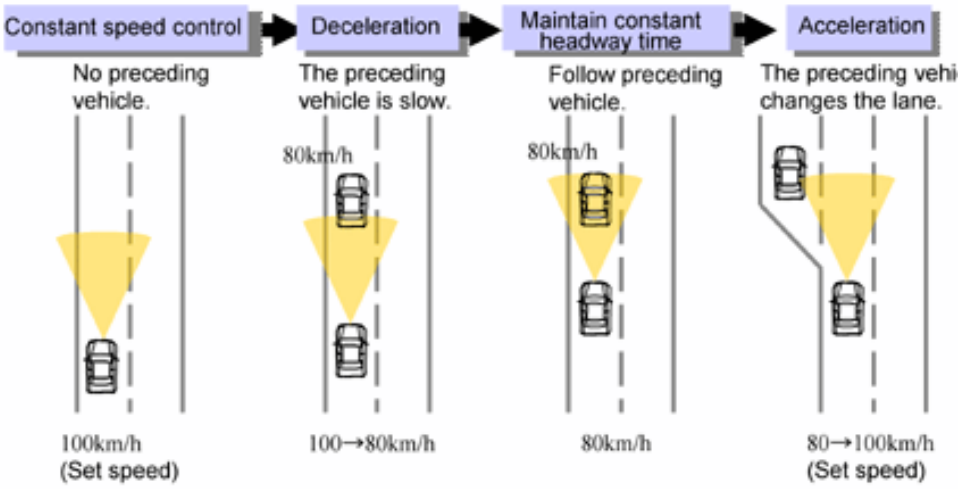

Figure 1.2: A Diagram of the Working Principle of ACC [1]

While safety was the primary focus in ACC development, it has provided gains in fuel economy by improving traffic flow on highways. By automatically reducing speed when approaching another vehicle, ACC removes the need for operator braking and re-acceleration to previous speeds to deal with slower traffic. ACC can also be tuned to maintain or change speed based on optimal fuel economy. However like ECC, it can be overridden by a driver who would rather overtake a slower vehicle than match its speed. Another recent cruise control technology to gain attention is Predictive Cruise Control (PCC). PCC uses both on-board sensors and external signals to infer an optimal trajectory in city driving situations [10]. PCC technology seeks to improve fuel consumption by communicating with traffic signals to reduce or eliminate time spent idling at red lights, which is the most inefficient state a vehicle can be in. With knowledge of the timing of an upcoming traffic-signal-controlled intersection, the PCC system derives a velocity

trajectory that minimizes braking, maintains safe vehicle distances, and results in arrival at the intersection under green light or with minimal stopping time. PCC technology still remains mostly theoretical but the concept has been proven on electric vehicles and should be readily extended to conventional autos [19].

Improved computing technologies have also made more complex driver Heads-Up Displays (HUDs) possible in today's cars. Many modern production models come equipped with digital gages with additional data accessible by drivers. Instantaneous, average, and past fuel economy data can now be displayed in real-time as a visual aid to promote driver consciousness of fuel efficiency.

Figure 1.3: Dashboard Fuel Economy indicators in a 2014 Corvette Stingray [42]

While usually implemented as purely an indicator, intelligent speed adaptation (ISA) systems do exist that can limit or even control speed based on speed limit data broadcast through GPS. These systems are mainly used as safety or punitive measures for speeding drivers but have been shown to improve fuel consumption through driver awareness [32].

1.3.4 Autonomous Driving

Continued advances in sensing, computing and actuation have made completely autonomous vehicles a reality today. Entities like Google's Waymo Project and Ford have spent a great deal of time and money developing autonomous vehicle platforms and have been road testing their products with an on-board engineer serving as a fail-safe. Autonomous vehicle technology provides a real opportunity to greatly reduce vehicle fuel consumption and emissions

by removing the driver from the equation entirely. Driverless cars could be programmed to prioritize fuel economy over travel time, which is usually not the case with a human behind the wheel. All of the gains from ACC and PCC systems would be compounded because they would be continuously running on an autonomous system.

Also, it has been shown that the high precision driving capable of autonomous vehicles makes coordinated fleet behavior possible. By driving in tight formation, groups of vehicles could achieve much greater fuel mileage by reducing their collective aerodynamic drag and improving traffic flow. The large scale deployment of platoon behavior on highway vehicles would make a drastic reduction in consumption and emissions possible [22]. Automotive road-vehicle technology is recognized today as having major potential to reduce fossil-fuel consumption however, many barriers remain to achieving large scale implementation. Regulatory, safety, and liability concerns still hamper research and development projects, mainly due to lack of certainty in the technology. In order to achieve the confidence level necessary for industry-wide adoption, improved models, testing apparatus and processes are necessary to create the flexible yet robust programming required for the reliable operation of an autonomous fleet.

Fuel Efficiency

Autonomous vehicle technology is well past its infancy but has not yet emerged fully into the automotive culture, and as yet, there are many different approaches being taken by competitors to achieve autonomy. In practice, driverless vehicles do not differ much from contemporary automobiles. This is because the most cost effective approach to creating an autonomous vehicle is to adapt a production car. A contemporary configuration is also necessary because at this point, drivers are still required to be present as a fail-safe measure and must be able to operate the vehicle. Discussions on the workings of a fully autonomous vehicle are beyond the scope of this work however autonomous control techniques relating to fuel efficiency will be reviewed. Manzie et al. [39] showed that the fuel consumption improvements offered by hybrid vehicles at the time could be matched by an “intelligent vehicle” using a contemporary engine with a predictive control algorithm. The intelligent vehicle was assumed to be equipped with autonomous driving technology plus a telematics system that informs the vehicle about traffic and intersection conditions in real-time. The authors combined three different drive cycles with varying traffic patterns to create simulated road conditions that were applied to a baseline production vehicle model, a hybrid, and the intelligent vehicle model constructed for the work.

Velocity profiles were derived and simulated to generate fuel consumption data for comparison. Fuel consumption was calculated from steady state engine maps. Results indicated that in all cases the intelligent system performed just as well as the hybrid in fuel consumed with only a small amount of previewed traffic information required.

The idea of an optimal vehicle speed for specific road situations is not a new one. One of the earliest works to study this was done by Schwarzkopf and Leipnik in 1977 [48]. They developed a nonlinear optimal control model to manipulate engine throttle under changing roadway conditions. They concluded that a steady state velocity was optimal for roads with unchanging grades. In 1988 Hooker built upon this work by creating a minimum fuel consumption model constrained by a fixed distance, speed and time constraints [29]. His work considered gradients and found that a constant speed was optimal for constant gradients. However his results were found to be only valid under certain road conditions. Since then, many additional models have been formed using variousl control strategies that conclude that a more or less constant speed is optimal for fuel consumption [33][15]. A more recent study that diverged from the constant velocity consensus was done by Kamal et al. in 2011. He applied optimal control theory to a simplified vehicle model to improve fuel efficiency in highway driving with changes in elevation [31]. They used a model predictive controller, a nonlinear optimization algorithm, and a minimum residual numerical strategy to derive an optimal velocity trajectory over a small fixed horizon that shifted as the vehicle progressed forward. They updated the horizon and optimal trajectories in real time to simulate an autonomous vehicle over a highway with elevation changes. They compared the fuel consumed by their optimized strategy to a simulated cruise controller. They realized up to 10% gains in fuel consumption using their control strategy over standard cruise control. They also demonstrated the viability of using numerical techniques with simple control theory to allow for real-time sensing, calculating, and carrying out of a trajectory. This is a crucial requirement if full autonomy is to be made possible.

Saerens et al. [46] used dynamic optimization to minimize the fuel consumption over an engine acceleration. They used a dynamometer test stand to validate their engine model, which was a two state engine model using intake manifold pressure and engine speed. In both simulation and experiments, they achieved 13% decreases in measured fuel consumption between an optimal and linear acceleration trajectories.

1.4 Scope and Objectives

During the course of this thesis work, an engine test bench was configured to support a variety of engine experiments and calibrations ranging from control testing to emissions studies. Equipment was initially arranged to test and validate control algorithms. A model predictive, optimal controller was developed using a simplified state space engine system and calibrated models obtained via steady-state experiments.

The algorithm was then deployed to a subject engine on a dynamometer test stand for evaluation. The objective of this optimal controller is to derive, in real-time, trajectories for engine speed and load that result in the least amount of fuel consumed. Simulated road conditions are limited to highway driving with changing elevation, longitudinal motion, and no traffic. Success of the controller is evaluated in this thesis by the amount of fuel savings achieved and its viability as an autonomous, real-time controller which is determined by the rate at which it can reliably predict and hold optimal operating points .

1.5 Thesis Structure

The remainder of this thesis will be structured into five additional chapters, a summary of which is provided here. Chapter two will describe the construction of the test facility and the equipment procured. A brief outline of the operating and safety procedures put in place will be given as well. Chapter three will detail the theory behind the modeling approaches taken and principles of optimal control used in this work.

Chapter four will summarize the engine characterization process that was performed to calibrate the optimal controller prior to experimentation. Chapter five will discuss simulations performed using the LabVIEW® programming environment to validate the engine model and tune optimal control parameters prior to deployment on hardware. Chapter five will also detail the hardware control programming, which was also done using LabVIEW, used to run the optimal control algorithm in real-time and guide the engine through experimental trials. The chapter will conclude with the design of experimental procedures, test cases, and benchmarking points used in this work. Chapter six will present the results of engine tests using the optimal controller and provide an analysis of the controllers performance and its viability as a strategy for autonomous driving. Final conclusions of this thesis work and potential future extensions will also be discussed.

CHAPTER 2

THE ENGINE TEST FACILITY

2.1 General Testing Facilities

Testing and validation play major roles in the development and regulation of combustion engines. Whether the testing is done on a stand-alone engine or on a vehicle, the devices and techniques used to study the operation and performance of engines has become quite sophisticated and versatile. At the heart of any test bench or facility is a dynamometer, which is used to load an engine and measure output RPM, torque and power. The types and configurations of dynamometers will be discussed below, but are dependent on the nature of tests being performed, the sophistication of the facility, and the size and power of engines to be tested.

A dynamometer test stand must be capable of rigidly fixing an engine in place and provide all subsystems necessary for sustainable operation. Crucial inputs such as fuel and ample airflow as well as some form of cooling must be present. Adequate ventilation to remove engine exhaust and waste heat is also very important. Also, most engines need electrical power for starting and some require a battery to be present to run electrical subsystems such as the engine control unit (ECU) and spark plugs. Depending on the test to be performed, the engine may need to be fitted with instrumentation to take measurements of in-cylinder conditions, or sensors in the input and output streams to measure fuel consumption and emissions composition.

All of these considerations or a subset of them must be accounted for depending on the type of engine being tested and the data to be gathered. The rest of this chapter is devoted to describing the features of the test cell used in this work as well as considerations that were taken in anticipation of future works in the facility.

2.2 The Marquette University Engine Observation Laboratory

2.2.1 Overview

A major aspect of this thesis project was the design and construction of the engine test facility as well as the installation of equipment necessary to complete the experiments required by this work. Marquette Universitys Engineering Hall was designed and constructed with specific space reserved for engine testing, however upon completion of the building, there were no current

or planned projects that could put an engine test bench to use so no infrastructure or equipment was put in place. At the inception of this thesis project in January of 2015, the test cell had been re-purposed as department storage, but funds for equipment and construction had been approved and the planning phase of facility construction was underway. With the help and generosity of many industry partners, a stand-alone facility was constructed capable of supporting various projects such as engine control, combustion studies, and emissions predictions. The remainder of this chapter will discuss the design, specifications, and installation of the test equipment, subject engine, measurement systems, and control procedures used in this study as well as a brief outline of the infrastructure decisions made to support this project and future work.

2.2.2 Design and Specifications

During the planning phase of the Engine Test Facility project, design requirements were fairly relaxed. Aside from the safety and integration requirements imposed by the university, the only specifications to be met were that all equipment be capable of supporting engines rated up to 100 horsepower, and that an equal amount of cooling power was available to maintain operation of said equipment. Considerations were made to ensure that plans took advantage of all existing infrastructure and that the configuration of the room and equipment be as flexible as possible to accommodate multiple experiments with minimal changeover of equipment. All of the restrictions and features that were considered during the planning of the facility were accommodated for in construction of the test cell and equipment designs.

2.2.3 Construction and Infrastructure

Construction of the facility took place between December of 2015 and February of 2016. During this time changes to the plumbing, HVAC, electrical, and monitoring systems of Engineering Hall had to be modified so the majority of the work was performed over a break in class so the effects of interruptions in building operation would be minimal. The fact that plans for an engine test cell had been incorporated into the building's original construction meant that most of the necessary infrastructure such as water, natural gas, electrical and high volume airflow had already been routed to the test cell and a steel surface plate had been laid into the concrete floor so construction did not need to extend beyond the immediate vicinity of the lab.

The first task to be completed was the removal of a moderate layer of rust that had accumulated over the surface plate as a result of the room being unused in the five years between

building construction and the start of this work. After the bedplate was restored to a satisfactory condition, work on cell infrastructure began with the installation of natural gas piping, engine exhaust ductwork, chilled water lines, and electrical conduit to various points in the cell. Some of this work was put on hold until the engine and dynamometer arrived from PowerTest®, the dynamometer manufacturer, to ensure all of the input streams were properly located. Exhaust, natural gas, and building water lines were all installed with capped off, "future" connections to accommodate additional engines and experimental setups as they become necessary.

Room ventilation and cooling modifications involved installation of a new temperature controller to the room inlet ductwork and additional control procedures to the room exhaust fan. The cooling air system is designed so that inlet air can be controlled to any temperature using a normal building thermostat, and the high capacity exhaust fan that the test cell shares with a utility closet will run during engine operation to maintain a slight negative cell pressure. This ensures that the specified cooling capacity is achieved as well as provides an avenue for rapid ventilation in the event of a gas or exhaust leak.

Engine exhaust is drawn away by a CAR-MON high volume static air exhaust fan mounted near the ceiling. This fan is controlled via the dynamometer's control system and runs at all times during engine operation. Engine exhaust is pulled upwards through an eight inch flexible exhaust hose to a solid duct that run along the ceiling to the fan as shown in Figure 2.1. An adapter was constructed to connect the catalytic converter to the flexible hose while allowing dilution air to enter the exhaust stream. This is desired to keep temperatures in the line and at the fan below the maximum safe temperature specified by the manufacturer. The fan pushes the exhaust out of the room and connects to a larger exhaust ventilation line that exits the building. The test cell shares this exhaust line with an emergency building generator. To ensure that no generator exhaust back-feeds into the test cell, a normally closed, motor driven butterfly valve was installed at the room's exhaust outlet to isolate the cell when the generator runs.

Figure 2.1: Test Cell Exhaust Ductwork and Fan

The natural gas plumbing was installed with a normally open, emergency solenoid shutoff valve that isolates the cell from building supply in the case of an emergency. Additional safety equipment such as emergency stop buttons, fire alarm and suppression system, as well as carbon monoxide and methane gas detectors were installed according to requirements imposed in the design phase. All of the sensors and safety equipment installed were interfaced with building and campus wide monitoring systems as required by the university. Once all equipment was installed, electrical and communication lines were routed between motor variable frequency drives (VFDs), dynamometer, monitoring equipment, building HVAC controllers, and the dynamometer control system at the command desk in the adjacent lab. The original command station, shown in Figure 2.2, consisted of a PC loaded with the PowerTest dynamometer control and monitoring software, a printer, and a physical emergency stop button.

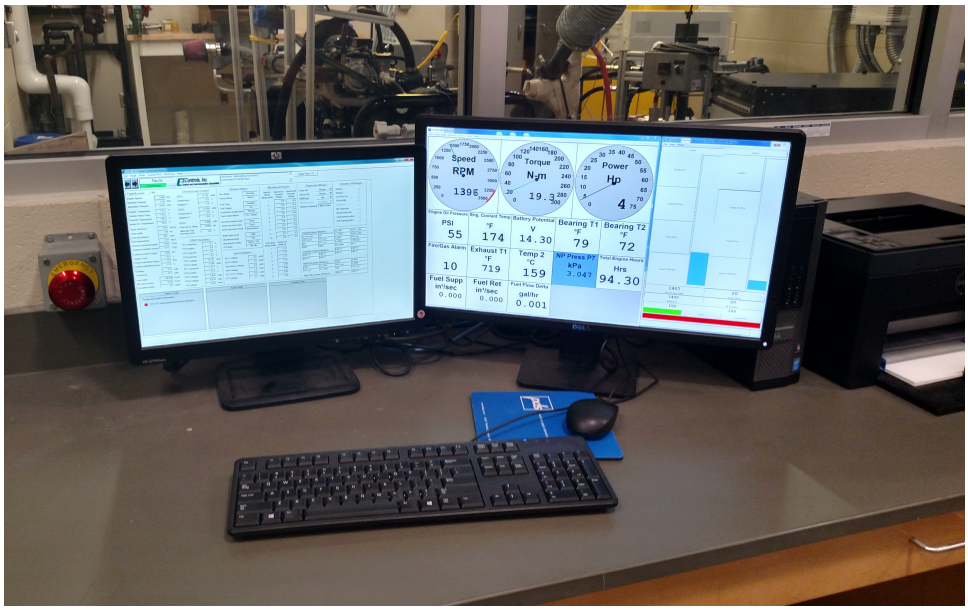

Figure 2.2: PowerTest Network (PNET) Control Station

2.2.4 Dynamometer

The most important piece of any engine testing facility is the dynamometer. An engine dynamometer is defined in [23] as a device that provides an external load to, and absorbs the power from a combustion engine or motor. Most modern dynamometers are either hydraulic or electric. Hydraulic dynamometers, sometimes known as "water brakes," are typically constructed of a vaned rotor, not unlike ones found inside a vane pump, mounted to an engine shaft. Water is allowed to flow over the spinning rotor at a fixed rate. The power from the engine is dissipated through fluid friction as the engine turns the rotor. Vanes on the stator, or outside casing of the water/rotor chamber, cause a resultant torque which is transferred via a lever arm to a load cell. By varying the flow rate into and out of the water brake, which controls the amount of water inside the dynamometer, the resistive torque from fluid power can be manipulated. Water brake dynamometers can be quite small in form and do not require much infrastructure except for ample water supply. For this reason they are popular in smaller test cells and with amateur enthusiasts. They also scale up very easily and can be employed in very high power applications. A simple schematic of a water brake dynamometer is displayed in Figure 2.3.

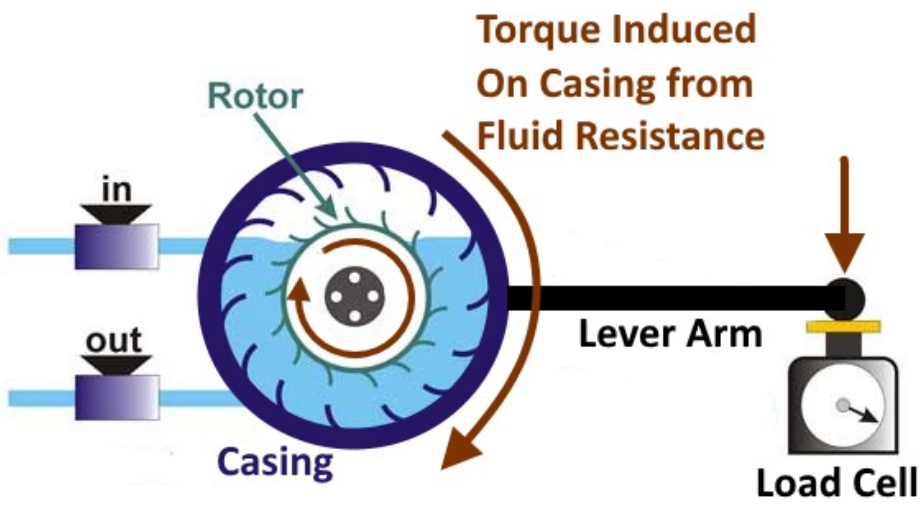

Figure 2.3: Working Principle of a Water Brake Dynamometer [2]

Electric dynamometers are classified by what type of current, alternating, direct or eddy, they generate. Eddy current dynamometers use electromagnetism to resist engine motion. The engine is attached to a disk of magnetic material, usually iron, that spins inside the dynamometer. The rotor is surrounded by a coil in which a current is induced which creates a magnetic field. The core rotating through the magnetic field is what loads the engine. Energy drawn from the engine is converted to heat by the dynamometer which requires cooling by either air or water [50].

AC and DC dynamometers use an induction motor attached to the engine's driveshaft to convert mechanical power from the engine to electrical energy and to load the engine. Both AC and DC dynamometers can rapidly change loads applied to an engine, are air cooled and are regenerative. A regenerative dynamometer can take the power produced by an engine and transform it into usable electricity to supplement a power grid [23]. The dynamometer chosen for this testing facility was a 100HP, dual ended, AC dynamometer manufactured by Powertest Inc and shown in Figure 2.4. This type of dynamometer was chosen for the added benefit of being able to motor the engine, which is the capability of a dynamometer to rotate the engine without combustion.

A dynamometer can derive many performance metrics, such as power, friction torque, brake and indicated mean effective pressures by measuring engine output speed and torque. Engine speed can be determined via either optical or electromagnetic means. On this dynamometer, a magnetic sensor placed on the dynamometer housing counts one revolution each

Figure 2.4: The PowerTest AC Dynamometer

time a magnetic pickup attached to the driveline of the unit passes. The pulse train produced by the pickup passing the magnet is used to derive an engine speed. Optical encoders are also commonly mounted to the drive-line to measure engine speeds. They produce a similar pulse train using a laser and a finned optical disk attached to a rotating engine component. A photocell is mounted across the disk from the laser. Light is periodically blocked by the rotating disk, which creates an intermittent signal from the photocell. This results in the pulse train needed to measure rotational velocity. The speed measurements supplied by a dynamometer are usually not resolved enough to be sufficient for crank-angle based studies so an independent optical encoder is employed on the engine itself to take such data. However, dynamometer readings are accurate enough for higher-level, steady-state and transient engine testing so no encoder was used for this work.

A torque transducer is used to determine the brake torque output of the engine. This device uses trunnion bearings, which support the drive-line inside a casing, and a strut that prevents rotational motion attached to the outer race of the bearings attached to a load cell. As the engine rotates it applies torque on the dynamometer that is transferred to the strut through the bearings. This load is proportional to the torque output of the engine and is used to derive the torque at the engine's flywheel [23].

Marquette's dynamometer is double ended which means that it has drive-lines on each end of the induction motor. While two engines cannot be connected at the same time, it significantly reduces the amount of downtime when switching between engines for different experiments. While this feature is irrelevant for the current study, future research plans include the procurement of a single cylinder research engine. The sharp contrast in size between the fixture and sensor configurations of this engine and larger engines, such as the one used in this thesis work would make changeover a very complicated and time consuming task. Dual end capability will mean that both engines can be set in place with their required sensing and control apparatus at the same time and the engine not currently in use would simply need its drive-line disconnected. The PowerTest dynamometer is rated at 100HP, which represents the amount of resistive power it can supply to an attached engine. The AC dynamometer is powered by a VFD, which is capable of modulating the voltage and input frequency supplied to the motor. This is required for the precise control of engine load using this type of dynamometer. A smaller VFD is also used to drive a motor attached on top of the dynamometer motor housing. This motor forces air from the room into the larger motor for a cooling effect.

2.2.5 Engine and Automotive Subsystems

The engine used in this study is a Kubota® WG1605 series engine which was generously donated by the Kubota Corporation. It is a naturally aspirated, spark ignited engine in an in-line four cylinder configuration. It has 93.8 cubic inches of displacement and is capable of 55 peak horsepower. The engine has an operating range of 750 to 3200RPM and 0 to 120 foot pounds of brake torque. The engine and mounting fixture is displayed in Figure 2.5.

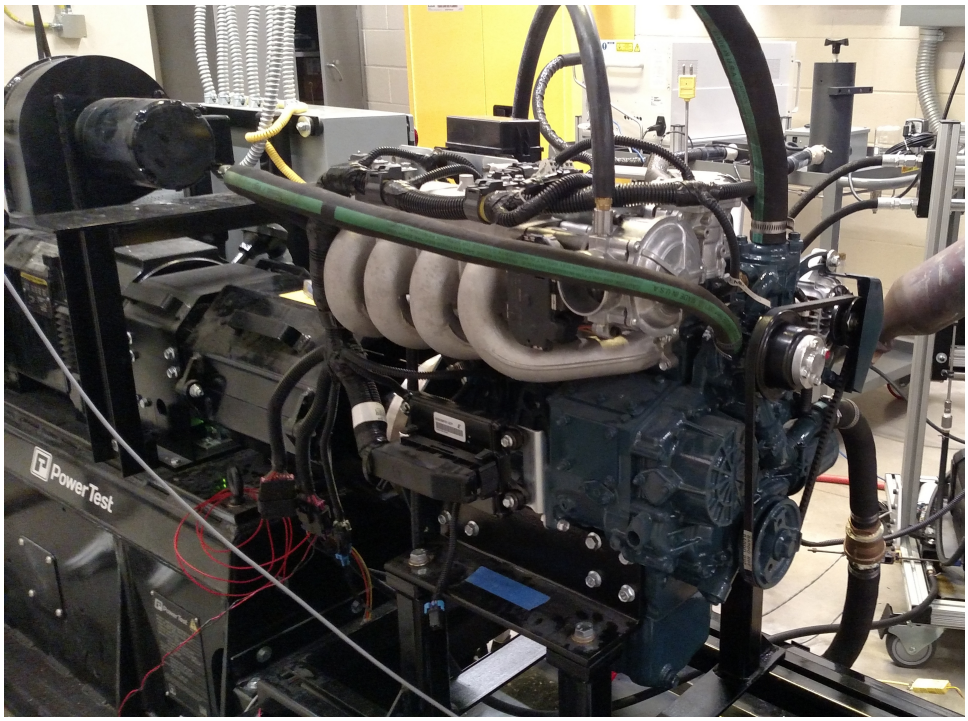

Figure 2.5: The Kubota WG1605 Engine

It is also multi-fuel capable, which means that it can run on gasoline, liquid propane, or natural gas and can be easily switched between the three modes. This is made possible by incorporating both in-cylinder and throttle body injectors simultaneously for liquid and vapor fuels respectively. Liquid fuel injection uses a fuel pump and pressure regulation manifold which is controlled in open loop by the engine control unit (ECU). Vapor fuel injection uses a vaporizer placed upstream of the throttle body. During natural gas operation, the vaporizer acts simply as a pressure regulator since the fuel is already in gaseous form. However, liquid propane (LP) must be vaporized before injection so during LP operation, the vaporizer converts liquid fuel to the usable vapor. The heat required for conversion is supplied by waste heat from the engine via tubes connected to the coolant lines. Schematics for each system are shown in Figure 2.7.

Management of fuel injection systems is handled by the ECU, where fuel selection is governed by a single, user controlled voltage signal that is either powered, connected to ground, or left open. This informs the engine which injectors to actuate and in what amount and sequence, the others are left inactive. A catalytic converter, oxygen sensors and intake air filter were provided by Kubota as well in compliance with EPA emissions standards [6].

Before the engine was installed at Marquette, it was delivered to the PowerTest facility to size and test the dynamometer pre-delivery. Additional equipment was designed and fabricated there to provide extra functionality to the testing facility. The engine and dynamometer drive shafts are attached with a drive-line supplied by Kubota and a torsional damper which was designed and manufactured after a rotational analysis of the system was performed at the PowerTest facility. This is necessary to dampen torsional vibration between the dynamometer and engine. Rotating components are fully enclosed in a guard casing as shown in figure 2.6.

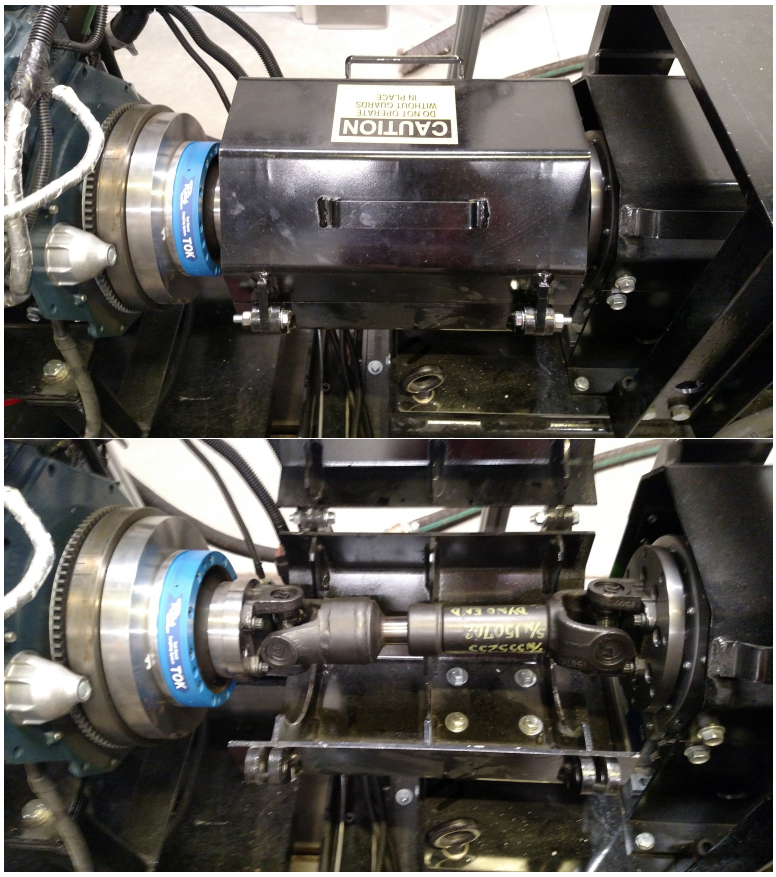

Figure 2.6: Engine/dynamometer drive-line with guard closed (top) and open (bottom)

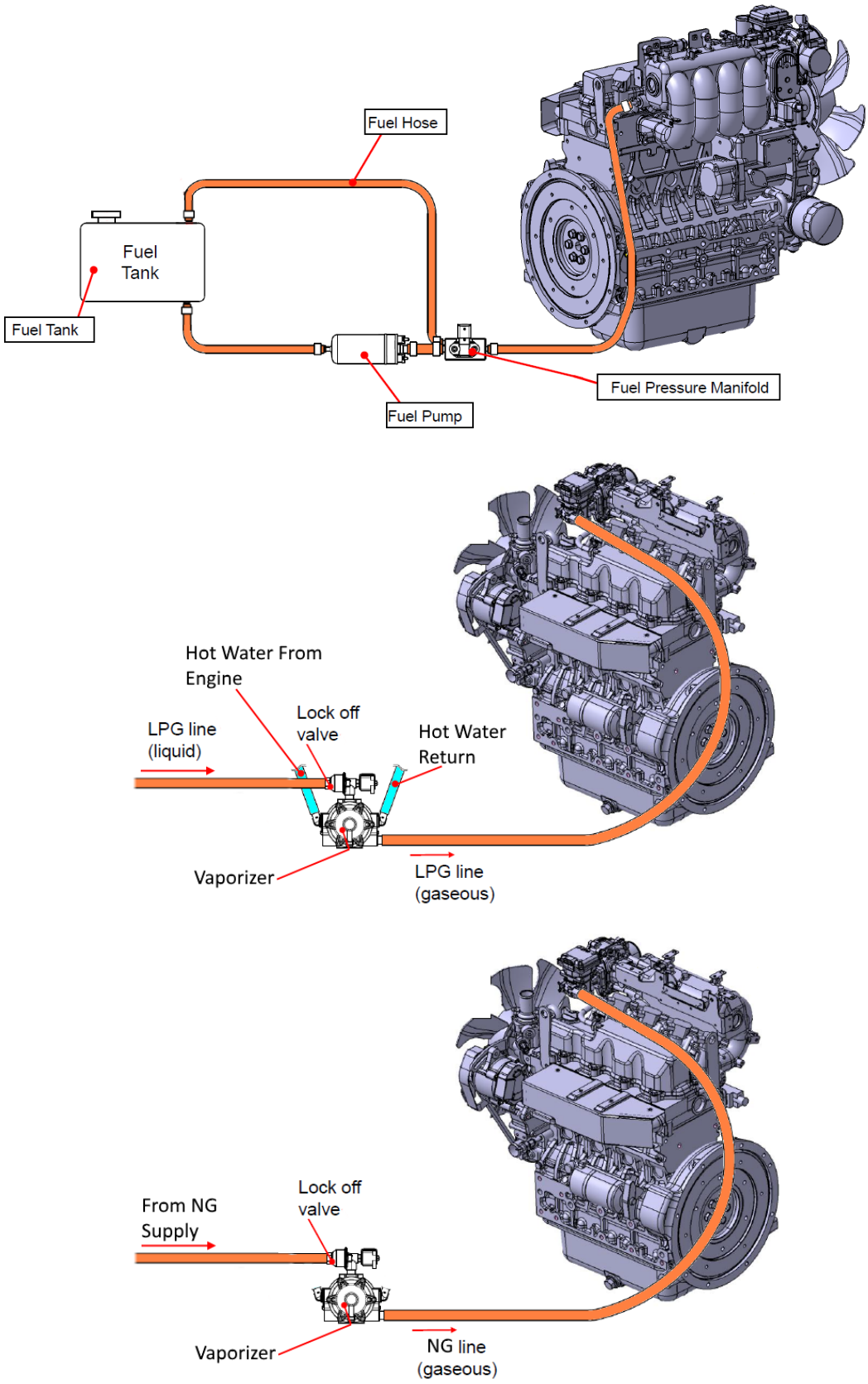

Figure 2.7: Fuel Delivery Configurations for Gasoline (Top), Liquid Propane (Middle), and Natural Gas Vapor (Bottom)

A rolling engine fixture was custom fabricated for the Kubota WG1605 by PowerTest and designed to attach to the dynamometer as shown in Figure 2.8. This provides a rigid connection between platforms and mobility when the two machines are detached. The attachment point on the dynamometer support can move vertically to ensure satisfactory alignment of driving and driven components. The weldment features an oil pan which serves to catch spilled engine fluids during oil changes and unanticipated engine issues. Once delivered to Marquette, various supports were created and attached to the cart to support coolant, exhaust, and intake lines.

Figure 2.8: A Rendering of the Engine Mounting Cart

Instead of using a radiator and fan to air cool the Kubota engine, a liquid cooling system, pictured in figure 2.9, was designed and implemented by PowerTest. It consists of a shell and tube heat exchanger remotely mounted from the engine. The tube side of the heat exchanger is connected to the engines coolant ports using $1x1/8''$ hoses and the shell side is connected to the test cells chilled water supply. A thermocouple is mounted to the outlet of the engine coolant stream and is connected to a temperature controller on the unit. The inlet of the shell stream is controlled via electronic butterfly valve which is normally closed and connected to the

temperature controller. Once engine coolant has reached a specified temperature threshold, the controller opens the butterfly valve, allowing chilled building water to flow through the heat exchanger shell, thereby cooling the water glycol mixture from the engine. This supplies a large cooling effect only after the engine has reached its optimal operating temperature. It also provides the benefit of less air cooling required of the test chamber,and allows for the removal of the engine fan, a major failure point and safety hazard. Upon arrival at Marquette University, the engine was fitted with a standard car battery, extended intake and exhaust streams, and a five gallon gasoline tank as required by the planned tests.

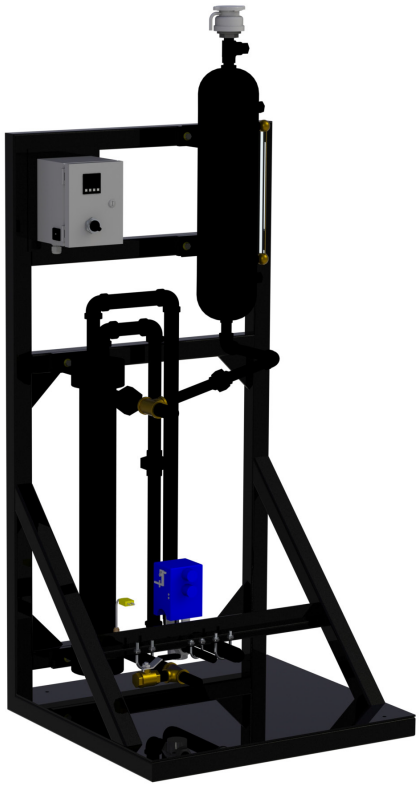

Figure 2.9: A Rendering of the Engine Cooling System

Finally, a custom fuel measurement system (FMS), pictured in Figure 2.10, was manufactured by PowerTest to provide accurate real-time fuel consumption data. The FMS uses turbine flowmeters installed in both the supply and return fuel lines. The readings from the supply and return lines are combined to give a net fuel flow measurement, representing the instantaneous flow rate to the injectors. The FMS also has a small shell/tube heat exchanger with

a temperature controller to cool the return fuel safely using building water. However, since all of the fueling components are external to this engine, no extra heat is supplied to the fuel so the heat exchanger has remained unused thus far. The FMS is contained in a rolling chassis and has a shelf designed to support fuel tanks as big as five gallons and the fuel delivery equipment. The fuel tank used in this configuration was donated by the Flambeau Corporation and was sized to fit within the confines of the FMS.

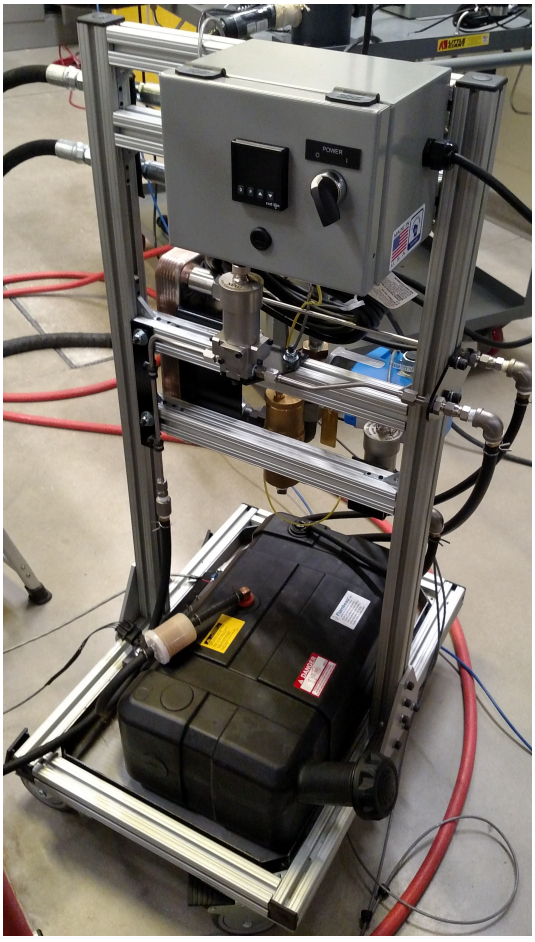

Figure 2.10: The Fuel Measurement System (FMS)

2.2.6 Control

The Kubota engine is a production model and therefore proprietary technology. As such, the specific programming routines governing the control of the engine's fuel injectors, spark plugs and throttle were inaccessible at the time of this study. Therefore, the only means of controlling

the engine is through the accelerator signal common to all automobiles. Despite this limitation, a good deal of functionality has been achieved through custom built controllers and sensing equipment for this facility which will be discussed in the subsequent sections.

Dynamometer Based Control

Included in the PowerTest dynamometer package is the PowerNet control system (PNET). This is a sophisticated control hardware and software suite that allows an operator to interface graphically with both the engine and load sides of the test equipment. This system has four main functions. Set points for driver command, analogous to foot pedal position (FPP) in an actual vehicle, and resistive torque from the dynamometer can be applied and held steady with either open loop or closed loop proportional integral (PI) control. Depending on the test to be performed, these controls can hold an engine operating condition based on a combination of two set-points in either speed, torque, power, or throttle percent. Ramping rates can also be applied. PNET converts signals from the torque and speed sensors, as well as any auxiliary thermocouples or pressure transducers that are present, into engineering units for monitoring and data gathering purposes.

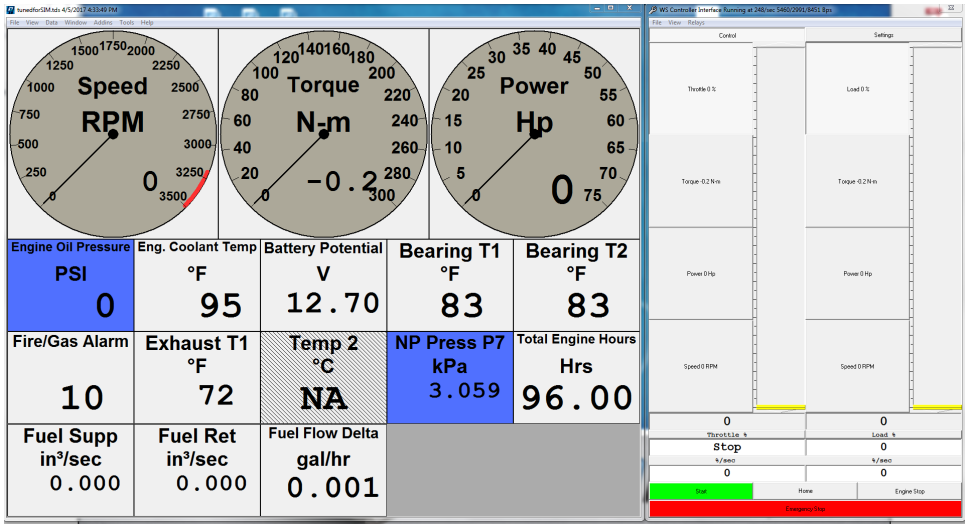

Figure 2.11: PNET User Interface with the Controller (right) and Sensor Data (left) pictured

The thermocouples and pressure transducers interface with PNET through terminals that were designed into the control box.

This system also has the capability to tap into the ECU's communications data using the CAN protocol and the SAE J1939 application layer, which is the standard communication protocol used in the automotive industry [52]. Information such as manifold absolute pressure (MAP), instantaneous spark and fuel injection timings, throttle plate opening, and fuel pressure can be read into the PNET software over the CAN connection.

PNET users can also create "calculated sensors" which are simply math operations performed on measured values that are represented as additional sensors. These are particularly useful for differential measurements or non-standard conversions. PNET can store data to memory by taking snapshots of its "database," or current speed and load set points and all measured and calculated sensors. It also has functions to format these data points into graphs and tables which it can design and build reports around.

Finally, PNET allows for the construction of "patterns." These are a series of set points with associated timing schemes that the software can apply to the engine autonomously. This is particularly helpful during mapping operations requiring a large number of steady-state set points that the operator would otherwise have to enter manually. The system has three redundant physical emergency stop (ESTOP) buttons, as well as one virtual ESTOP button in the PNET user interface. When employed, the ESTOP function immediately cuts off power from the battery to the engine. This stops fuel flow as well as ignition. An ESTOP event also causes the VFD to apply its maximum load at a very high ramp rate to forcibly stop engine rotation in the shortest time possible. This forced stop can damage the engine so it is intended only to be activated in the most extreme of circumstances. Figure 2.12 shows the PNET control box mounted on the dynamometer with one of the ESTOP buttons.

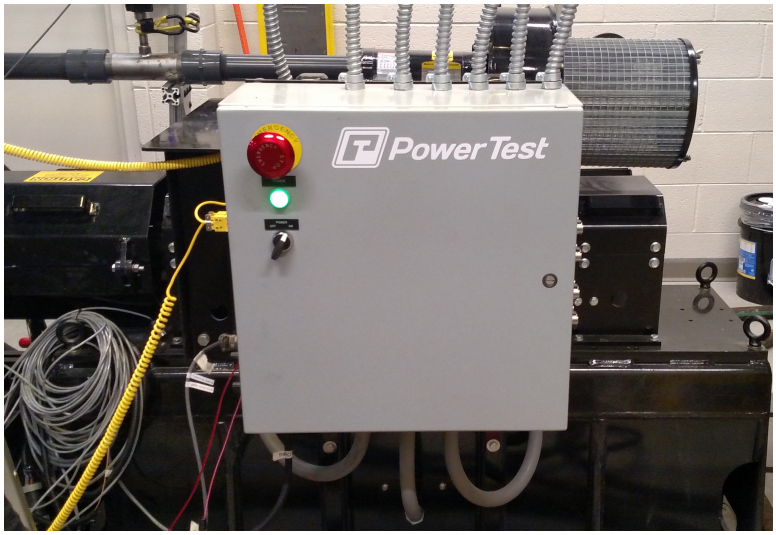

Figure 2.12: PNET Control Box with Attached E-Stop

Engine Control System(ECS)

The functionality of PNET is sufficient for many top-level engine operations such as steady-state mapping and slow transient testing when only bulk operating conditions such as speed, load, and power need to be manipulated. However, the package is quite limited when rapid transients and high data collection rates are required. To supplement the PNET controller, a National Instruments Engine Control System® (ECS) was purchased. The ECS is a very sophisticated, LabVIEW based hardware and control package that can be used to actuate any engine component, and accept inputs from the variety of sensors that may be used in engine studies. It contains two independent field programmable gate array systems (FPGA) as well as multiple National Instruments CompactRIO® chassis that can accept a variety of different control drivers or sensor modules. All of this results in a fully customizable system capable of supporting complex testing procedures and instrumentation as well as fully taking over all of the calculations and cycle-to-cycle control that are normally handled by an independent ECU. Please reference the ECS user manual [7] for a full description of ECS functionality. The specific control and measurement tasks used in this thesis work as well as a more detailed description of the programming written for experiments is outlined in chapter five.

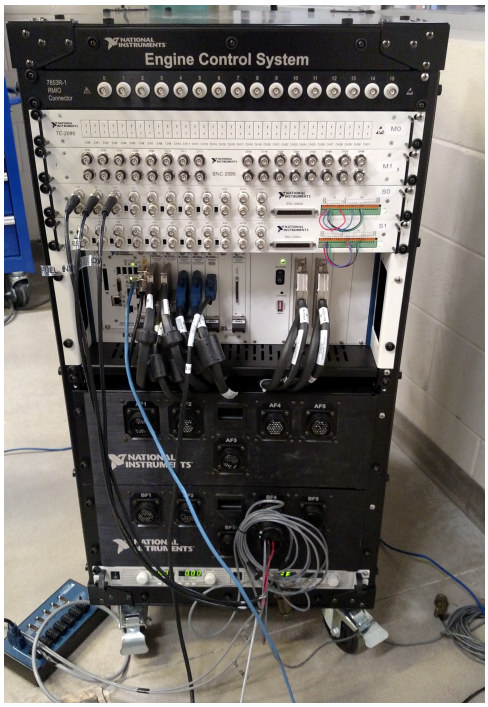

Figure 2.13: The Engine Control System (ECS)

2.2.7 Sensors

Many additional sensors and measurement devices were installed during test cell construction. While some were deemed necessary for this study, most of the additional equipment was purchased in anticipation of future engine studies. In addition to the CAN data stream from the engine, thermocouples were placed at multiple locations in the exhaust line for emissions purposes and to ensure that the exhaust lines were not overheating. Prior to cell construction, two Magnetrol® hot wire mass flow meters were purchased to monitor natural gas and air mass flows into the engine. The natural gas sensor was installed into the utility piping near the room inlet. This is justifiable since there will only be one flow path ever open at once, fuel flow rate into an engine could be monitored anywhere in the stream. The meter is designed specifically with combustible gas flow in mind and the probe is shielded to prevent any accidental ignition.

The second, larger flow meter was sized to the Kubota engines air intake port and is used to measure the real-time air mass flow rate into the engine. In order to satisfy the upstream and downstream straight pipe requirements of the meter, a PVC extension was built into the system and extends the intake line by ten feet on either side of the flow meter. Both meters emit a voltage

signal proportional to the flow rate and are read using the ECS.

The other major piece of measurement instrumentation procured for the Engine Testing Lab was an MKS Systems® FTIR device. Using Fourier Transform Infrared Spectroscopy (FTIR), the instrument can quantify and classify over 30 gas species simultaneously in an emissions stream accurate to the parts per billion (ppb) level. FTIR technology cannot measure diatomic molecules like oxygen, so a separate General Electric oxygen analyzer was purchased as well. These two instruments were combined in a sample delivery system designed and built in the test cell to create a gas analysis suite that will be used, although not for the present work, to perform emissions studies.

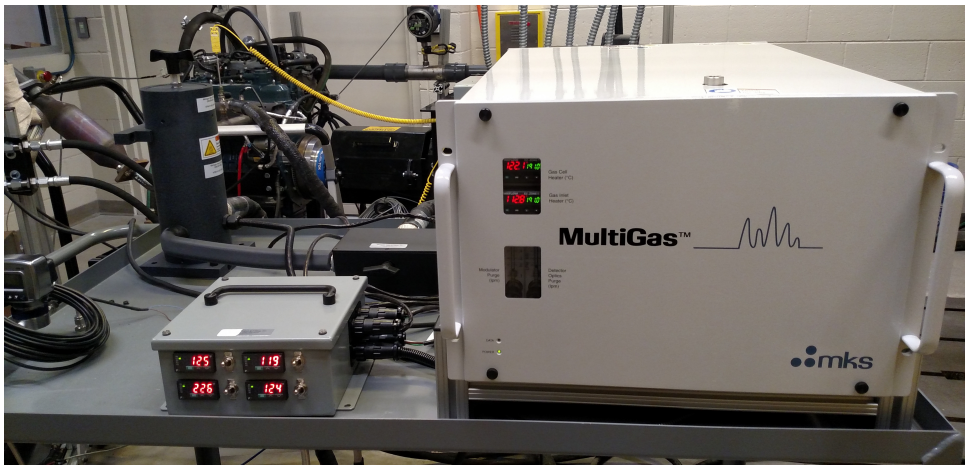

Figure 2.14: The MKS FTIR Gas Analyzer

2.2.8 Test Facility Procedures

Much care and thought went into both the planning and construction of the Engine Testing Facility to ensure that the proper equipment and procedures were in place to mitigate damages from both catastrophic and minor events that can take place in engine test cells, as well as to operate the equipment in the most efficient way possible. The final paragraphs of this chapter will outline general test cell operation procedure, in the context of the equipment installed for this thesis project, and the emergency procedures that were created as part of test cell construction.

Normal Operating Procedures

General dynamometer operation in the test cell is fairly simple. Before starting the Kubota engine, an operator must physically power on the PNET system at the control box and the temperature controller on the cooling tower. If no additional sensing equipment needs to be connected, the ECU is then manually connected to the battery terminals. The operator then starts the exhaust fan remotely from the command desk and gives the start command. When the exhaust fan is powered on, a signal is sent to the isolation valve at the exhaust outlet which causes it to open.

Once PNET receives the start command it motors the engine, rather than using the engine's starter, until combustion takes over. Once the dynamometer senses torque being produced from the engine, it ceases motoring and goes to the "home" position which is at engine low idle speed and zero resistance torque. While the engine is running, PNET gives off an "operating" signal that is used to trigger the room ventilation system and notifies campus security that the test cell is operational. Under certain circumstances the operator may need to enter the test cell while the engine is running. If that is the case, the operator must find someone else familiar with dynamometer operation to man the command desk and stop the engine if need be.

When the operator is finished running the engine, the home command should be given before the engine "soft stop" command is sent. A soft stop cuts off fuel and power to the engine and lets it coast to a stop, just like turning a car engine off normally. The exhaust fan should then be closed after allowing a few seconds for any remaining engine exhaust to clear the isolation valve. Turning the exhaust fan off triggers the valve to close as well.

Once the engine operating status indicates that the engine has been turned off, the room ventilation runs for a few additional minutes in a purge cycle. The purge cycle will be explained in the next section. Once testing has completed, the battery should be disconnected and the cooling tower and PNET control box turned off.

Emergency Procedures

Emergency procedures refer to the routines that are programmed automatically execute in response to an event such as a fire or operator ESTOP triggering. Instructions given to operators in the event of emergencies in the test facility were not part of this thesis work and will not be discussed here. When designing the emergency procedures, events were placed into two

categories, “ESTOP required” and “ESTOP not required.” Given that an actual ESTOP has the potential to catastrophically damage the engine, the procedures are in place to ensure that all intermediate steps are attempted before an ESTOP is initiated. The only events that warrant an immediate ESTOP are an explosion or mechanical failure that causes debris to be flung about the cell. Also if a fire or breakdown occurs while an operator is present in the cell an ESTOP should be triggered.

Upon initiation of an ESTOP, in addition to the engine being forced to a stop, the natural gas and exhaust valves close automatically and a purge cycle is initiated. During a purge cycle the room ventilation is increased to provide additional cooling air as well as force any exhaust or harmful gas out of the enclosed space. It should be stated here that in the event that the cell registers that a fire has broken out, the purge cycle is overridden to prevent extra oxygen from making any flame worse. Once an ESTOP has been triggered, a reset must be performed at the master ESTOP switch on the PNET control box and using the virtual ETSOP at the dynamometer command desk.

ESTOP not required events are further categorized into “action” and “warning” categories. A warning event, such as a gas leak or high temperature alarm will trigger audio and visual indicators inside the test cell that will prompt the operator to immediately soft stop the engine.

For convenience the cell is programmed to initiate a purge cycle whenever the engine is shut down, except in the case of a fire alarm as previously stated. There are only two action events that will automatically trigger a soft stop in the test cell. A fire, both in the test cell or elsewhere in the building, will shut the engine down and close the natural gas solenoid valve, and the powering on of the generator that the test cell shares exhaust ventilation with. Any emergency event registered by either the fire, high temperature, or hazardous gas alarms triggers an alarm with campus security who will contact the proper emergency response service.

2.3 Summary

Through collaborations between the Mechanical Engineering, Campus Safety and Facilities departments at Marquette University, contractors, and industry partners, the Engine Testing Facility was designed and constructed over the course of 13 months from January of 2015 to February of 2016. A PowerTest dual-ended, AC dynamometer and a donated Kubota WG1605 tri-fuel engine were installed as well as numerous sensing and control hardware. Steps were taken

to ensure that equipment and infrastructure fully support unplanned, but anticipated future experiments. Upon completion, the cell can accommodate a variety of engine operations such as steady-state mapping, controller verifications, and emissions studies. Safety equipment and operating protocols were implemented to ensure safe, reliable and efficient operation. The finished test cell is capable of supporting a variety of combustion experiments employing up to 100 horsepower engines.

CHAPTER 3

METHODS

3.1 Problem Definition

The objective of this thesis study is to develop an autonomous control algorithm that functions in a more fuel efficient manner than contemporary cruise control. It is hypothesized that this can be accomplished by allowing moderate variations in speed in order to negotiate changes in environmental conditions more efficiently. Only the forward longitudinal motion of an isolated automobile is considered. This approach is taken under the assumption that for highway driving, lateral motions, primarily lane changes, are made with no significant variation to speed or effort and therefore have no bearing on overall fuel consumption. The brief but frequent accelerations and decelerations required to drive in traffic have been shown to have a substantial influence on fuel economy, however this phenomenon is heavily tied to driver behavior and traffic density and not applicable here. Any application of this strategy to an individual vehicle could readily be extended to groups of vehicles driving in formation during highway situations, which can reduce both individual and bulk fuel consumption considerably [22].

In order for an autonomous controller to be viable, it must perform all sensing, calculating, and actuating tasks at a high enough frequency to prevent instability and to respond to changing road conditions. It must also be insensitive to small variations in speed and load that result from cycle-to-cycle variation inside engine cylinders. Although operation optimized around fuel efficiency is desired, the control must not perform in an unsafe manner or put passengers in uncomfortable situations. Therefore the optimal control strategy must be constrained to reasonable highway speeds and to keep accelerations to a minimum.

As stated in chapter two, the programming that governs the control of the Kubota engine's actuators is proprietary and was not made available for this work. Given this fact and limitations of the testing equipment, some simplifications to the scope of this work were made. The scenario to be applied to the engine controller will be analogous to a passenger vehicle traveling at highway speeds over hilly terrain. The transmission is assumed to be manual and gear shifting is neglected. This allows for a justifiable transition from a vehicle reference frame to that of an independent engine. Also since no traffic will be present, braking will be excluded from the control logic. Since focus is on the engine and engine braking via down-shifting is prohibited,

the lowest engine output would be while the vehicle is coasting regardless so the engine/dynamometer configuration that is in place for this study is appropriate.

3.2 Models

Before the engine model is derived, it will be useful to outline a simplified vehicle model so analogies may be drawn. A simplified model of the longitudinal motion of an automobile is assumed to be taken in state space form as:

$$\dot{x} = f(x, u) \tag{3.1}$$

where the vector x is made up of the state variables, namely position x_1 and velocity x_2. The variable u represents the input to the system, which in this case is the tractive effort produced by the engine and available at the wheels. The state equation for velocity is governed by a force balance on the vehicle by:

$$M\frac{dx_2}{dt} = u - F_R \tag{3.2}$$

where M is the equivalent mass of the vehicle. Equivalent mass is required for dynamic analysis because the forces required to propel a vehicle forward are influenced by curb weight, inertias of the drive-train and wheel assemblies, and the transmission ratio. This is a convenient way to simplify vehicle models when such details are not important [35]. F_R is the sum of motion resistance forces applied to the vehicle [31]. The major components of motion resistance are aerodynamic, rolling, and gravitational resistances which are represented by:

$$F_R = \frac{1}{2}C_{Da}A_V x_2^2 + \mu Mg\cos\theta(x_1) + Mg\sin\theta(x_1) \tag{3.3}$$

where C_D, ρ_a, A_V, μ and $\theta(x_1)$ are the drag coefficient, the air density, frontal area of the vehicle, rolling resistance coefficient, and the road slope angle as a function of location x_1 respectively. Equations 3.1 through 3.3 can be re-written in state space form as [31]:

$$f(x, u) = \begin{bmatrix} x_2 \\ \frac{u}{M} - \frac{1}{2M}C_D\rho_a A_V x_2^2 - \mu g\cos\theta(x_1) - g\sin\theta(x_1) \end{bmatrix} \tag{3.4}$$

3.2.1 Engine Model

This simplified vehicular model can be translated to the reference frame of an engine by making the following correlations: the states position x_1 and velocity x_2 are analogous to the

engine rotational position (revolutions) and rotational speed (RPM)., respectively. Tractive effort u is analogous to the net torque output at the flywheel T_N. An AC dynamometer like the one used in this study is capable of replicating any pattern of torques and torque rates that may occur in a reasonable driving environment as well as transients from the transmission. Therefore, it is assumed that all motion resistances F_R, as well as all inertial forces due to rotating hypothetical wheels, axles, transmission, and other components downstream of the flywheel can be lumped into a resistive torque term T_R which will be simulated by the dynamometer at the flywheel.

The effective mass of the vehicle M can then be replaced by the rotational inertia of the reciprocating components of the test engine I. Due to the experimental configuration, the inertia term must also include the inertias of the dynamometer, drive-line, and torsional coupling between the drive-line and flywheel. It is also assumed that the net torque is the difference between new input engine indicated torque u, and parasitic effects taking place inside the engine (T_P). Equation 2 is re-stated in the engines reference frame as:

$$I\dot{x_2} = u - T_P(x_2) - T_L(x_1) \tag{3.5}$$

The engine indicated torque u refers to the amount of instantaneous torque produced by combustion processes inside the cylinders [28]. T_P represents the total resistive torque of the engine which is made up of three components, friction torque, pumping torque, and accessory torque. Friction torque is the torque required to overcome the friction that develops from moving parts inside the engine. Pumping torque is the torque required to intake, compress, and exhaust a volume of air during the four strokes of the combustion cycle. Accessory torque is required to drive components such as the alternator, coolant and oil pumps which are powered by the rotation of the crankshaft. Friction torque is a good approximation for the total power loss inside an engine.

Mean effective pressure (MEP) is defined as the work produced per engine cycle divided by the volume of air displaced. It is most useful when comparing different engines as it normalizes a performance metric by the engines size, thus allowing for a meaningful comparison of two dissimilar engines. According to Heywood, the total frictional mean effective pressure MEP_{tf}, or the component of MEP effected by losses in an engine, can be effectively modeled as a polynomial function of crankshaft rotational speed only. Since the relationship between MEP_{tf} and resistive torque is linear [28], it is assumed that a calibrated function can be used to directly model total friction torque T_P as a function of engine speed. A dynamometer experiment was

conducted which resulted in a model of the form:

$$T_P(t) = a_0 + a_1 x_2(t) + a_2 x_2(t)^2 + a_3 x_2(t)^3 \tag{3.6}$$

The process used to derive coefficients for the friction torque model will be explained in chapter four. For this study, the resistance to motion applied by the environment T_L will be expressed as an arbitrary function of accumulated engine revolutions x_1. This is analogous to instantaneous road angle being a function of how far the vehicle has traveled along that road. The new system in the engines frame can be expressed in state space form as:

$$f(x,u) = \begin{bmatrix} x_2 \\ u - a_0 + a_1 x_2 + a_2 x_2^2 + a_3 x_2^3 - T_L(x_1) \end{bmatrix} \tag{3.7}$$

3.2.2 Fuel Consumption

From [28], specific fuel consumption of an engine is defined as the mass flow rate of fuel $\dot{m}_f$ into the engine divided by the power P produced. It can also be expressed in terms of fuel conversion efficiency η_f as:

$$\eta_f = \frac{P}{\dot{m}_f q} \tag{3.8}$$

where q is the higher heating value (HHV) of gasoline in kJ/kg. While there are several different heating values associated with hydrocarbon fuels, their magnitudes do not normally differ by more than a few percent [16] so HHV was chosen for this case. Fuel conversion efficiency is defined as the amount of work produced by the combustion of the air fuel mixture during an engine cycle divided by the amount of fuel energy injected into the cylinder for the given cycle [28]. By substituting the product of engine speed and net torque for power in equation 3.9, and then solving for the mass flow rate of fuel, a relation for fuel consumption in terms of model states and inputs is given by:

$$\dot{m}_f = \frac{x_2 T_n}{q \eta_f(u, x_2)} \tag{3.9}$$

An accurate model for fuel conversion efficiency can be quite complicated since it has been shown to depend on engine geometry, engine state, and in-cylinder conditions [16]. However, according to Heywood, fuel conversion efficiency can be adequately modeled using engine speed and load when specific cycle-to-cycle behavior of engines is not needed. Since equation 3.10 for fuel consumed is linear, it is assumed that a calibrated model can be built for fuel consumption using engine speed x_2 and input u as well. In fact, it is common practice in the

automotive industry to generate steady state brake specific fuel consumption (BSFC) maps for use in ECU programming and performance analysis. A polynomial model for fuel consumption as a function of engine speed x_2 and torque u will be built using a fuel consumption map generated experimentally. It is assumed the model will take the form shown in equation 3.11. See chapter four for further explanation of calibrations.

$$\dot{m}_f = b_0 + b_1 x_2 + b_2 u \tag{3.10}$$

3.3 Optimal Control

3.3.1 Theory

To control the engine efficiently at a prescribed cruising speed, a model predictive optimal control algorithm will be applied to the model described above. The control problem can be classified as a non-linear, receding horizon control problem with state and input constraints [37]. Optimal state and input trajectories for optimal fuel consumption over a prescribed time horizon, from t_0 to T, can found by minimizing the performance index:

$$\min_{x,u} J = B(x_T, T) + \int_{t_0}^{T} L(x(t), u(t))dt \tag{3.11}$$

with initial conditions being the measured engine states x_{t_0} at time t_0. Function B represents some penalty function on the state of the system at final time T, and L represents the objective function of the problem. The solution to equation 3.12 will be bound by the following constraints:

1. The maximum allowable input to the system $u_{max.}$ is the peak indicated torque achieved by the engine at wide open throttle (WOT) which has been measured experimentally on the dynamometer.
2. Since coasting but not braking will be allowed in the control strategy, the lower bound on the control input $u_{min.}$ will be equal to the friction torque T_R at idle speed.
3. Engine speed $x_{2,min.}$ and $x_{2,max.}$ will be bound by the operating envelope of the Kubota engine.

To aid in computational speed, these constraints will be applied numerically in the solving of the boundary value problem described below.

3.3.2 Performance Index

The objective function to be minimized takes the form:

$$L = \frac{R}{2}\left[\frac{\dot{m}_f(x_2,u)}{x_2}\right]^2 + \frac{S}{2}\left[u - T_r(x_2)\right]^2 + \frac{Q}{2}\left[x_2 - V^*\right]^2 \tag{3.12}$$

The first term is the calibrated fuel mass flow rate model divided by engine speed which is also the inverse of fuel mileage. When minimized, this term ensures that the maximum number of revolutions per unit mass of fuel is achieved. This is necessary because if gross fuel consumption were the parameter being optimized, the engine would instantly decelerate to the lowest speed possible. Introducing a mileage term ensures that the most fuel efficient trajectory is chosen. The second term is designed to minimize inputs that are not expressly required to overcome changing road conditions. By keeping accelerations to a minimum, this will ensure rider comfort and avoid fuel inefficiencies from rapid accelerations.

The third term penalizes deviation from the prescribed cruising speed. It is in place to ensure that the optimal trajectory does not deviate substantially from the speed setpoint. The final state penalty function B is in place to keep the searching space of the solution optimizer small and, while it has no bearing on the overall optimal trajectory keeps the computations fast and stable. It penalizes the final engine speed at time T from deviating from the cruising speed V^*

$$B = \frac{P}{2}\left[x_{2,T} - V^*\right]^2 \tag{3.13}$$

Constants R, S, Q, and P are weights which will be manipulated to prioritize efficiency or cruise speed. The weights will be tuned to keep the magnitudes of the three terms similar to each other for computational efficiency. This cost function approach allows for the functionality of the proposed controller to change from fuel efficient operation to normal cruise control simply by changing the weight on each term. This feature was taken advantage of when collecting data for benchmarking purposes.

3.3.3 Boundary Value Problem

The solution to the minimization problem is achieved by forming the Hamiltonian function from equation 3.13 as:

$$H(x,u,\lambda,\psi) = L(x,u) + \lambda^T f(x,u) + \psi^T C(x,u) \tag{3.14}$$

where λ is the n-by-one vector of Lagrange multipliers attached to the n state space model equations, also known as co-states, and ψ is the vector of lagrange multipliers attached to the constraint equations [37]. Since the system constraints are not applied until later, C is equal to zero so the constraint term is omitted. Inserting equations 3.13 and 3.8 into 3.15, the final form of the Hamiltonian is given as:

$$H(x,u,\lambda) = \frac{R}{2}\left[\frac{\dot{m}_f(x_2,u)}{x_2}\right]^2 + \frac{S}{2}\left[u - T_r(x_2)\right]^2 + \frac{Q}{2}\left[x_2 - V^*\right]^2 + \lambda_1 x_2 + \frac{\lambda_2}{I}\left[u - T_R(x_2) - T_L(x_1)\right] \tag{3.15}$$

The conditions for minimization can be derived through calculus of variations as the following system of differential equations [37]:

$$\frac{dH}{d\lambda_1} = \dot{x}_1 = x_2 \tag{3.16}$$

$$\frac{dH}{d\lambda_2} = \dot{x}_2 = \frac{1}{I}\left[u - T_R - T_L\right] \tag{3.17}$$

$$\frac{dH}{dx_1} = -\dot{\lambda}_1 = \frac{\lambda_2}{I}\frac{dT_L}{dx_1} \tag{3.18}$$

$$\frac{dH}{dx_2} = -\dot{\lambda}_2 = -R(\frac{d\dot{m}_f}{dx_2})\frac{\dot{m}_f}{x_2} + S\frac{dT_R}{dx_2}(u - T_R) - Q(x_2 - V^*) - \lambda_1 + \frac{\lambda_2}{I}\frac{dT_R}{x_2} \tag{3.19}$$

$$\frac{dH}{du} = 0 = R(\frac{d\dot{m}_f}{du})\frac{\dot{m}_f}{x_2} + S\left[u - T_R\right] + \frac{\lambda_2}{I} \tag{3.20}$$

Equation 3.21 is the "stationary condition" for minimization and can be rearranged to obtain an equation for input u as a function of states x_1 and x_2 and co-states λ_1 and λ_2. By differentiating equations 3.7 and 3.11 and substituting into 3.21, the relation for optimal input trajectory is:

$$u_{opt} = \frac{-Rb_2(b_0 + b_1 x_{2,opt}) + ST_R(x_{2,opt}) - \frac{\lambda_{2,opt}}{I}}{Rb_2^2 + S} \tag{3.21}$$

Equations 3.17 through 3.20 constitute a two-point boundary value problem (TPBVP) in states x_1 and x_2 and co-states λ_1 and λ_2. Known boundary conditions are initial states x_{1,t_0} and x_{2,t_0} and final co-states given by the relation $\lambda_T = \nabla_x S(T, x_T)$ [37]. From equation 3.14 it can be determined that the boundary condition for $\lambda_{1,T}$ is unspecified and the remaining boundary condition is:

$$\lambda_{2,T} = P\left[x_{2,T} - V^*\right] \tag{3.22}$$

The TPBVP can be solved numerically using any of a number of numerical methods. The approach employed in this study is a shooting method that uses known and guessed initial conditions to solve the system of four, first order differential equations from t_0 to T. The final

value of $\lambda_{2,T}$ is compared to the value defined by equation 3.23 to determine the performance of initial guesses. The shooting method will run until the value of $\lambda_{2,T} - P(x_{2,T} - V^*)$ is minimized according to some user specified convergence criterion.

3.4 Control Strategy

The solution to the TPBVP constitutes the optimal state and co-state vectors over the horizon t_0 to T for a given weighted objective function. From this solution equation 3.22 can be used to derive the optimal input trajectory. To control the subject engine in real time, the TPBVP will be solved repeatedly at some time interval with boundary conditions being continuously updated based on the measured state of the engine. The size of the horizon will remain constant, yet the road conditions that are factored into the solution will be changing as the horizon moves forward in time.

Once a solution has been generated, an instantaneous optimal set-point will be drawn from the solution and passed to the engine/dynamometer system. Each set-point is derived based on the most recent solution that is updated in real time. Figures 3.1 is a block diagram of the control strategy. This allows the engine to respond quickly to changing road elevation. It should be noted that the optimal solution is independent of the rate of optimal trajectory generation so the length of horizon T_H can be independent of sampling interval since only a single optimized input is used in real-time. Therefore, horizon characteristics can be chosen based on the desired performance of the control algorithm.

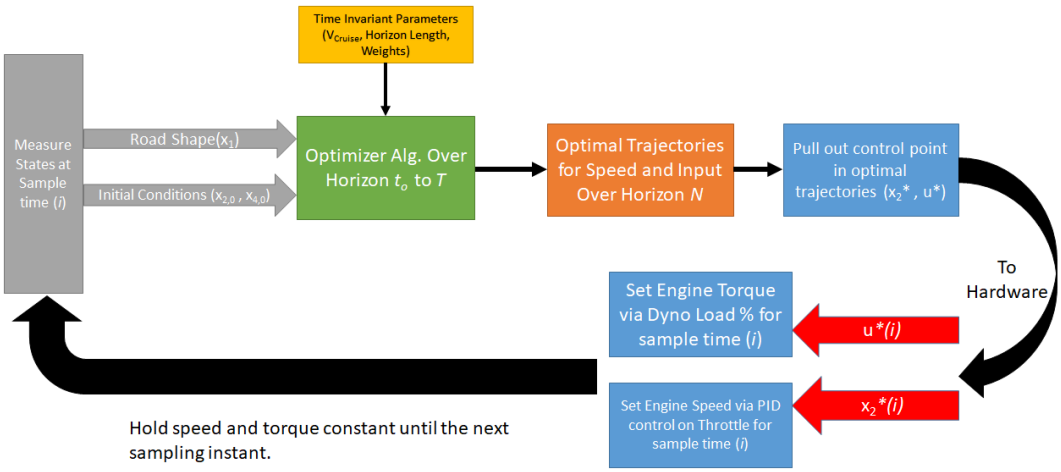

Figure 3.1: Block Diagram of Overall Control Strategy

CHAPTER 4

ENGINE CHARACTERIZATION

Before simulations or experiments could be performed, certain engine parameters needed to be characterized. This chapter will discuss the processes and results of calibrations for resistive torque T_R and fuel mileage $(\frac{\dot{m}_f}{x_2})$.

The rotational inertia of the system needed to be accounted for as well. As discussed in chapter 3, not only is the rotational inertia of the engine needed, but all of the reciprocating components in the drive-train and dynamometer system need to be accounted for as well. A rotational analysis of the engine and dynamometer was performed prior to delivery by PowerTest. The purpose of this analysis was to derive the design requirements for the torsional dampening coupler that was installed. The results of that analysis were used to generate the final value of system inertia used in this study and can be found in table 4.1.

Table 4.1: Results of Torsional Analysis performed at PowerTest Inc.

Component	Value	Units
Dynamometer	0.192	$kg * m^2$
Kubota WG1605	0.102	$kg * m^2$
Torsional Coupling+Drive-line	0.0536	$kg * m^2$
Total Rotational Inertia	0.3476	$kg * m^2$

4.1 Resistive Torque

Total resistive torque is defined in [28] as the sum of all speed dependent resistances to engine motion that happen inside the engine up to the flywheel. The three major components are the friction, pumping, and accessory torques as discussed in chapter three. Since each component is a function of engine speed only, they can be lumped together and calibrated as a bulk torque term. This was accomplished by performing motoring tests where the engine was disconnected from electrical power, so no ignition could take place, and incrementally accelerated from 800 to 3000 RPM by the dynamometer. The intake and exhaust streams were left intact and no spark plugs or injectors were removed, as is sometimes the case in motoring tests. This was to ensure air flow into and out of the engine would be consistent with actual engine operation. The steady state

torque required to reach and maintain each engine speed was measured.

Since a motored engine produces no torque of its own and no other forces are acting in the system, it can be assumed that the steady state torque input from the dynamometer is equal to the total friction torque for a given speed. Figure 4.1 shows the distribution of total resistance torque versus engine speed which was fit to the third order polynomial assumed in equation 3.7. The outliers that fall above the main groupings represent data points that were measured while the engine was coasting from the maximum engine speed back to idle and were thus ignored. Table 4.2 shows the polynomial coefficients determined via regression analysis.

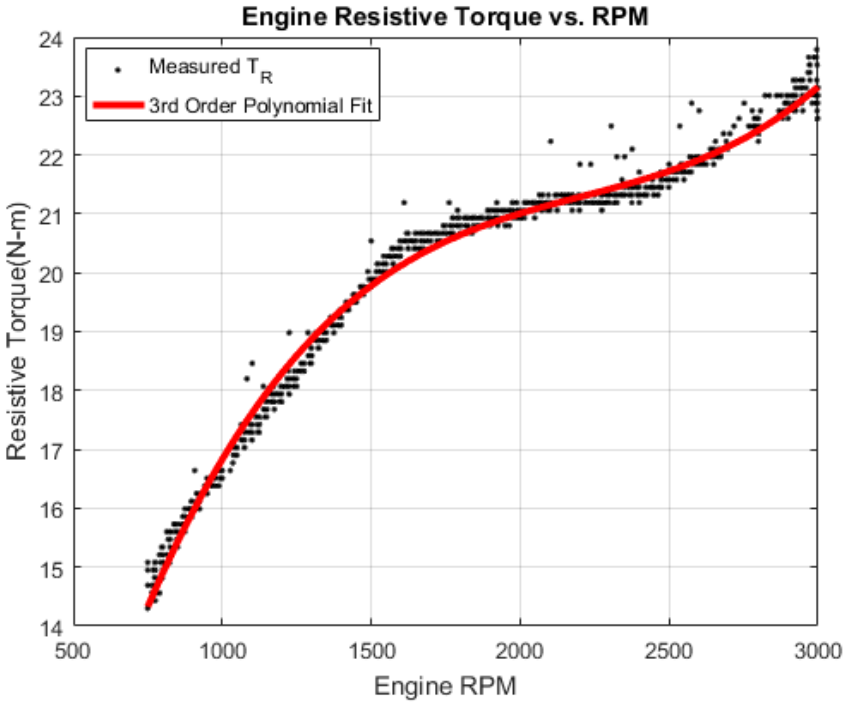

Figure 4.1: Plot of Resistance Torque T_R versus Engine Speed

Table 4.2: Resistance Torque Polynomial Coefficients

Model	$T_R = a_0 + a_1 x_2 + a_2 x_2^2 + a_3 x_2^3$
a_0	0.906
a_1	0.025
a_2	-1.07$x10^-5$
a_3	1.69$x10^-9$

4.2 Fuel Mileage

In order for the optimal control algorithm to function properly, accurate data on the fuel consumption behavior of the Kubota engine had to be obtained. Two methods of tracking fuel volume flow rate into the engine were available. The Fuel Measurement System (FMS) used its twin turbine flow meters to output a very accurate but sensitive flow reading. Also the Kubota engines control unit (ECU) broadcasts a real-time volumetric flow rate reading over the CAN data stream. It was observed that readings from the FMS were subject to intermittent injections of noise that made measurements unreliable. The source of this noise remains unknown at the time of writing. While readings from the ECU were very stable, no information on how the value of fuel consumption was being generated since access to the ECU programming was prohibited. Thus, a calibration experiment was performed to generate a map of steady-state fuel consumption as a function of engine speed x_2 and net torque output T_N. Consumption data from both the FMS and ECU systems were measured and compared. A plot of the raw data collected from both sources can be seen in Figure 4.2.

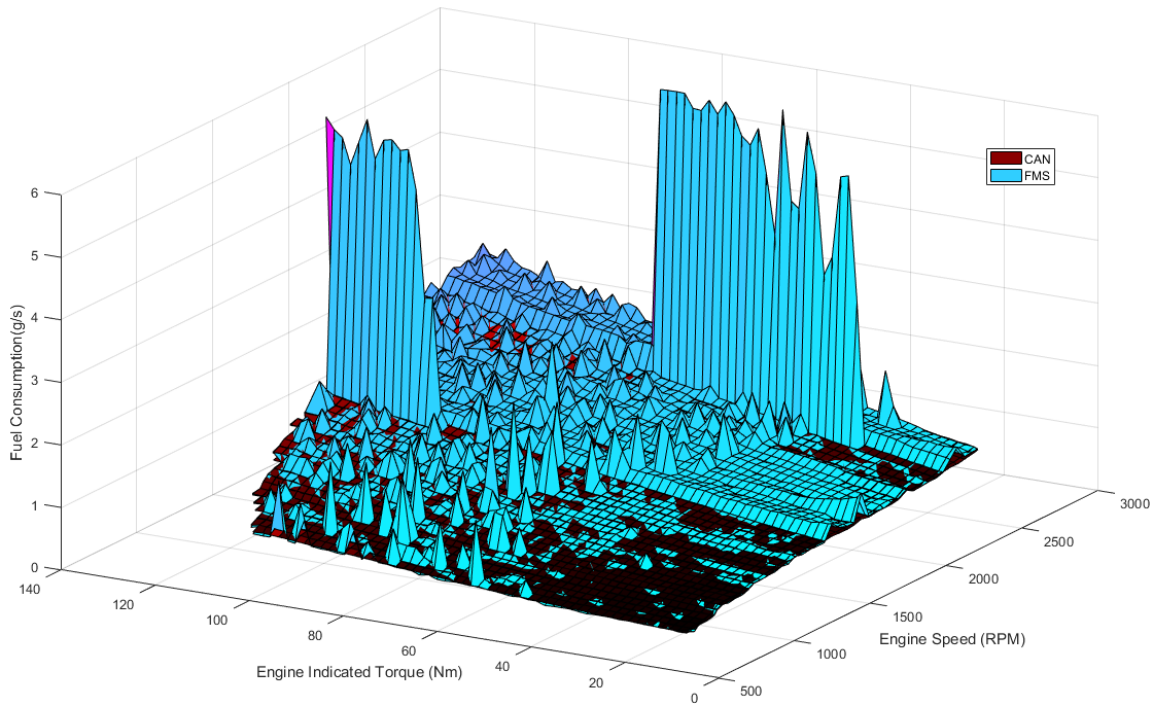

Figure 4.2: Raw Fuel Consumption Map from both ECU and FMS

Data measured by the ECU appears to trend smoothly, as expected. However, there are clear divergences in the FMS data. Before any manipulation of the data was made, the mean percent error between the two methods was 12.9%. The two large peaks in the data were a result of data being taken when the fluid level in the fuel tank dropped too low for the fuel pickup to function properly. This resulted in a much higher flow rate since the fluid being measured was mostly vapor rather than liquid gasoline. The data points making up these two peaks were discarded and replaced by a first order central difference estimation using the surrounding points. Figure 4.3 shows the data after the correction with an average percent error of 7.8%. With the large deviations removed, the surfaces appear indistinguishable in parts with smaller spikes in the FMS data. It was hypothesized that the remaining spikes in the FMS data resulted from engine not given enough time to reach steady state after a change in operating condition.

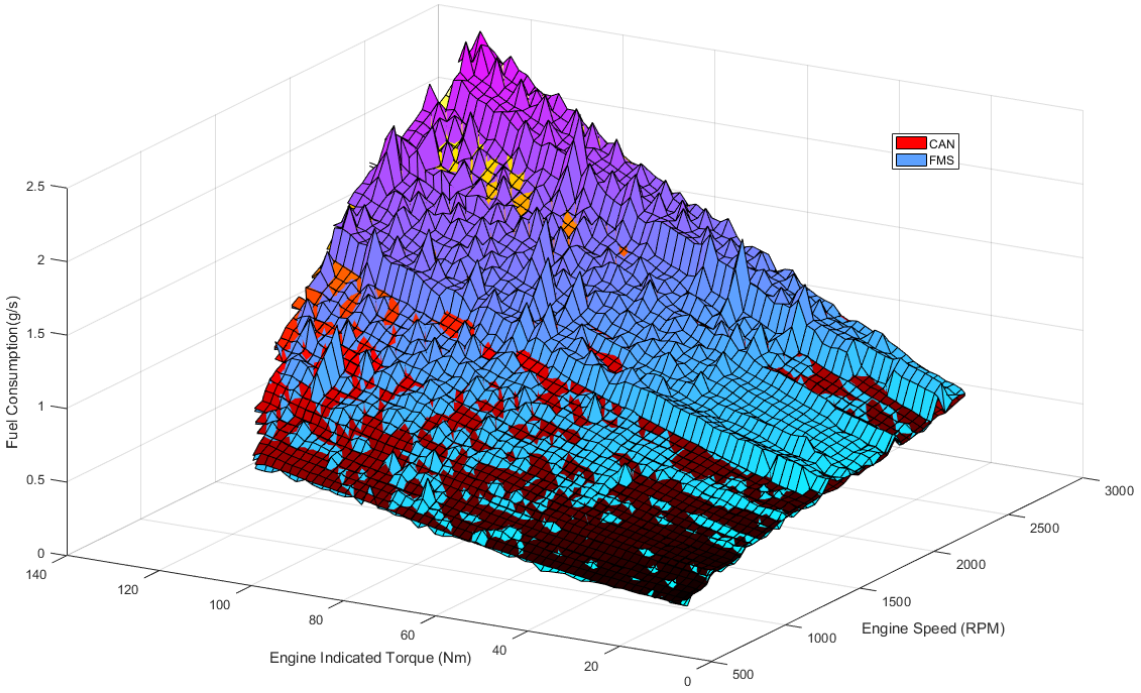

Figure 4.3: Consumption Data from both sources with problematic data removed

This would result in extra fuel, consumed during transition to a different load condition, included in the time averaged steady-state data, thus yielding an erroneous result. The hypothesis was tested by randomly selecting five data points assumed to be in error and re-conducting the experiment at those points with extra time given between changing conditions and data

gathering. Table 4.3 displays the results. The extra allowed time resulted in an average reduction of error in the small data set from 141% to 2.8%. Assuming this hypothesis holds for the other flawed data points, fuel consumption as determined by the ECU was considered accurate enough for use in the model. Figure 4.4 is a contour plot of the engine fuel consumption, measured by the ECU,converted from volumetric flow rate to mass flow rate, as a function of engine speed and load.

Table 4.3: Re-measured Fuel Consumption Data Points

Speed (RPM)	Torque $(N*m)$	FMS Old $(\frac{in.^3}{sec})$	FMS New $(\frac{in.^3}{sec})$	ECS $(\frac{in.^3}{sec})$	Error Old (%)	Error New (%)
850	64.5	0.113	0.03	0.032	253	6
1200	89.6	0.137	0.058	0.057	140	2
1550	80.6	0.186	0.066	0.064	191	3
1850	121.3	0.444	0.118	0.115	286	3
2050	123.7	0.169	0.130	0.129	31	0.8
2100	22.4	0.066	0.03	0.031	113	3
2150	93.0	0.195	0.102	0.10	95	2
2400	128.1	0.181	0.156	0.155	17	0.7
2750	65.7	0.208	0.091	0.087	139	5

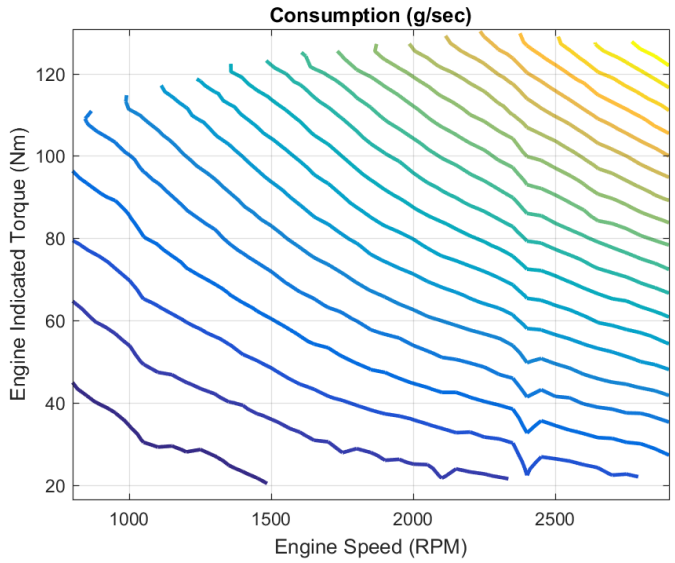

Figure 4.4: Contour Plot of Engine Fuel Consumption as a Function of Engine Speed and Torque. Fuel consumption increases from purple contours to yellow.

An opportunity was taken in this phase of the project to simplify the mathematical model by building an inverse fuel mileage map as a function of speed and engine torque. This was done by dividing the fuel consumption map by steady-state engine speed. This resulted in the map found in figure 4.5 which appears to be approximately planar, so a linear surface was fit using a regression analysis. Figure 4.6 is a contour plot of the inverse fuel mileage map. The model and coefficients can be found in table 4.3.

Table 4.4: Inverse Fuel Mileage Polynomial Model Coefficients

Model	$\frac{\dot{m}_f}{x_2} = b_0 + b_1 x_2 + b_2 u$
b_0	4.45×10^{-3}
b_1	-1.55×10^{-6}
b_2	3.65×10^{-4}

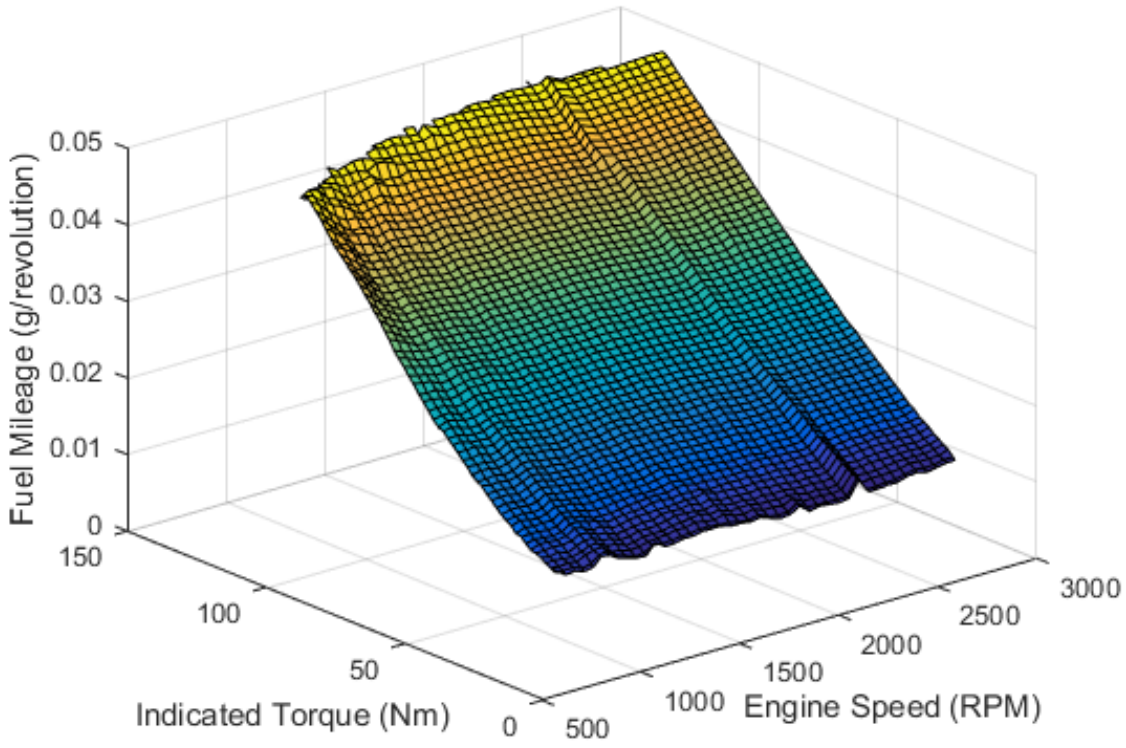

Figure 4.5: Inverse fuel mileage as a function of engine speed and torque

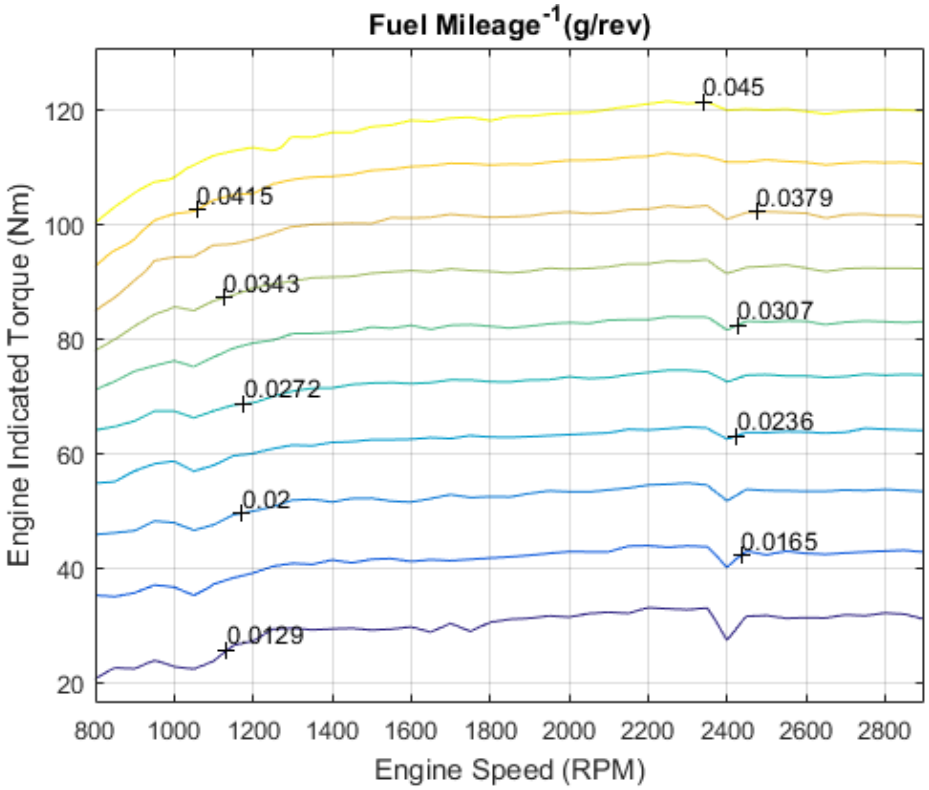

Figure 4.6: Contour Plot of Inverse Fuel Mileage as a function of Engine Speed and Torque

CHAPTER 5

SIMULATION AND EXPERIMENTAL SETUP

5.1 Overview

Prior to testing the optimal control algorithm described in chapter three, various experiments on the mathematical model were performed using MATLAB® and LabVIEW programming environments. This was done in order to gain a deeper understanding of the relationships between model parameters and any limitations of the control strategy. It was soon discovered that the algorithm had issues solving the minimization problem for certain weighting values and simulation parameters which caused a poorly conditioned problem or numerical instability. Systematic approaches to defining the reliable operating envelope of the algorithm and weighting sets were taken. Results of these investigations will be provided in this chapter.

Once a sufficient understanding of the mathematical behavior was gained, transition of the controller from MATLAB to the LabVIEW environment began. Additional small adjustments to the controller were made to work better in the new environment. Once satisfactory simulation performance was observed, the system was again transitioned from simulation to the control hardware for engine testing. More adjustments to the controls and hardware were made after initially observing poor performance.

This chapter will detail the model studies done in MATLAB and their results, simulations performed in both MATLAB and LabVIEW environments, and the adjustments necessary to take the optimal controller from theory to physical implementation on the engine control system. Also, a description of the design of hardware experiments will be given as well as metrics that were used to analyze the results.

The general control strategy is the same on both MATLAB and LabVIEW platforms. Once a trial is initiated, optimal horizon trajectories are generated based on time-invariant parameters and measured engine conditions. After generation, the optimal control set-point in engine speed and torque is derived and passed to the engine and dynamometer controllers corresponding to the sampling interval chosen. The process repeats itself until a total distance traveled threshold is met.

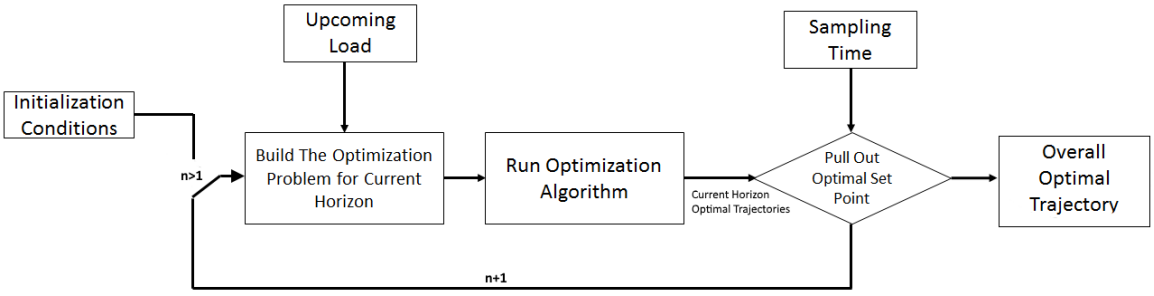

Figure 5.1: Block Diagram of Simulated Control Algorithm

In simulation space, the first set of initial conditions is set by the operator prior to initiation. In MATLAB, the solution to the current receding horizon optimal control problem is generated using the *"fmincon"* function which is a part of the MATLAB optimization toolbox. This specific function minimizes a programmed objective function subject to nonlinear equality and inequality constraints using a trust-region algorithm [13]. Subsequent initial conditions are taken from the previous optimal trajectory at the sampling time t_s since there is no physical system to take measured states from. The optimal set-points from each trajectory compiled and stored in overall speed and torque vectors which are then used to calculate the fuel consumed at that point using equation 3.11. Total fuel consumption over an entire test is calculated by integrating the instantaneous fuel flow rate measurements. The programming that governs simulations in the LabVIEW environment are analogous to the MATLAB programs except for the default mathematical method employed for solving nonlinear constrained optimization problems differ. It will be demonstrated that the simulation results between the two programs agree well with each other.

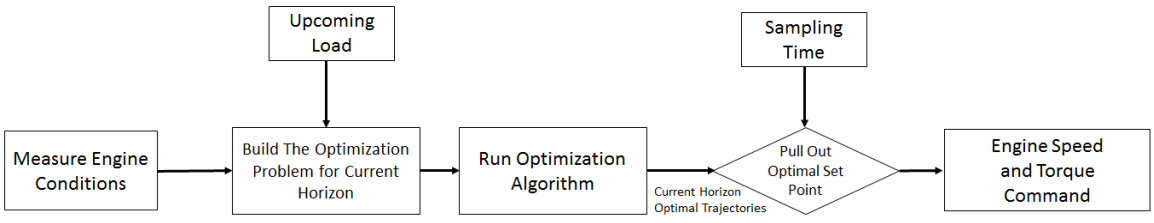

Figure 5.2: Block Diagram of Experimental Control Strategy

Once deployed on the actual test hardware, the control strategy becomes somewhat different. The initial conditions for the first solution are measured immediately upon trial initiation. After the first horizon is found, optimal set-points are derived and passed to the engine and dynamometer controllers. Subsequent initial conditions are re-measured for each horizon generation and are dependent on the engine's response to the previous command. Since this study is operating in an engine reference frame, load must be simulated by the dynamometer since there is no road to change shape and cause varying load conditions on the engine. Therefore the optimal speed set-point is set via PID throttle control on the engine, and output torque is controlled through PID control on dynamometer current using net torque as the process variable. See figure 5.2 for a depiction of the control strategy. The general practice of determining instantaneous control input from a predicted optimal trajectory is employed regularly in optimal control applications [37] however the specific application of this control strategy to an engine and dynamometer was not found in the review of literature relevant for this work.

5.2 Preliminary Studies

Before tests of the optimal controller were performed on actual driving scenarios, single horizon generation tests were conducted to check viability and to observe convergence behavior. This proved to be critical since one full test of the controller over a road profile required over a minute to complete in simulation and several minutes to perform on the actual engine.

5.2.1 Parameter Limits

Through the initial tests, it was determined that success of solution generation was sensitive in varying degrees to weight values, desired cruising speed parameter, the shape and intensity of the outside torque profile, and simulation settings such as horizon length, sampling interval, and numerical solver type and minimum time step. Given the large number of apparent variables and an incomplete understanding of their relationships, a multi-step experiment to determine the limits on, and relationships among, these variables was performed. The results of which were used as constraints on simulation and hardware tests moving forward.

Initially only the limits on variables that yielded successful convergence with no consideration given to solution performance were desired. To find these limits efficiently, a single horizon test under a constant environmental torque was run for individual parameter sets. Successful sets were classified by whether or not a reasonable solution could be found. Reasonable

solutions are ones where all points of the optimal velocity trajectory remained within the range of zero to 8000 RPM. The values of the upper bound is well outside the speed range of the engine but the solution for a single horizon does not need to remain inside the range since only a single point is pulled from each horizon and passed to the engine. A check on rotational speed is necessary because under certain circumstances, a solver would successfully converge, but return an obviously infeasible solution so single pass/fail criterion would be insufficient in this case.

Sets of variables to be tested were generated via latin-hypercube sampling which is a common approach to generate random parameter sets from a multi-dimensional distribution [30]. Variables included were model weights R, Q, S, and P, horizon length T, sampling rate t_s, and the initial guess of co-state λ_{2,t_0}. 10,000 randomly distributed sets were generated and a single horizon was solved for each. If the algorithm reached a solution which fell inside the reasonable velocity bounds, it was classified as passing. Table 5.1 lists all of the variables and the ranges on each. Ranges on each variable were determined through observations during initial testing of the algorithm. It should be noted that the sampling rate was restricted to increments of 0.25 seconds and the horizon was restricted to 0.5 second increments to reflect limitations on the physical control hardware. Figure 5.3 shows histograms of the passing values of each variable.

Table 5.1: Variables and Ranges of Possible Values for each used in Preliminary Dependency Analysis

Variable	Range	Units
R	$\{R \in \mathbb{R} \mid 0 < R \leq 1.00 \times 10^{10}\}$	-
Q	$\{Q \in \mathbb{R} \mid 0 < Q \leq 1000\}$	-
S	$\{S \in \mathbb{R} \mid 0 < S \leq 1000\}$	-
P	$\{P \in \mathbb{R} \mid 0 < P \leq 1000\}$	-
T	$\{T \in \mathbb{R} \mid 3 \leq T \leq 10\}$	s
t_s	$\{t_s \in \mathbb{R} \mid 0.25 \leq t_s \leq 3\}$	s
λ_{2,t_0}	$\{\lambda_{2,t_0} \in \mathbb{R} \mid -1000 \leq t_s \leq 0\}$	-

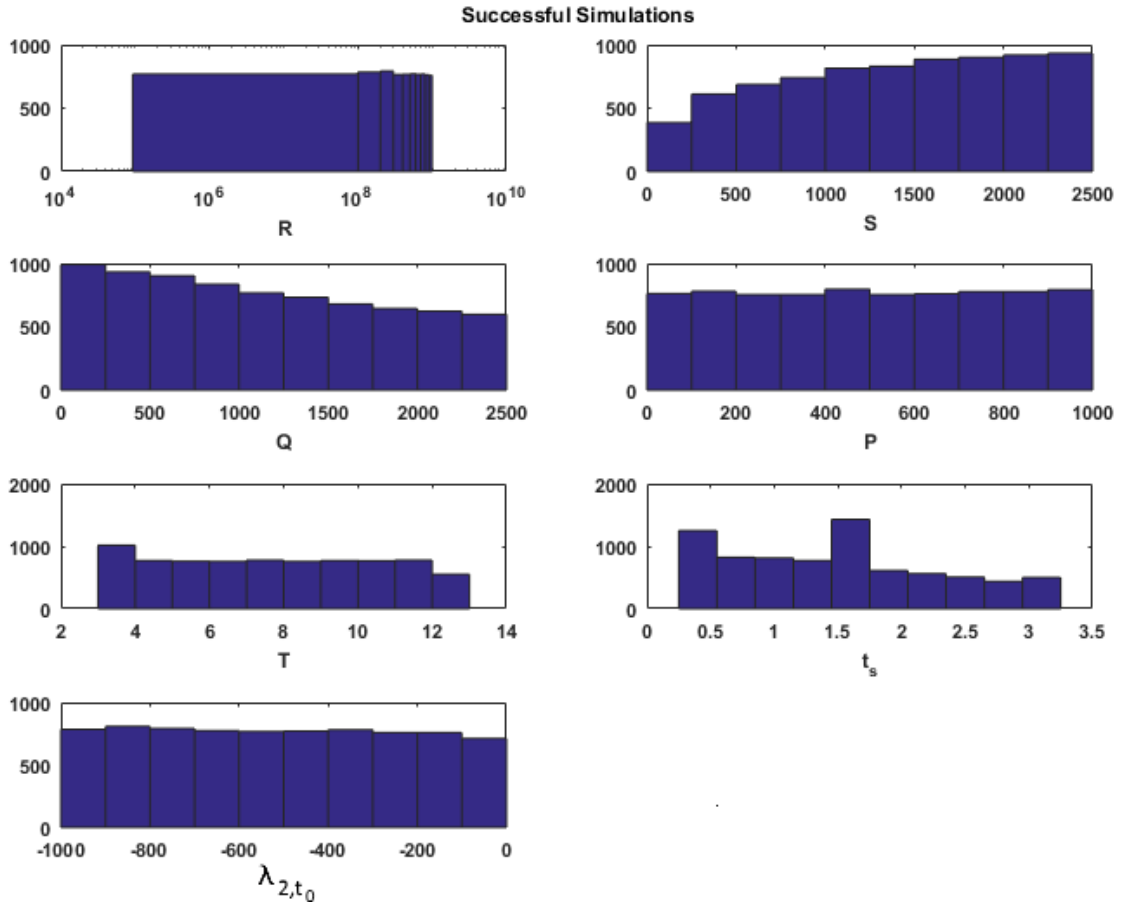

Figure 5.3: Histograms of Successful Variables in the Latin Hypercube Study

Results shown in Figure 5.3 were used to define limits on simulation parameters as well as some general rules to follow when choosing model weights. It is clear from the histograms success of the algorithm is not very sensitive to P, initial guess λ_{2,t_0} or horizon length T. Hardware performance indicated that horizon length should be kept in the three to six second range for reliable simulations. There also does not seem to be a dependence on sampling interval t_s, so the general rule will be the faster trajectories can be generated the better. There appears to be some relationship between success and weights S and Q relative to each other, however when plotted against each other in figure 5.4, there is no clear region where the solution fails so no additional rules can be made in this regard. The only definite guideline taken from this experiment is that the value of weight R should not fall below 10^4.

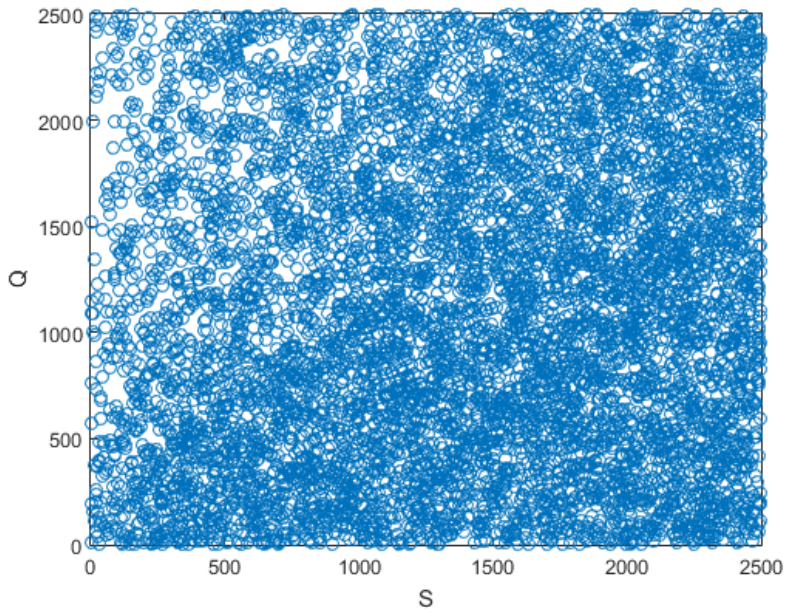

Figure 5.4: Successful trials plotted against Weight Values S and Q

5.2.2 Weight Selection

Once better understanding of algorithm limitations and weight behavior was gained, a genetic algorithm was employed in MATLAB to systematically select weight values for the two situations of interest which will be described below. Genetic algorithms are useful computational technique that uses the principle of genetics and evolution to find a global minimum of some multi-dimensional function when the relationships between variables are not well defined [53].

For both tests, a population of 50 candidate sets, or "chromosomes", were generated by random pairings of each variables and evaluated. More description on the case specific constraints and evaluations will be explained in the subsequent paragraphs. Five "elite" chromosomes, the five lowest scoring sets of weights were automatically passed to the next "generation" or pool of candidates. The remaining 45 candidate sets are chosen by parenting, mutation, or random selection.

Parenting is the process by taking characteristics from one set, in this case one or more weight values, and combining it with another set to create a candidate. This is what allows the algorithm to converge to the proper minimum through "natural selection." A "mutation" is when a chromosome randomly jumps, in one or more dimensions, to a different part of the domain. If

the mutation performs poorly, it is discarded. However if the mutation performs well during evaluation, it is retained in the chromosome pool and used as a parent. This mechanism serves to reduce the chance that the algorithm becomes stuck in a local minimum. Normally, the rate of mutation is reduced by some function of the number of generations that have passed, otherwise the algorithm could run indefinitely.

Any remaining candidate sets needed to fill the population of 50 chromosomes are randomly generated according to the constraints imposed upon the problem. This process is repeated until the best chromosome score falls below a specified threshold, or the change in population mean score falls below some relative tolerance. Common parameters were a four second horizon length, a sample interval of 1 second, and all initial co-state guesses were set to negative one. No absolute threshold was set and the relative tolerance in mean values was set to 1×10^{-4} for both cases.

Cruise Control

The first weight set generated was chosen to simulate a contemporary cruise control system. The genetic algorithm for cruise control used an evaluation function that scored the amount of deviation from the prescribed speed and the total computation time needed to complete the profile. Total deviation was determined by summing the root mean squared error between each point in the optimal velocity vector and the desired speed. It was weighted ten times greater than computational time. The optimal cruise control weighting set is the candidate that minimized this value. Limits on weights were kept identical to the ones imposed on the latin-hypercube test except for R which were set to generate values in between 1.00×10^4 and 1.00×10^8. Figure 5.5 shows plots of best candidate score and mean value of candidate scores for each generation. This plot is updated at completion of each generation and is useful for tracking convergence behavior.

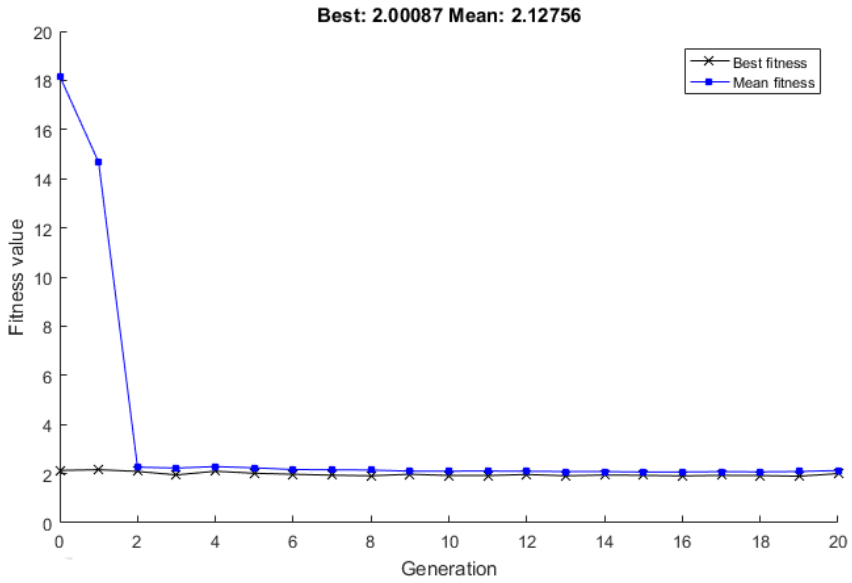

Figure 5.5: Convergence Behavior for the Cruise Control Genetic Algorithm Study. The best and mean score of the final generation is displayed above the graph.

Maximum Fuel Efficiency

For the optimal fuel efficiency weighting, the candidate optimal velocity and input vectors were input into the first term in equation 3.13. Again, this term represents the inverse of fuel mileage which is appropriate in this minimization problem. Minimization conditions were kept the same as the minimum fuel consumption case in all respects. Figure 5.6 shows the results of the genetic algorithm for this study. The final weights chosen for both cases will be discussed later in the chapter.

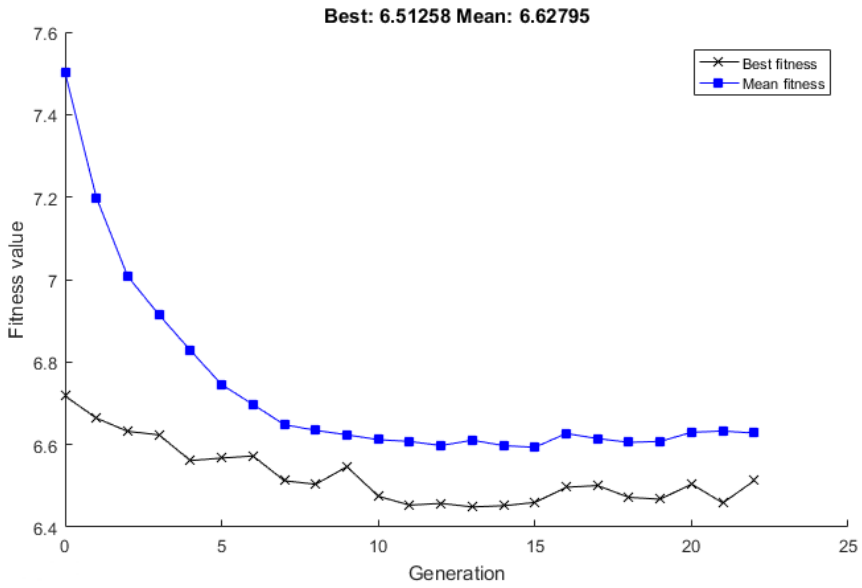

Figure 5.6: Convergence Behavior for the Fuel Efficient Genetic Algorithm Study. The best and mean score of the final generation is displayed above the graph.

5.3 Road Design

Different driving scenarios for the control algorithm to negotiate are imposed via load profiles, the $T_L(x_1)$ term in the mathematical model, referred to as "roads." At different points in this thesis work, certain roads were used to test certain functionalities and controller performance in both the simulation and hardware spaces. A brief description of the roads used and the stages at which they were employed will now be given.

5.3.1 Flat

For initial algorithm testing and weight verifications, constant values of T_L were used to verify that the numerical solutions remained in a viable domain. Flat roads were quickly discarded for trigonometric profiles once controller configurations had proved to be functional over the entire range of engine operation.

5.3.2 Trigonometric

Before the engine was put through complicated road profiles, simple road shapes were employed to check general algorithm behavior and for preliminary hardware testing. These profiles were advantageous to work with because they were easily generated and could be simply

shifted and scaled to observe trends in behavior. These function are also easily differentiable so they mesh well with the control strategy.

Positive and negative versine and vercosine load profiles were generated using MATLAB functions. The trigonometric functions were bound between positive and negative one so that constants representing the intensity of the desired road shape and the magnitude of the baseline could be applied during simulation and control to simplify changing shapes. The period of these shapes was set so that one profile was completed in approximately 5000 revolutions of the engine. This was arbitrarily chosen to be slow enough to fully observe the engines behavior but not too long to waste unnecessary time and fuel. These shapes were then approximated by sixth order sum of sine waves models using a MATLAB curve fitting tool. The approximations were used in the model to avoid needing look-up tables in the programming. Eventually, the look-up table approach was necessary to verify the programming before more complicated road profiles were inserted. At minimum, a positive shift in road intensity was always required to keep the optimal torque solution from dropping below zero, which violated the mathematical constraints. The four trigonometric road profiles used for preliminary studies can be found in figure 5.7.

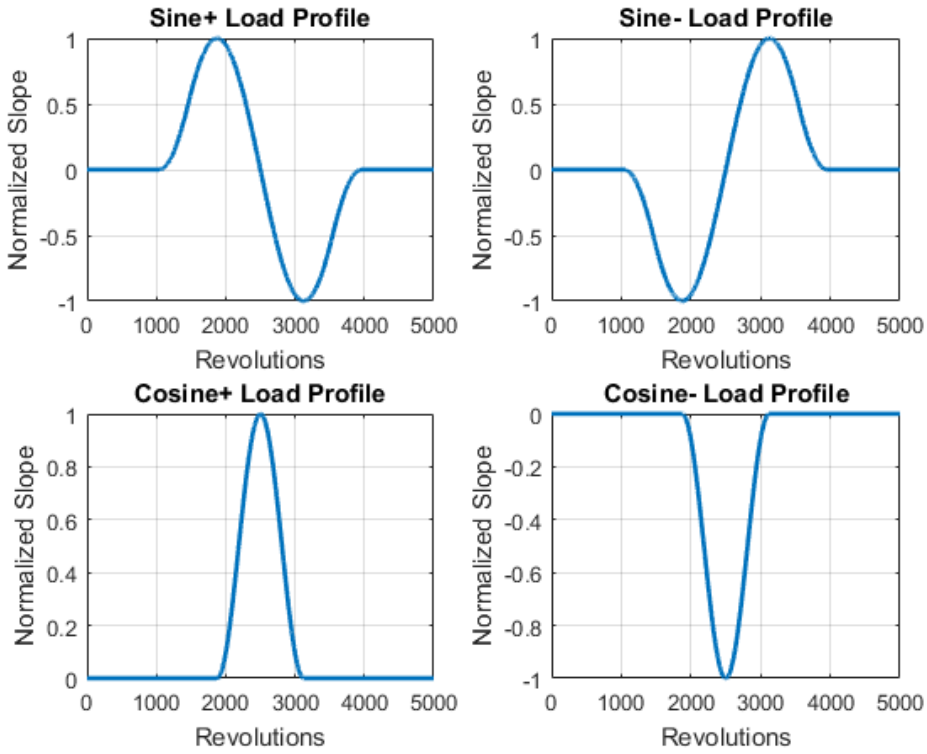

Figure 5.7: Normalized Trigonometric Load Profiles as a function of Accumulated Revolutions used in Simulation and Experiments with designation above

5.3.3 Complex Spline

A more rigorous road profile was desired for an in-depth performance test of the control algorithm. This was generated in MATLAB using a random number generator and a smoothing spline function. The spline function was constrained between the bounds of negative and positive one so that the same shifting and multiplication functions that were used for the trigonometric roads could be applied here. The T_L and $\frac{dT_L}{dx_1}$ values were passed to the model and control system via look-up tables and finite difference approximations. Figure 5.8 is an example of a complex spline road shape before any shifting or intensifying.

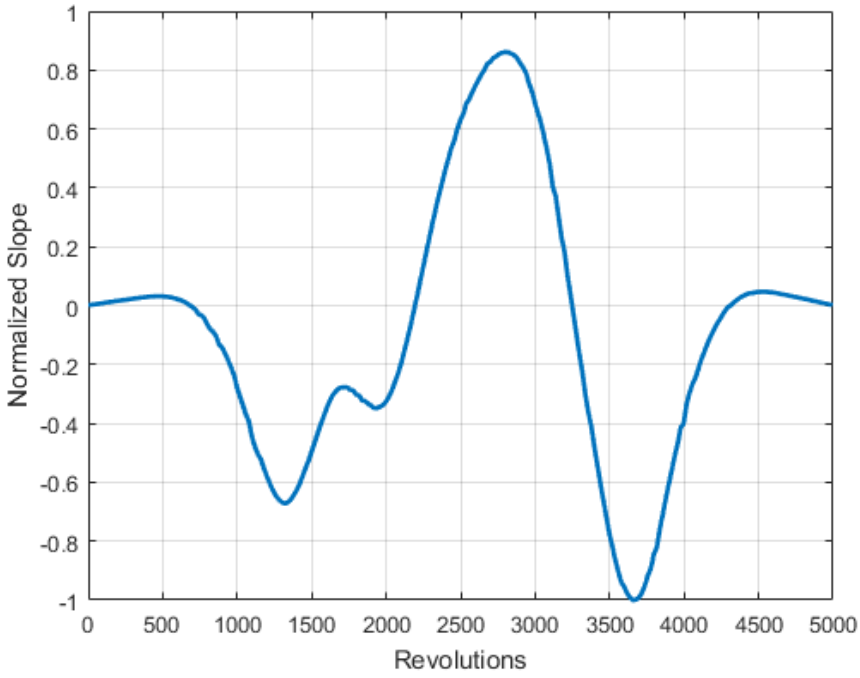

Figure 5.8: Example Normalized Spline Load Profile as a function of Accumulated Revolutions used in Simulation and Experiments

5.4 Simulations

Once candidate weights were chosen, they were put through a battery of tests in MATLAB on full trigonometric and splined road cases described above. The manipulated variables for these validations were engine cruising speed and baseline torque shift. This was done to ensure that the weights were valid for the entire operational speed and torque envelope of the physical engine system. Some small adjustments were made to the weights to achieve total validity and the final resultant weight candidates can be found in table 5.2.

Table 5.2: Weight values for both Control Strategies

Weight Set	R	Q	S	P
Cruise Control (CC)	1.00×10^4	1.5	2.5	10
Fuel Efficient (EFF)	2.50×10^8	0.01	1×10^{-5}	10

Next, a LabVIEW virtual interface (VI) was constructed to simulate an experimental trial. This was beneficial for a few reasons. The simulation VI offered an opportunity to ensure the LabVIEW programming functioned as intended before deployment to the engine test stand. The simulations also allowed for rapid validation of both the mathematical model and the candidate weights for many different road profiles and road load intensities using the unproven programming. These simulations were compared with analogous simulations done in MATLAB for verification. Results of this comparison will be presented in chapter 6. Once validated, the programming was modified to run on the real time hardware and transitioned to the physical test setup.

5.5 Experimental Configuration

To integrate the software programming with the hardware-in-the-loop equipment, some fundamental adjustments to the code needed to be made. This section will detail the control hardware setup and control procedures as well as the adjustments made to the optimal control algorithm in order to transition from simulation to actual engine experiments.

5.5.1 Control Hardware

The engine and dynamometer control strategy used for this experiment was designed according to the capabilities and limitations of the test cell equipment, and to best accommodate the specific experiments intended for this study. In order to take advantage of the fast computing power of the National Instruments Engine Control System (ECS), the VIs in charge of formulating and solving the optimization problem were re-written to be compatible with the real-time architecture (RT) of the ECS. Input parameters and monitoring were handled on an operator's computer running the "host" side of the real-time LabVIEW architecture, henceforth referred to as RTHOST. The programming details of the ECS and RTHOST relationship fall outside the scope of this work, refer to [7] for an in-depth guide to the National Instruments real-time control architecture. It will be sufficient to say that the optimal trajectory computations were performed on the high speed ECS system which was passed inputs and parameters from the RTHOST. Also, safety precautions and shutdown capabilities existed on the RTHOST that could terminate experiments and shut down engine systems if needed. The actual control and measurement of the engine and dynamometer states took place outside the real-time architecture so bridges had to be formed to allow for real-time optimal control of the entire system. Engine output speed and

torque were measured using the PowerTest network (PNET) and input speed and torque set-points had to be sent to the engine and dynamometer there as well. So a small VI named PCOM was written to pass these parameters from RTHOST to PNET via Ethernet. CAN data (see chapter three) were also read from the engine directly into the ECS system. Since engine speed could be monitored at a higher rate using the CAN communication protocol, these measurements were used in the optimal control programming. Figure 5.9 is a diagram that depicts the relationships between the hardware systems.

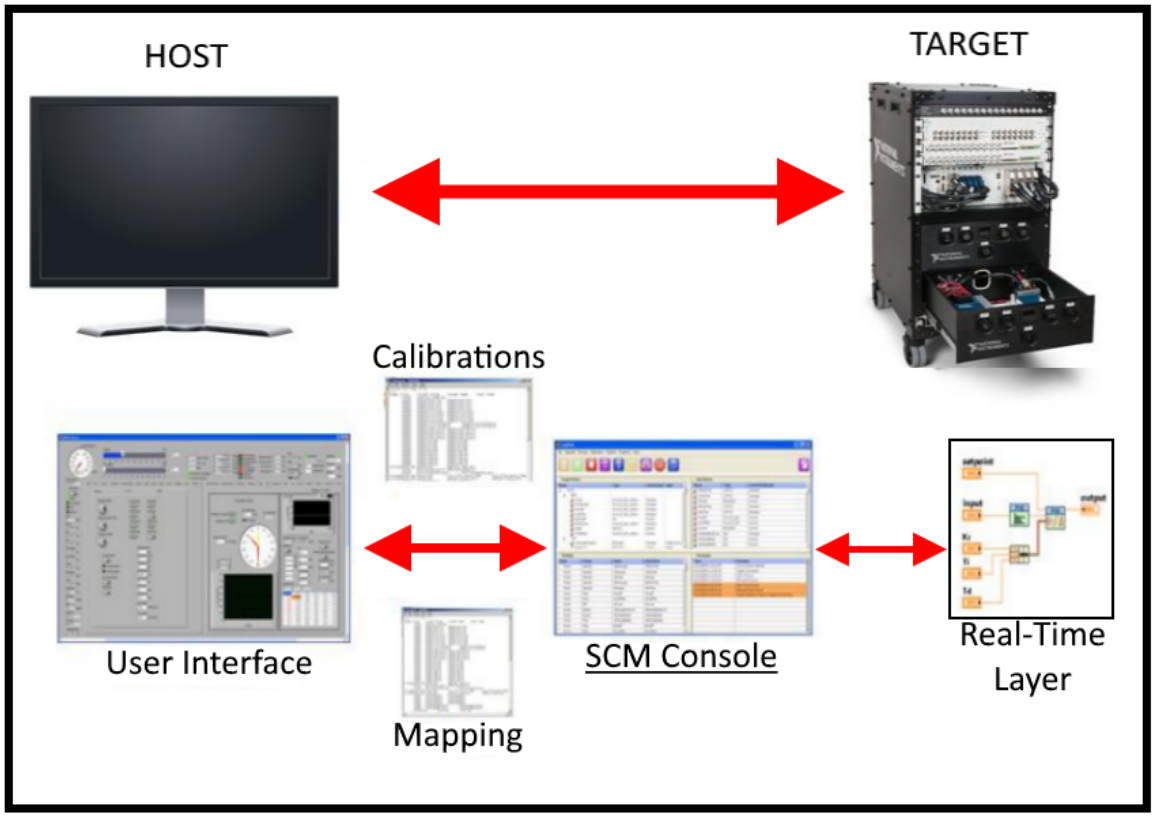

Figure 5.9: Target and Host Relationships in the Control Architecture

5.5.2 Control Software

The basic control strategy and flow during experimental trials is as follows: First, simulation parameters such as weighting, load profile conditions, desired cruise speed, horizon and sampling time conditions are set in the RTHOST. Then, the engine and dynamometer must be set to the desired cruise speed and baseline load value so the proper first initial conditions are

read by the algorithm. It is assumed that a hypothetical vehicle would already be traveling at or near the desired speed and load upon deploying the optimal controller. This assumption is necessary because if the initial conditions are very different from the expected speed and load profile, the optimization algorithm will not be able to find a valid solution.

The test run is then initiated from RTHOST. A single horizon, optimal trajectory is calculated by measuring the instantaneous engine speed and torque in PNET, which are then sent via PCOM to the RTHOST. The initial condition of engine position $x_{1,0}$ is determined in RTHOST by integrating engine speed in real time. Initial engine speed $x_{2,0}$ is read from CAN data, and a transformation of the measured dynamometer torque to an initial condition for co-state $\lambda_{2,0}$ is performed in RTHOST using equation 3.22. These initial conditions are passed to the ECS and the optimal trajectories are calculated. Vectors for x_1, x_2, λ_1 and λ_2 are passed back from ECS to RTHOST where the optimal instantaneous set-points in speed and dynamometer torque are derived and then sent to PNET via the PCOM VI.

Engine speed is used as the set-point for the proportional-integral (PI) controller linked to the engine foot pedal signal, which is the process variable for speed control. Dynamometer torque is set via PI control over the dynamometer motor voltage. The optimal set-points are tracked in a continuously updating vector that is stored in the RTHOST as they are generated. These are compared to real-time engine and dynamometer data that is sampled at a rate of 10Hz. Fuel flow rate into the engine is also measured from CAN data at the same sampling rate and stored as well. Once the experiment has finished, a total value of fuel consumed in grams is generated by integrating the flow rate profile in time. Figures 5.10 and 5.11 show the plots of outside load, engine speed, and engine torque versus time, and fuel consumption vs. time respectively.

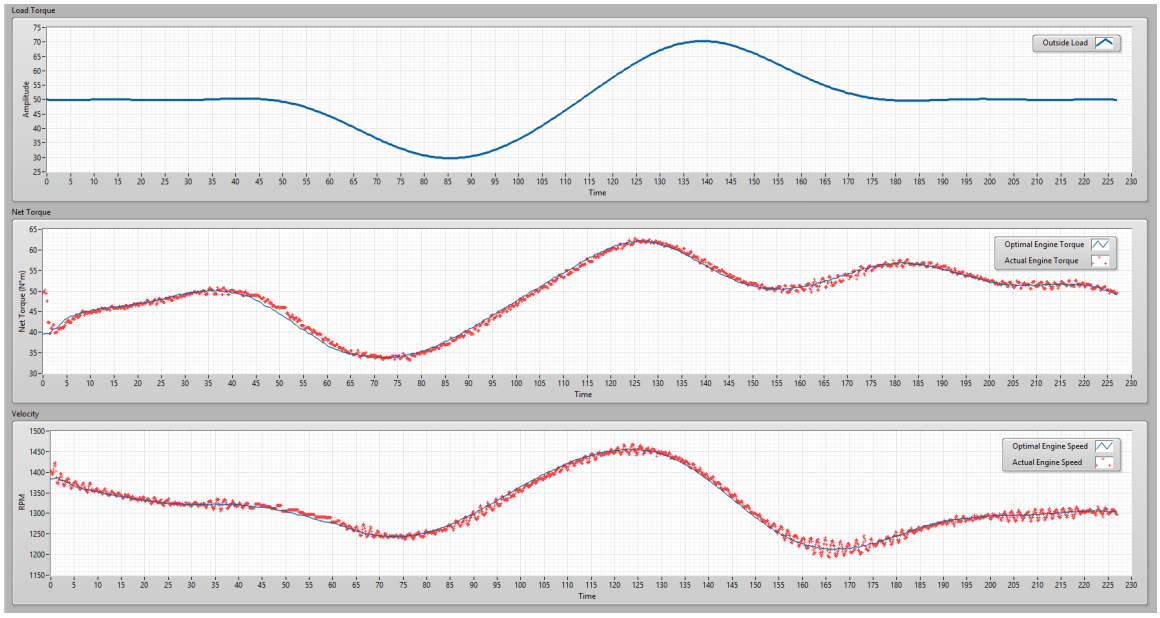

Figure 5.10: Time (seconds) Plots of Outside Load (N*m) (Top), Predicted Optimal vs. Actual Engine Net Torque (Middle), and Predicted Optimal vs. Actual Engine Speed (Bottom) used in the RTHOST VI during a Sine- Experiment

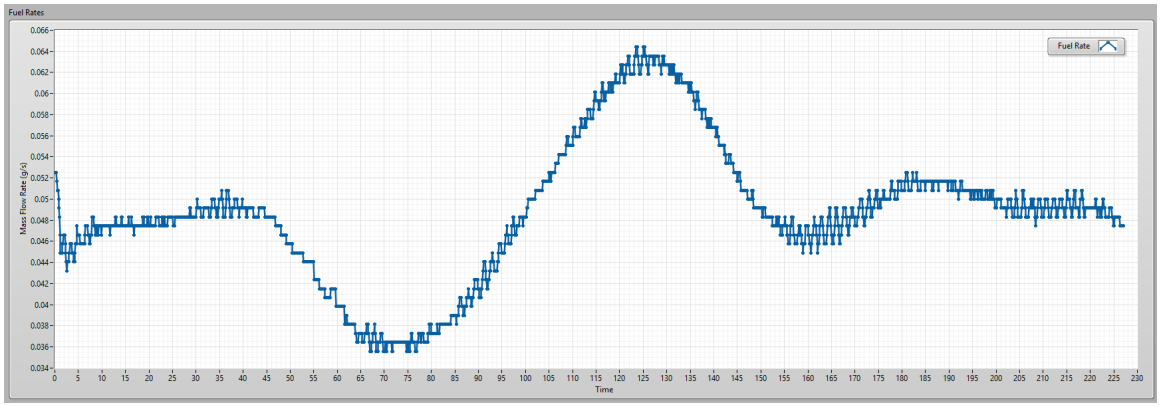

Figure 5.11: Fuel Consumption Measured by the ECU vs. Time Plot used in the RTHOST VI during a Sine- Experiment

RTHOST plus PCOM combined can fully replicate the functionality of the PNET controller software to set any operating points and ramp rates required by an operator for steady state dynamometer functions. Real-time charts of speed and net torque allow for adequate system monitoring and shutdown if necessary. The only function not provided for in RTHOST is the

emergency stop (ESTOP) capability. However the physical ESTOP button is near enough to the RTHOST machine to not make a software addition necessary. Figure 5.12 is a screen shot of the RTHOST main controller user interface.

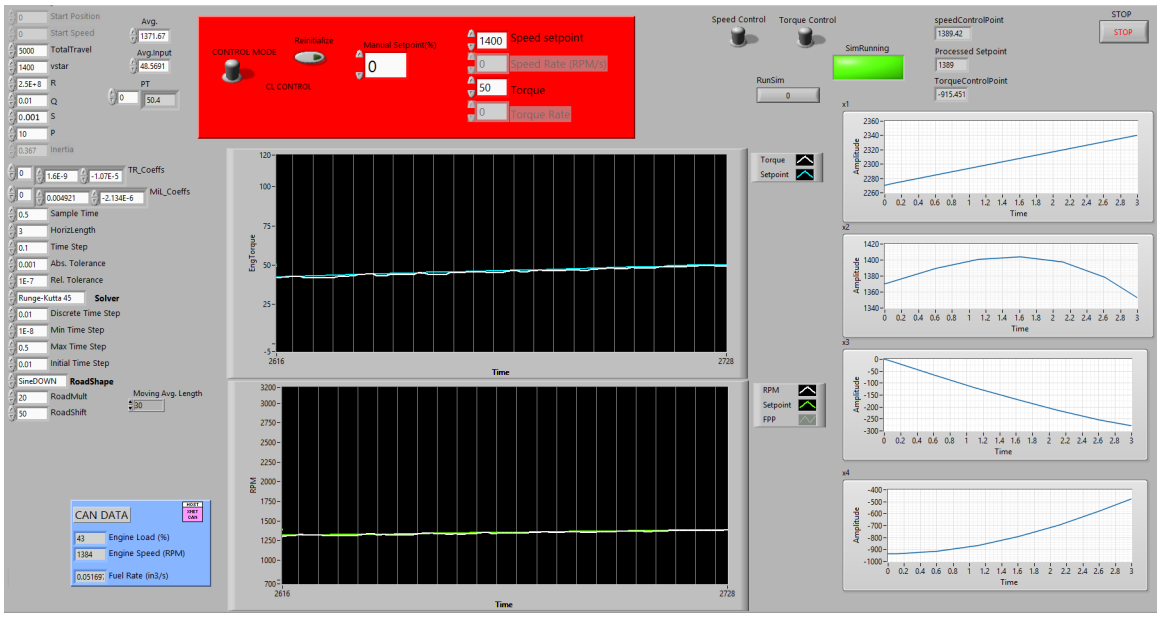

Figure 5.12: Screenshot of the RTHOST Main User Interface during an Experiment

An added benefit of the LabVIEW control environment was the possibility of quickly adding functionality to the base control programming as it became needed. Initial tests of the autonomous control system on hardware indicated that initially the cycle-to-cycle variations in engine RPM and torque were too intense for the PI controllers and set-point generation rate to keep up with and stability was quickly lost at the beginning of a trial. To remedy this, two steps were taken. First the gains on the speed and load PI controllers in PNET were tuned using factory settings as a baseline to achieve a more desirable closed-loop response. This had a profound effect on system stability for moderate changes in speed and torque. However the variability in sampled engine speed continued to cause system instability due to initial conditions being outside of the expected range. For example; during steady speed operation (cruise control), a positive fluctuation in measured engine speed caused the optimal control solution to increase dynamometer torque in order to bring speed down. The controller would overshoot the cruising speed slightly which caused the next sampled engine speed to be below the desired cruise speed so the engine would cut torque and throttle up to compensate. The process would oscillate out of

control until the test was manually stopped. This behavior was fixed by taking a three second moving average of the engine past speeds and torques to dampen the noise introduced by cycle-to-cycle variations in engine output. With the equipment operating to satisfaction, experimental test cases were designed and run. Chapter six will detail the results and conclusions that could be drawn from them.

5.6 Test Cases and Performance Evaluation

To evaluate the optimal control algorithm on the Kubota engine, it was deployed on the five outside load profiles discussed above. For each profile, the weights in table 5.2 will be compared. Two set points for both baseline speed and environmental load will be used to test the algorithm's performance of the engine's entire operating range. Low and high baseline speeds will be set at 1400 and 2000 RPM respectively. Low and high environmental load ranges will be from 10 to 30 Nm and 30 to 70 Nm respectively. All 40 trials will be compared against simulation data to ensure validity. For each run, optimal vs. actual engine speed and torque will be compared as well as fuel flow rate vs. time. Total fuel consumed and time required to complete the profile will be calculated. A successful implementation of the optimal control algorithm will be characterized as follows:

1. The algorithm should be able to navigate all load profiles without failing to generate a single horizon or allowing the engine to run outside its typical operating range, which would hypothetically cause unsafe conditions on an actual road.
2. The algorithm will run fast and stably so that real-time operation is stable and reasonably comfortable to hypothetical passengers. This means that no undue acceleration will be experienced.
3. The algorithm will demonstrate that fuel savings can be achieved under any conditions without overly sacrificing engine speed and overall trip time.

The results of both simulation and experiments as well as an analysis of results will be presented in the following chapter.

CHAPTER 6

RESULTS AND CONCLUSIONS

This chapter presents and compares the results of initial MATLAB and LabVIEW simulations, and hardware experiments. A brief explanation behind the motivation and process for each experiment will be provided. Results of all trials will be compiled and presented without analysis in Appendix A. Once all the results have been presented and justified, conclusions and potential for future work will be discussed.

Only the positive sine (Sine+) profile, low speed, and high load scenario will be presented for analysis. It should be noted that all results are given in terms of state x_1 rather than the time domain. This is because testing scenarios take varying amounts of time to complete due to different baseline speeds and accelerations resulting from the optimization process. All profiles were generated using a final distance of 5000 revolutions. Since the magnitude of load to overcome is also dependent on other factors and varies during experiments, road elevation has been normalized for clarity.

As stated in previous chapters, the prescribed loading profile T_L is the outside load the engine must surpass. While the shape and magnitude of this profile is technically arbitrary, the profiles used in this study were chosen to simulate smooth changes in elevation that can be expected along a highway. When analyzing the following results, it will be helpful to contextualize the data using a theoretical road profile. By assuming that T_L represents the slope of this "road" with respect to accumulated revolutions x_1, the integral with respect to x_1 will give the road's elevation as a function of distance traveled. Figure 6.1 is an example using the positive sine profile.

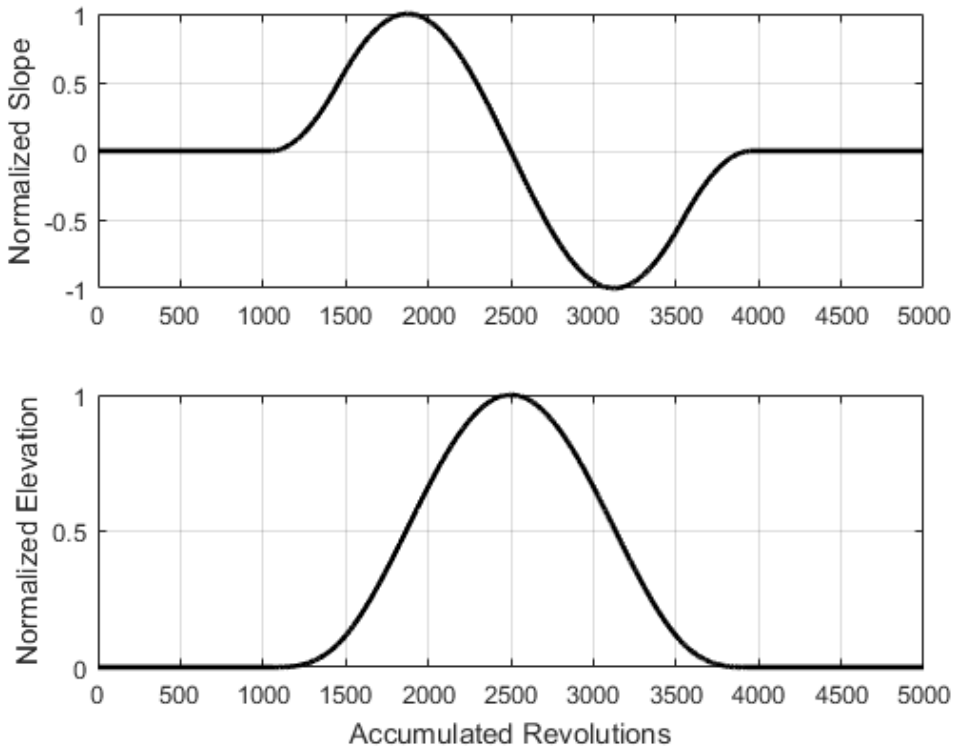

Figure 6.1: Example Road Elevation and slope profiles

6.1 Simulation Results

Initial tests between MATLAB programming and LabVIEW simulations indicated that the optimal control algorithm yielded identical results on both software platforms as expected. Slight differences in solution robustness and required computational time were observed. It is hypothesized that this is a result of differences in the optimization strategies employed on the different platforms. With the LabVIEW algorithm validated, all simulation test cases were run. Figure 6.2 shows example simulated optimal trajectories for the positive sine slope case.

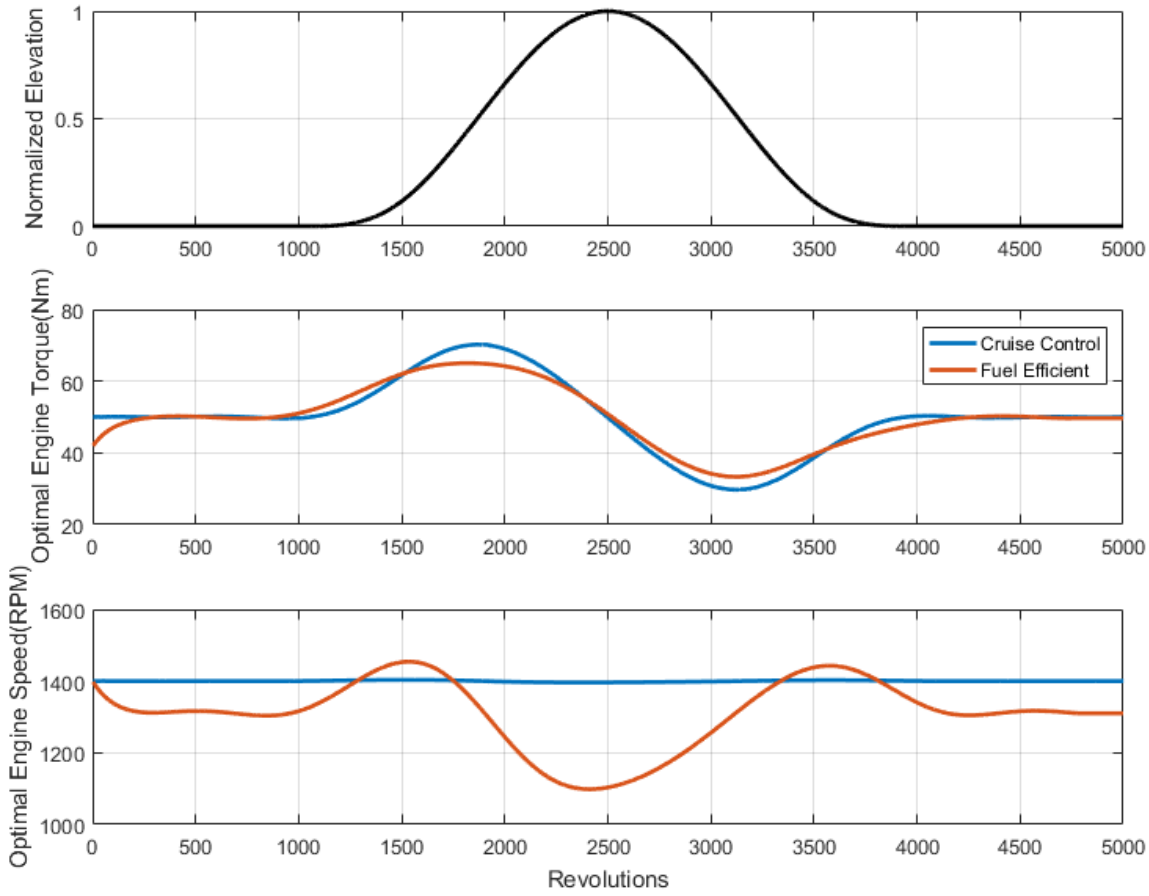

Figure 6.2: Simulated Optimal Trajectories using both weight sets for the Sine+ trial

An explanation for the observed optimal behavior will accompany the experimental results below since qualitatively, behavior is consistent across both simulation and experimental platforms. Figure 6.3 shows total fuel consumed over each load profile for cruise control and fuel efficient behaviors. Figure 6.4 shows the averages of total fuel consumed over the five load profiles for each speed and load setting. Bars are labeled with their corresponding total fuel consumption and each group is labeled with the percent savings experienced for each case between the cruising and fuel efficient settings. Since LabVIEW simulations are mainly intended for validation, only total fuel consumed was calculated and reported. It can be seen that simulations predict some form of fuel savings for all cases, however the spline simulations seem to perform significantly worse. It is hypothesized that this can be contributed to the control horizon strategy not being able to account for the rapidly changing road conditions at the simulated generation rate.

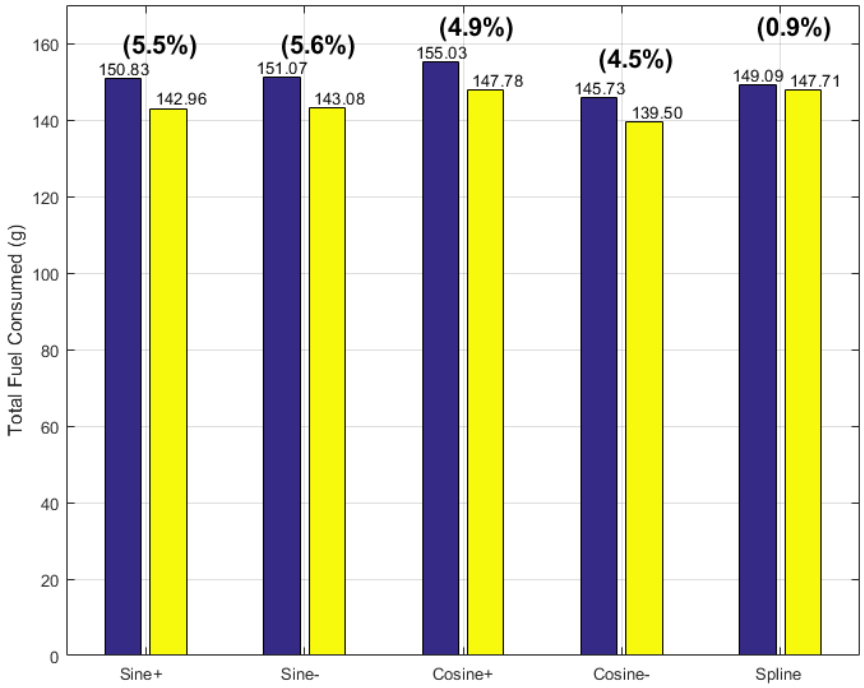

Figure 6.3: Cruising (Left) vs. Efficient (Right) Total Fuel Consumed for each road shape in Low Speed/High Load Simulations.

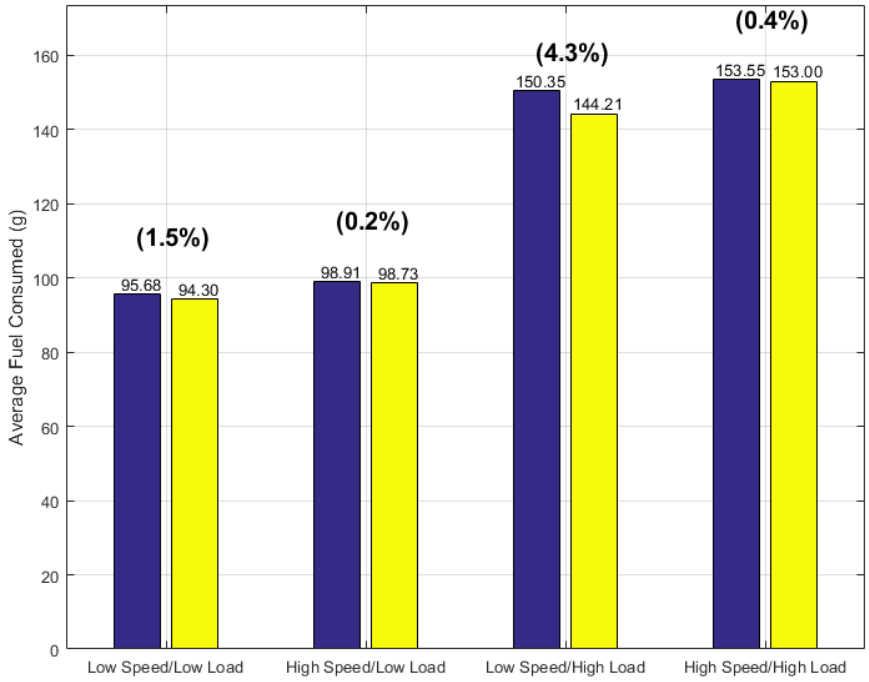

Figure 6.4: Cruising (Left) vs. Efficient (Right) Average Total Fuel Consumed across all simulated road shapes for each Speed/Load Category

6.2 Experimental Results

LabVIEW simulations yielded results that were consistent with expectations so the transition to the experimental configuration could commence. First the optimal strategies predicted by the algorithm running on hardware were compared to the simulation predictions. Results of the comparison for the positive sine profile for both cruising and efficient scenarios are displayed in Figure 6.5. Optimal engine torque and speed in the cruise control trial match simulation curves very well. The deviations in engine speed can be attributed to cycle-to-cycle variations inside the engine causing noise in the data. Due to this variation, engine speed can only reasonably be controlled to within ± 20 RPM so the experimental velocity is considered acceptable for the cruise control case.

Overall profile shape does deviate from a constant 1400 RPM, which was observed for all high load cases. There are two possible reasons for this, either the rate of load change is too dynamic for the PI controllers to maintain a fixed speed, or the weights on the performance index do not sufficiently prioritize holding speed when terms affected by outside load T_L are too high.

Attempts were made in simulation to increase cruising priority however the difference in weight magnitudes became too high for the TPBVP solver. As the deviation is well within the bounds of the engine noise, this result is also considered sufficient for cruise control operation.

A significant disparity between simulated and experimental optimal trajectories is observed for the fuel efficiency case, although the algorithm trends similarly in both. The reason for this is hypothesized as the following: During simulation, initial conditions for each horizon were taken from the previous optimal trajectory. This implies that the engine performs ideally, or responds exactly as prescribed by the algorithm over the starting point of the previous horizon to the next sampling instance. It should be clear that the engine and controller cannot achieve ideal behavior, and therefore engine conditions at the start of each horizon generation process should not be expected to match the previous horizons predictions. Some unknown, however assumed, nuances in the engine, dynamometer, controllers, or a combination of the three must effect the dynamics enough to cause deviation from the optimal solution on the real hardware when the operating state is changing significantly. This is why the effects during cruise control tests were much smaller. This is why PID control was employed initially, because precise knowledge of system dynamics was not required or known. However, since similarities in the shape of both results are clear, fuel efficient behavior on the actual hardware can still be expected and the decision was made to continue testing with the current control strategy.

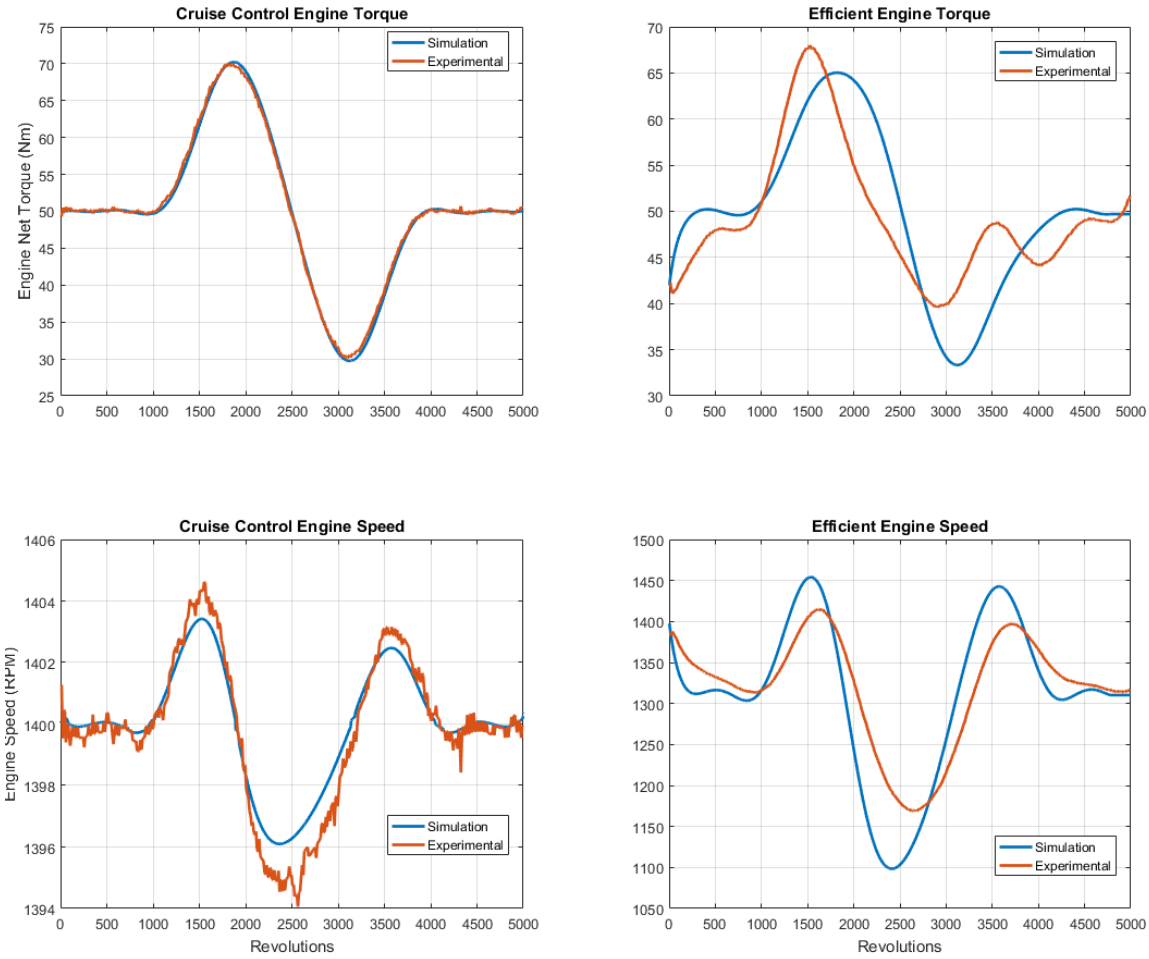

Figure 6.5: Optimal Trajectories calculated by both Simulations and Hardware Experiments

Figure 6.6 shows the optimal control trajectories predicted by the control algorithm compared against actual engine output. It is observed that the engine and controller are fully capable of matching the desired optimal set points derived by the optimal algorithm and is unaffected by PID tuning or the moving average approach. Figure 6.6.c shows the optimal velocity for the cruise control, positive sine case. The cycle-to-cycle engine noise is very apparent, however the variation in RPM remains within the acceptable tolerance. Figure 6.7 is the output of an experimental trial of the positive sine load scenario for both cruise control and fuel efficient driving. Cruise control is obviously achieved according to the engine speed, however the engine torque plot could also be used independently to validate the result. In order for constant velocity to be achieved, the engine net output must exactly match the T_L profile at all times. Comparing

Figure 6.7 to Figure 6.1 demonstrates that this is the case. For the remaining analysis of the fuel efficient case, it is worthwhile to note the following: At any point, if the fuel efficient engine output is greater than the cruise control output, which is equivalent to T_L, the engine will be in a state of acceleration. The opposite applies when the engine torque trajectory falls below the trajectory required for cruising.

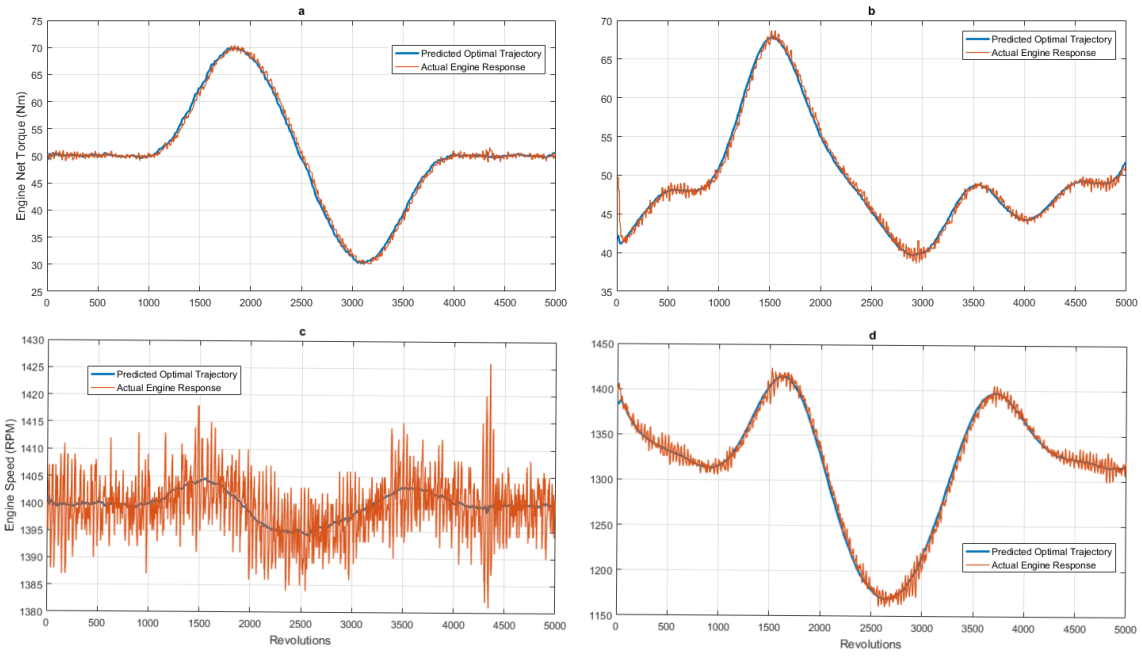

Figure 6.6: Optimal vs. Actual Trajectories from the Low Speed/High Load, Sine+ Experiment using both Cruise Control (Blue) and Efficiency Weightings (Orange)

Attention should be paid to several points along the fuel efficient trajectory during analysis. At the initiation of the experiment (zero revolutions), engine torque sharply drops off and the engine decelerates accordingly. This is a result of the optimal controller inferring that a different base cruising speed will be more efficient than the programmed desired speed. In this case, the optimal engine speed appears to be around 1300 RPM however load conditions appear to change too fast for the engine to reach a new steady speed. This is corroborated by the fact that this phenomenon scales proportionally to the weight given to fuel efficiency R. Further discussion of this behavior will be touched upon in the conclusions section. Once the controller sees changing road conditions approaching, it preemptively increases its output to accelerate before encountering the increased load demand. It continues to accelerate and increase output until it

deems it has gained enough speed to get over the “hill” at which point it decreases output and decelerates over the top of the hill. Comparing the size and location of the peak in both profiles, it is observed that instead of increasing torque until the inflection point of the uphill, as the cruise controller does around 1900 revolutions, the engine peaks early and coasts over the hill. This allows for a longer period of decreased torque and deceleration. If relative fuel consumption can be approximated using the same rational as engine acceleration, the duration of time spent under the cruise control output curve is time spent in a more fuel efficient state. When the cruise control and efficiency torque curves intersect near 1600 revolutions, engine speed should be expected to be equal to the desired cruising speed. This is also reflected by the velocity graph. Once the engine crests the peak of the elevation graph at 2500 revolutions, the rate of change in torque begins to increase in order to bring the engine back up to the newly derived optimal baseline speed. It appears to reach this speed around 3200 revolutions, overshoots and then the torque oscillates until the engine speed settles which is familiar PI control behavior.

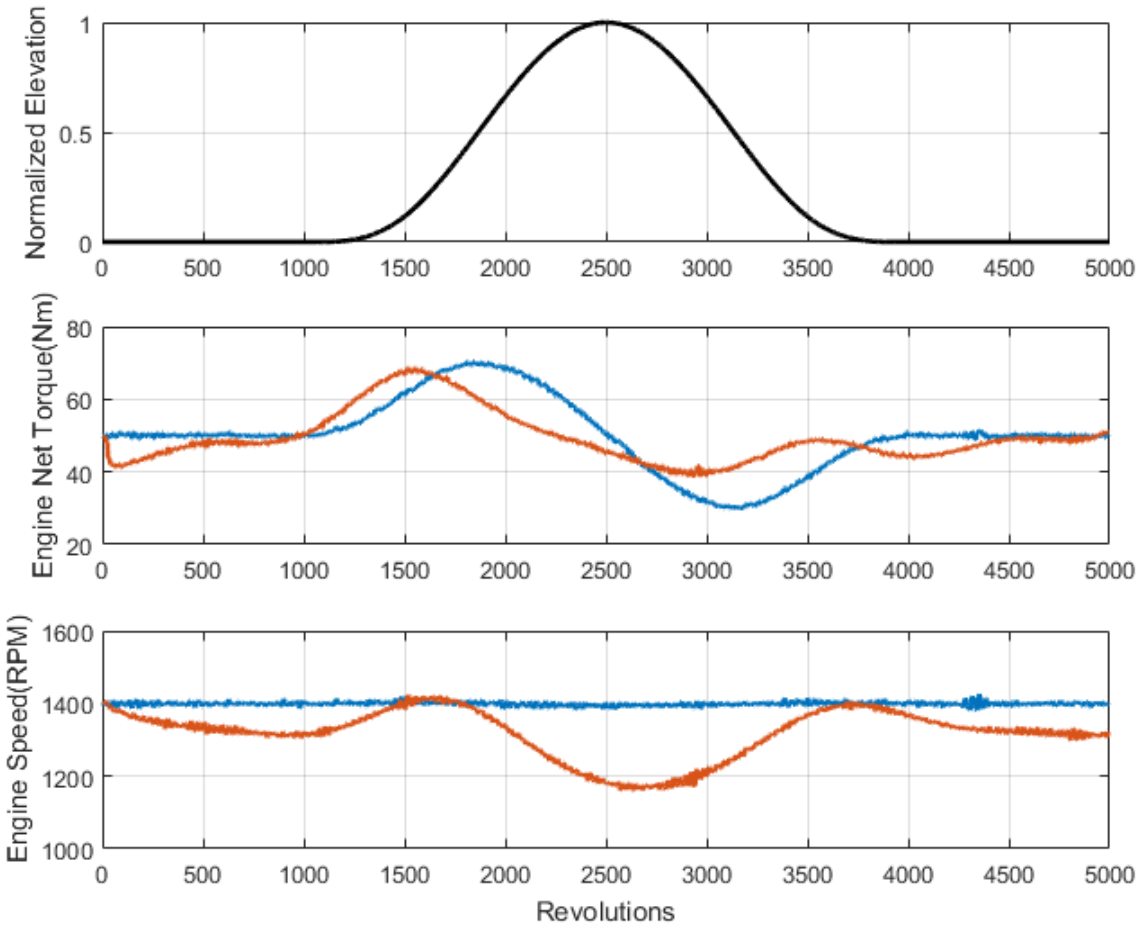

Figure 6.7: Engine Output Speed and Torque from the Low Speed/High Load, Sine+ Experiment using both Cruise Control (Blue) and Efficiency Weightings (Orange)

Figure 6.8 is the result of the complex spline case for the low speed, high load scenario. Note that the elevation plot was derived from the complex spline shape discussed in the previous chapter by integrating that profile with respect to revolutions x_1. As expected, similar behavior to the trigonometric cases is observed. The engine corrects to a new optimal baseline speed and then reacts to the upcoming road shape. Preemptive accelerations can be observed around 1200, 2000, and 3500 revolutions. However, the road appears to be changing too dynamically for the engine to reach the new steady-state optimal speed. Even the cruise control case seems to have difficulty maintaining constant speed during the most dynamic portion between 1300 and 2000 revolutions, as is evidenced by the increased noise in the velocity chart over that interval. This indicates that profile might be too extreme to employ the subject algorithm effectively.

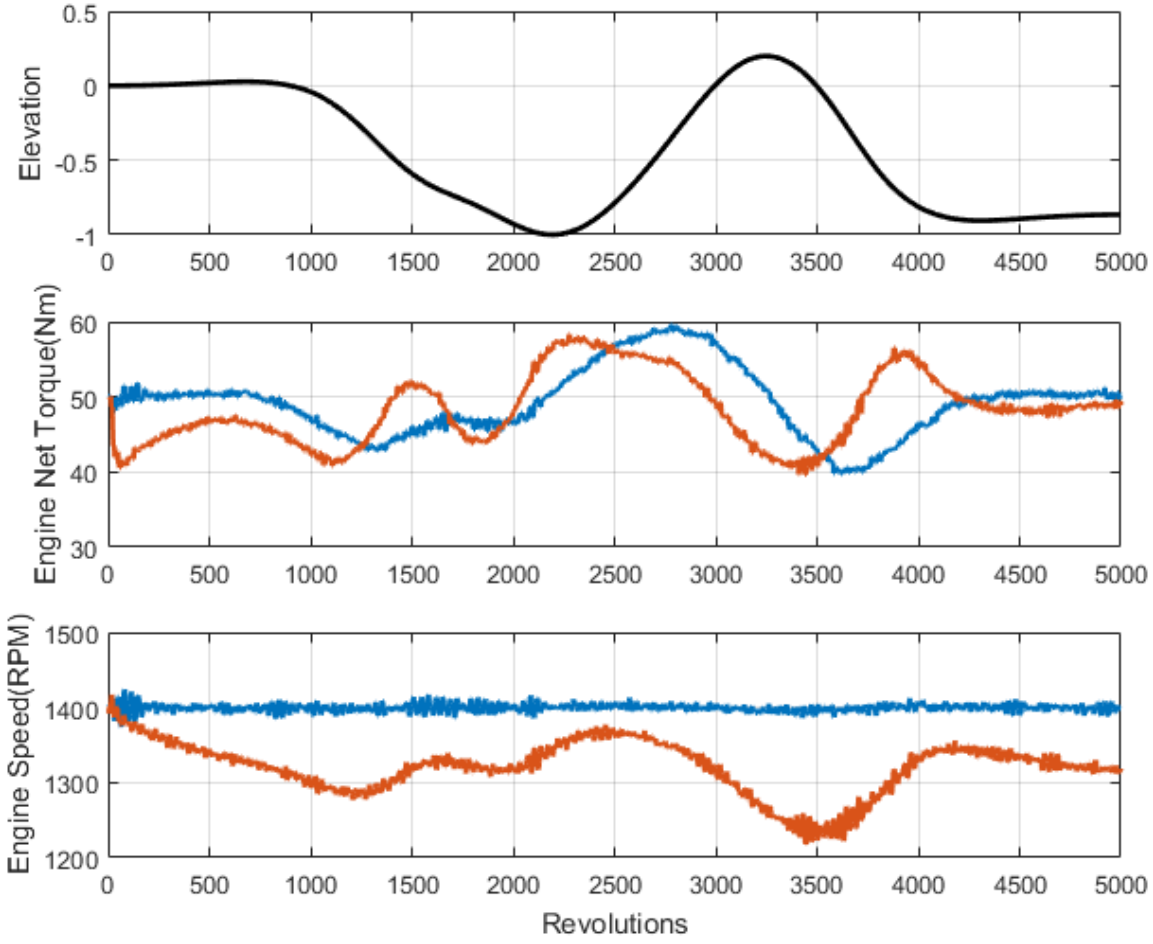

Figure 6.8: Engine Output Speed and Torque from the Low Speed/High Load, Spline Experiment using both Cruise Control (Blue) and Efficiency Weightings (Orange)

Figures 6.9 and 6.10 show total fuel consumption compared to the equivalent simulation cases analogous to figures 6.3 and 6.4. Percent change from cruise control to efficiency strategy, referencing the cruise control case, is displayed over each bar grouping. It appears that the simulations over-predict both fuel consumption levels and the amount of savings achieved by using the fuel efficient algorithm. The latter over prediction is attributed to the previously stated fact that in simulation, the engine is operating ideally and each horizon is generated assuming that the engine navigated the previous optimal horizon exactly. The consistent over prediction between simulation and engine fuel consumption data could have a few possible causes, the most likely of which is a disparity between the fuel consumption model outlined in chapter 4 and actual engine fuel consumption behavior. This may have resulted from the engine not having

been fully "broken in" during the months between calibrating the fuel model and running the experiments. This would certainly cause the components of the engine fuel system to behave differently. This claim is somewhat supported by the fact that the level of over-prediction appears to be near constant across all speed and load cases, however without detailed knowledge of the calculations taking place inside the ECU a root cause cannot be confidently determined. Since the actual engine performance is of primary interest in this study and time was limited, no further investigation was conducted into this disparity.

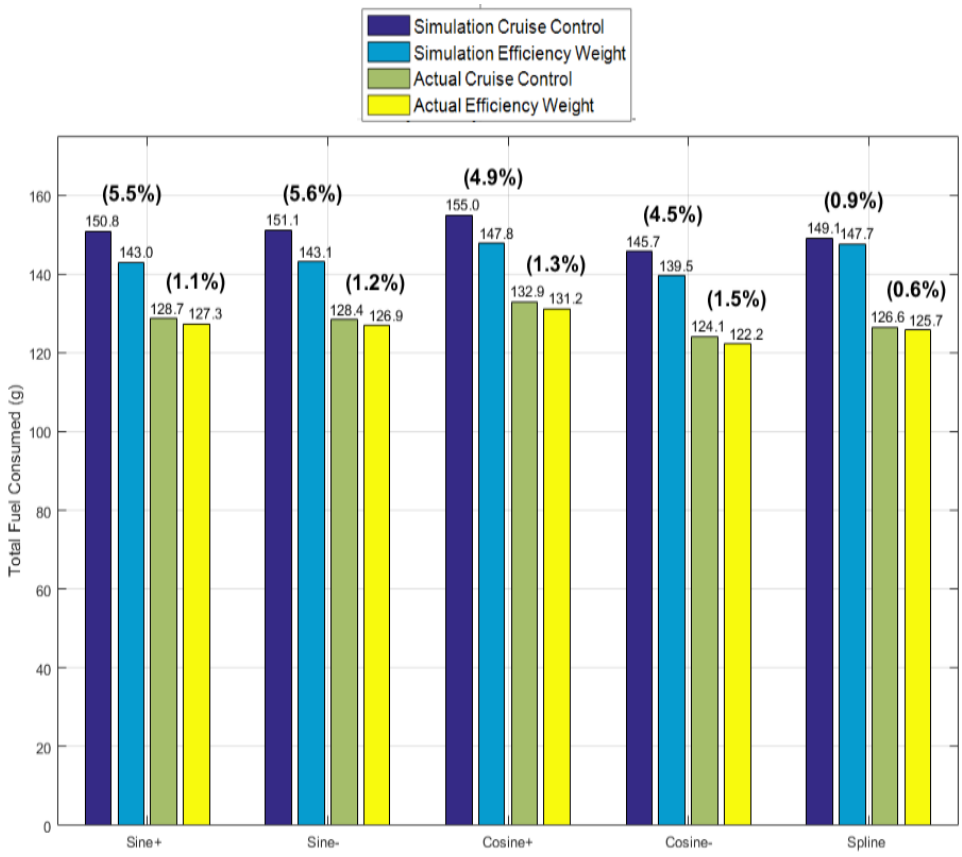

Figure 6.9: Simulated Cruise Control, Simulated Efficiency, Experimental Cruise Control and Experimental Efficient Total Fuel consumption along each road shape for the Low Speed/High Load case

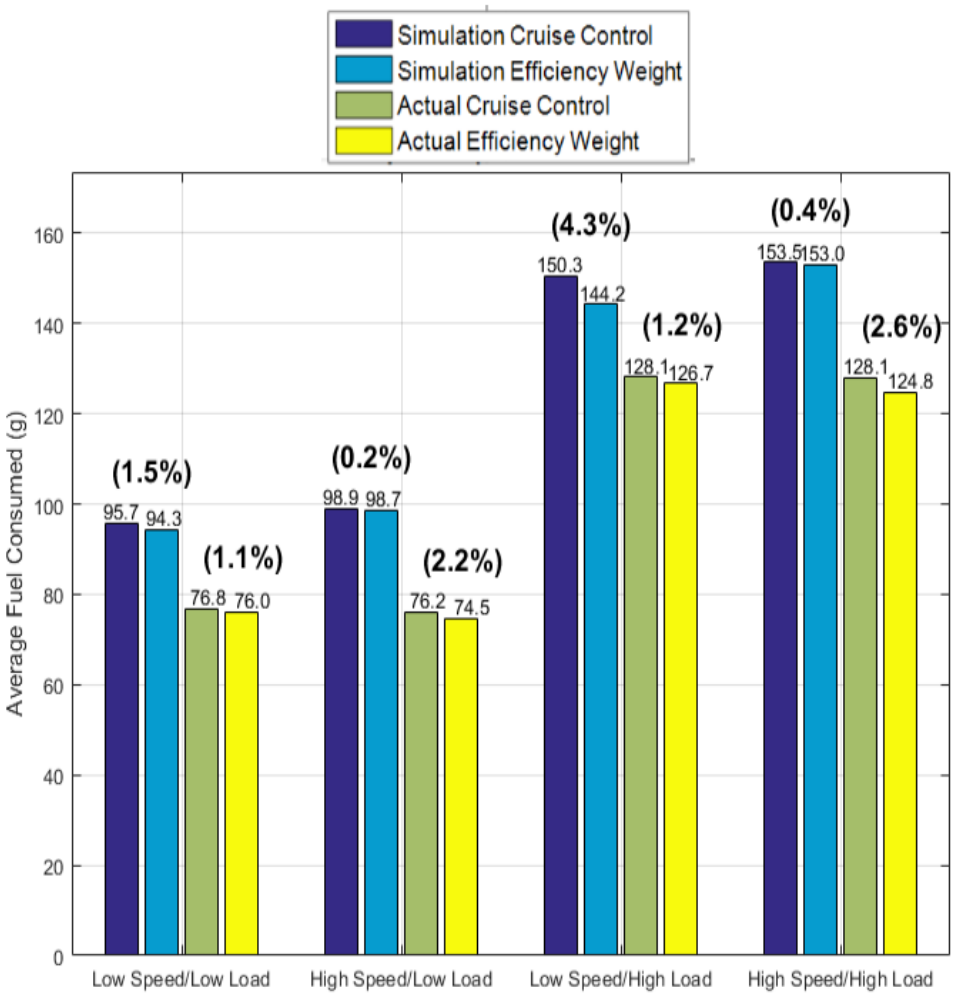

Figure 6.10: Simulated Cruise Control, Simulated Efficiency, Experimental Cruise Control and Experimental Efficient average fuel consumption across all road shapes for each Speed/Load Category

Finally, figures 6.11 and 6.12 show bar graphs for experimental fuel consumption and experimental average fuel mileage, with values and percent improvements over each. Mileage was calculated using the engine measured velocity profile divided by the mass flow rate of fuel into the engine, measured by the ECU. Note that increases in fuel mileage from the cruising to efficient cases are desired. Results indicate that in all scenarios, a small measure of improvement in fuel mileage and consumption was experienced. As expected, for a single load/speed setting, fuel consumption and fuel mileage levels were fairly consistent across all load profiles. Better fuel mileage was experienced at the low load setting which is also an intuitive result since less fuel

was required to go the same distance.

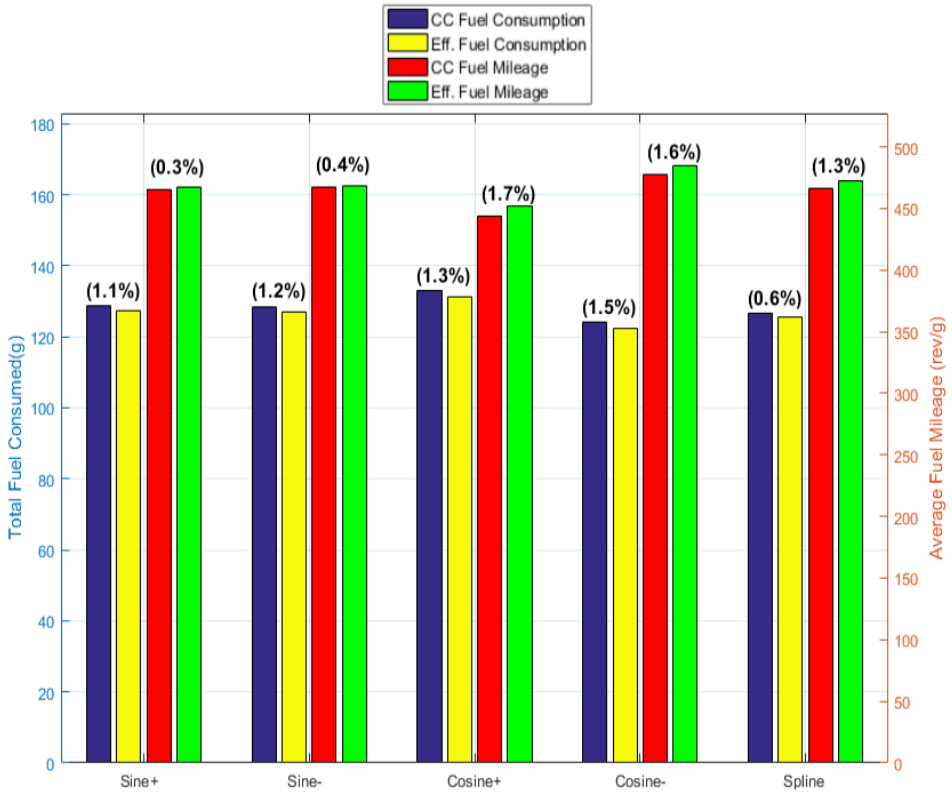

Figure 6.11: Total Cruise Control and Efficient Fuel Consumed and Average Cruise Control and Efficient fuel mileage for each road shape during Low Speed/High Load Simulations and Experiments

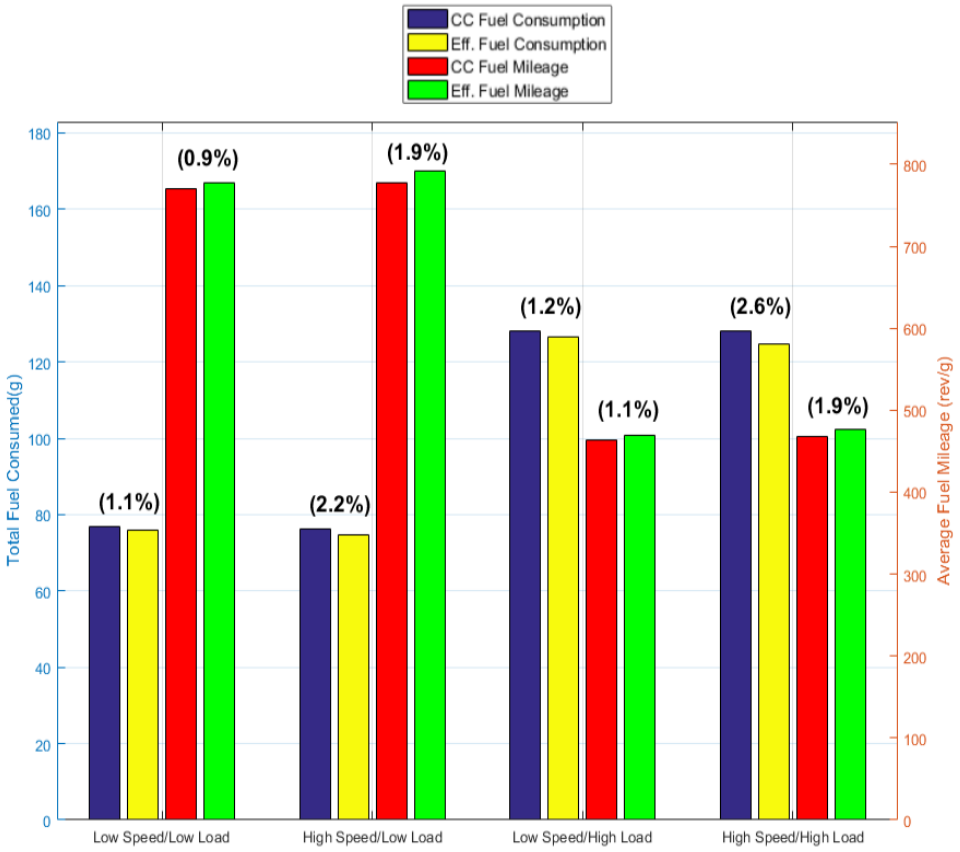

Figure 6.12: Total Cruise Control and Efficient Fuel Consumed and Average Cruise Control and Efficient Fuel Mileage Averaged across all Simulated and Experimental road shapes for each Speed/Load Category

6.3 Conclusions

The objectives of this study were to develop a fully functional engine test stand to support different experiments and to develop a control algorithm to operate an engine efficiently in highway driving scenarios. The experiments performed over the course of this work demonstrate the efficacy of the infrastructure and equipment put in place towards an efficient and versatile testing facility that is capable of supporting many different engines and experiments. In fact, during fuel consumption experiments, emission levels were measured using the FTIR. Trends in emissions data were observed that appeared to be engine state dependent, however as emissions studies are not in the scope of this work, no analysis was performed.

Results indicate that the optimal controller was able to achieve between one and two percent reductions in fuel consumption for each scenario without any fault or failure. While this indicates the objectives outlined in the scope of this work are satisfied, a few caveats must be highlighted.

First, a fuel savings of at most two percent is significantly lower than expected. Preliminary testing prior to the final algorithm deployment indicated that greater reductions could be achieved, but this behavior was not produced by the controller. The reason for this is unclear, but suggests that other control methods might yield better results. Also, the subject engine used for this study can be partially blamed for improvements lower than expected. The fuel efficiency map presented in chapter four indicates that inverse of fuel mileage (the term to be minimized in fuel efficient trials) is approximately linear and changes very slowly in both speed and engine torque, which is not ideal behavior for nonlinear optimal control theory. What this means is that any minimization strategy will seek to simply reduce speed and load in response to changing conditions. This behavior needed to be specifically counteracted in order to maintain viable highway driving conditions so it is intuitive that this control strategy would have very limited results unless full priority was given to minimizing consumption. It is hypothesized that a higher speed engine with more dynamic fuel efficiency behavior would see better results using this control strategy.

Second, it has been proven that the current form of optimal controller is capable of generating solutions to the optimal control horizon at a rate fast enough to ensure stable and smooth engine operation. The controller is also capable of negotiating the load profiles set before it without failing to find a solution numerically. However this success was found to be highly dependent on weight values and the intensity of the incoming load. This suggests that in order to be capable of navigating any reasonable highway environment, frequent changes to the optimal control programming would have to be made to keep the controller viable. This issue stems from the constrained optimization solver native to LabVIEW programming, which was employed for this control problem, being susceptible to failure when the terms in the performance index cause the numerical problem to be poorly conditioned or the solution to fall outside the established constraints.

It is the author's opinion that results prove that an optimal control strategy applied to internal combustion engines can make robust, fuel efficient control possible. This has strong economic and environmental implications. Results will vary based upon methods used in optimal

trajectory generation and the hardware chosen to employ the strategy. However, this work shows proof of the concept and provides a foundation for future works to improve upon to achieve more significant fuel savings.

6.4 Future Work

There are some aspects of this study that would benefit from further study. First, the gap in knowledge of the Kubota engine's fuel consumption should be addressed. Due to high noise in the FMS data, the fuel consumption map integral to this work was built using ECU data. This was gathered without a clear indication of how those values are being measured or calculated. If access to the ECU programming cannot be made possible, the FMS and fuel delivery system should be modified so that a clearer signal can be obtained which would provide certainty to fuel consumption measurements. Alternatively, a different engine with more accessible fuel flow data could be used. This might also have the added benefit of more dynamic consumption behavior that is better suited for the optimal control problem.

Secondly, a more sophisticated control strategy could be devised and used to replace or supplement the dual PID controllers used to control engine speed and dynamometer resistance torque. The National Instruments ECS is more than capable of supporting routines to precisely manage engine systems. Taking all aspects of engine control away from PNET may free up computational resources to allow for tighter control of the dynamometer and open up new opportunities for fuel efficient strategies.

Lastly, there is room for improvement in the approach taken to solve the optimal control problem. Future work could employ more sophisticated algorithms to solve the boundary value problem in a more robust manner without having to manipulate weights between scenarios.

Extensions to this work should include additions to the modeling strategy to account for less obvious engine dynamics that may affect the overall system. Also, work to extend driving scenarios to reflect changing vehicle conditions, such as transmission, aerodynamics, traffic effects and even urban driving could greatly supplement the work done to improve fuel efficiency undertaken by this thesis.

6.5 Summary

The objective of this thesis project was two-fold. The first was to develop the Marquette University Engine Testing Facility into a versatile platform capable of running combustion,

emissions, and control experiments on a variety of subject engines and reactors. A PowerTest AC dynamometer and a Kubota gasoline engine were installed along with infrastructure, control, and measurement systems. The resulting test environment was used in the design and testing of an optimal control algorithm capable of operating the engine over a prescribed load profile, simulating changing elevations over a highway, in a manner that improved fuel efficiency over contemporary cruise control systems. To accomplish this, a nonlinear, receding horizon, optimization problem was solved continuously in time to derive instantaneous optimal engine states based on predicted loading conditions.

Experiments indicate that the current algorithm is capable of a one to two percent reduction in fuel consumption across all simulated road profiles. It is hypothesized that this could be improved with further modifications to the numerical approach taken to trajectory generation, improved control strategies imposed on the engine and dynamometer, and a more precise method of measuring and modeling fuel consumption. The testing environment and control approach taken reported in this thesis project does provide a foundation for further development of strategies for minimizing IC engine fuel consumption and emissions levels.

REFERENCES

[1] Cruise Control: A Walkthrough. http://www.drivelinesr.com/2014/12/cruise-control-walkthrough.html/. Accessed: 2017-01-03.

[2] Dynamometers: Everyone Talks Horsepower, but How do you Measure it? http://dealernews.prod.as2.guidance.com/dealernews/article/dynamometers-everyone-talks-horsepower-how-do-you-measure-it?page=0,1/. Accessed: 2017-01-03.

[3] U.S. Federal Highway Administration, Highway Statistics, Summary to 1995. http://www.fhwa.dot.gov/ohim/ohimstat.htm. Accessed: 2017-01-05.

[4] H.R. 6 110th Congress: Energy Independence and Security Act of 2007.. https://www.govtrack.us/congress/bills/110/hr6. Accessed: 2016-12-30.

[5] S. 622 94th Congress: Energy Policy and Conservation Act.. https://www.govtrack.us/congress/bills/94/s622. Accessed: 2016-12-30.

[6] *Kubota Installation Instructions. CARB/EPA certified engine, WG1605 and WG2503*. Kubota Corporation, 2014.

[7] *NI Engine Control System Configuration Guide*. National Instruments, 2014.

[8] William G Agnew. Fifty years of combustion research at general motors. *Progress in Energy and Combustion Science*, 4(2):115–155, 1978.

[9] Kevin Anderson and Glen Peters. The trouble with negative emissions. *Science*, 354(6309):182–183, 2016.

[10] Behrang Asadi and Ardalan Vahidi. Predictive cruise control: Utilizing upcoming traffic signal information for improving fuel economy and reducing trip time. *IEEE Transactions on Control Systems Technology*, 19(3):707–714, 2011.

[11] K J Åström and Richard M Murray. *Feedback Systems: An Introduction for Scientists and Engineers*, volume 36. 2008.

[12] Bert Brunekreef and Barbara Hoffmann. Air pollution and heart disease. *The Lancet*, 388(10045):640–642, 2016.

[13] Richard H Byrd, Robert B Schnabel, and Gerald A Shultz. A trust region algorithm for nonlinearly constrained optimization. *SIAM Journal on Numerical Analysis*, 24(5):1152–1170, 1987.

[14] White House Press Secretary Jay Carney. Obama administration finalizes historic 54.5mpg fuel efficiency standards. 2012. https://www.whitehouse.gov/the-press-office/2012/08/28/obama-administration-finalizes-historic-545-mpg-fuel-efficiency-standard. Accessed: 2016-12-29.

[15] David J Chang and Edward K Morlok. Vehicle speed profiles to minimize work and fuel consumption. *Journal of transportation engineering*, 131(3):173–182, 2005.

[16] Robert Todd Chang. *A modelling study of the influence of spark-ignition engine parameters on engine thermal efficiency and performance*. PhD thesis, Massachusetts Institute of Technology, 1988.

[17] K.C. Colwel. Porsche is working on the most entertaining cruise control ever: It can corner up to 0.70 g. `http://blog.caranddriver.com/porsche-is-working-on-the-most-entertaining-cruise-control-ever-it-can-corner-up-to-0-70-g` Accessed: 2017-01-03.

[18] I. De Vlieger. On-board emission and fuel consumption measurement campaign on petrol-driven passenger cars. *Atmospheric Environment*, 31(22):3753–3761, 1997.

[19] Julian Eckstein, Kai Schäfer, Sebastian Peitz, Patrick Friedel, Sina Ober-Blöbaum, and Michael Dellnitz. A Comparison of two Predictive Approaches to Control the Longitudinal Dynamics of Electric Vehicles. *Procedia Technology*, 26:465–472, 2016.

[20] Ottmar Edenhofer, Brigitte Knopf, Terry Barker, Lavinia Baumstark, Bertrand Chateau, Patrick Criqui, Morna Isaac, Alban Kitous, Socrates Kypreos, Marian Leimbach, Kai Lessmann, Bertrand Magné, erban Scrieciu, Hal Turton, and P Van Vuuren. The Economics of Low Stabilization : Model Comparison of Mitigation Strategies and Costs Source. *The Energy Journal Special Issue 1 : The Economics of Low Stabilization*, 31, 2016.

[21] Jiyong Eom, Jae Edmonds, Volker Krey, Nils Johnson, Thomas Longden, Gunnar Luderer, Keywan Riahi, and Detlef P Van Vuuren. The impact of near-term climate policy choices on technology and emission transition pathways. *Technological Forecasting and Social Change*, 90:73–88, 2015.

[22] Daniel J. Fagnant and Kara Kockelman. Preparing a nation for autonomous vehicles: Opportunities, barriers and policy recommendations. *Transportation Research Part A: Policy and Practice*, 77:167–181, 2015.

[23] Colin R Ferguson and Allan T Kirkpatrick. *Internal combustion engines: applied thermosciences*. John Wiley & Sons, 2015.

[24] David L. Greene. Why CAFE worked. *Energy Policy*, 26(8):595–613, 1998.

[25] David L. Greene. Measuring energy security: Can the United States achieve oil independence? *Energy Policy*, 38(4):1614–1621, 2010.

[26] Sarath K Guttikunda and Rahul Goel. Health impacts of particulate pollution in a megacitydelhi, india. *Environmental Development*, 6:8–20, 2013.

[27] Arie J Haagen-Smit and MM Fox. Photochemical ozone formation with hydrocarbons and automobile exhaust. *Air Repair*, 4(3):105–136, 1954.

[28] John Heywood. *Internal combustion engine fundamentals*. McGraw-Hill Education, 1988.

[29] JN Hooker. Optimal driving for single-vehicle fuel economy. *Transportation Research Part A: General*, 22(3):183–201, 1988.

[30] Ronald L Iman. Latin hypercube sampling. *Encyclopedia of Quantitative Risk Analysis and Assessment*, 2008.

[31] M. A S Kamal, Masakazu Mukai, Junichi Murata, and Taketoshi Kawabe. Ecological vehicle control on roads with up-down slopes. *IEEE Transactions on Intelligent Transportation Systems*, 12(3):783–794, 2011.

[32] Thomas Klier and Joshua Linn. New Vehicle Characteristics and the Cost of the Corporat Average Fuel Economy Standard. *The RAND Journal of Economics*, 43(December):186–213, 2012.

[33] H Kormanski, S Mazurek, and K Rudzinska. Analysis of real and optimal vehicle driving strategy. Technical report, 1983.

[34] Pamela I Labuhn and William J Chundrlik Jr. Adaptive cruise control, October 3 1995. US Patent 5,454,442.

[35] Jeongwoo Lee, Douglas J Nelson, Michael W Ellis, and Charles F Reinholtz. Rotating Inertia Impact on Propulsion and Regenerative Braking for Electric Motor Driven Vehicles By Rotating Inertia Impact on Propulsion and Regenerative Braking for Electric Motor Driven Vehicles. 2005.

[36] Jonathan I Levy, Jonathan J Buonocore, and Katherine Von Stackelberg. Evaluation of the public health impacts of traffic congestion: a health risk assessment. *Environmental health*, 9(1):65, 2010.

[37] Frank L Lewis, Draguna Vrabie, and Vassilis L Syrmos. Optimal control, hoboken, 2012.

[38] John a. Maga and Gerhardt C. Hass. The Development of Motor Vehicle Exhaust Emission Standards in California. *Journal of the Air Pollution Control Association*, 10(5):393–414, 1960.

[39] Chris Manzie, Harry Watson, and Saman Halgamuge. Fuel economy improvements for urban driving: Hybrid vs. intelligent vehicles. *Transportation Research Part C: Emerging Technologies*, 15(1):1–16, 2007.

[40] Rose McCallen, Fred Browand, and James Ross. *The aerodynamics of heavy vehicles: trucks, buses, and trains*, volume 19. Springer Science & Business Media, 2013.

[41] J Van Mierlo, G Maggetto, E Van De Burgwal, and R Gense. Driving Style and Traffic Measures Influence on Vehicle Emissions and Fuel Consumption. *Proceedings of the Institution of Mechanical Engineers Part D*, 218(v):43–53, 2004.

[42] Rain Noe. For the corvette stingray, a user-configurable dashboard. `http://www.core77.com/posts/25374/for-the-corvette-stingray-a-user-configurable-dashboard-25374/`. Accessed: 2017-01-03.

[43] J.G.J. Olivier, M. Muntean, and J.A.H.W. Peters. Trends in global CO2 emissions: 2015 report. *PBL Netherlands Environmental Assessment Agency & European Commission's Joint Research Centre (JRC)*, pages 1–78, 2015.

[44] Intergovernmental Panel on Climate Change. Climate change 2014: Mitigation of climate change. 3, 2015.

[45] Joeri Rogelj, Gunnar Luderer, Robert C Pietzcker, Elmar Kriegler, Michiel Schaeffer, Volker Krey, and Keywan Riahi. Energy system transformations for limiting end-of-century warming to below 1.5 [deg] c. *Nature Climate Change*, 5(6):519–527, 2015.

[46] B. Saerens, J. Vandersteen, T. Persoons, J. Swevers, M. Diehl, and E. Van den Bulck. Minimization of the fuel consumption of a gasoline engine using dynamic optimization. *Applied Energy*, 86(9):1582–1588, 2009.

[47] Evangelia Samoli, Richard W Atkinson, Antonis Analitis, Gary W Fuller, David C Green, Ian Mudway, H Ross Anderson, and Frank J Kelly. Associations of short-term exposure to traffic-related air pollution with cardiovascular and respiratory hospital admissions in london, U.K. *Occupational and environmental medicine*, 2016.

[48] AB Schwarzkopf and RB Leipnik. Control of highway vehicles for minimum fuel consumption over varying terrain. *Transportation Research*, 11(4):279–286, 1977.

[49] United States. Inventory of U . S . Greenhouse Gas Emissions and Sinks : 1990 1998. *IPCC*, pages 1990–1998, 2000.

[50] Akinori Sugimoto and Hiroshi Sugimoto. Electric dynamometer, April 9 1985. US Patent 4,509,374.

[51] The Internation Council on Clean Transportation. United States Efficiency and Greenhouse Gas Emission Regulations for Model Year 2018-2027 Heavy-Duty Vehicles, Engines, and Trailers. (August), 2016.

[52] Wilfried Voss. *A comprehensible guide to J1939*. Copperhill Technologies Corporation, 2008.

[53] Darrell Whitley. A genetic algorithm tutorial. *Statistics and computing*, 4(2):65–85, 1994.

APPENDIX A

SIMULATION AND EXPERIMENTAL RESULTS

A.1 Simulation Results

In the following figures displaying simulation results, blue curves represent cruise control simulations while orange curves represent trials prioritizing efficiency. Blue bar graphs represent total fuel consumed in simulated cruise control trials and yellow bar graphs represent simulated efficiency results.

A.1.1 Low Speed, Low Load

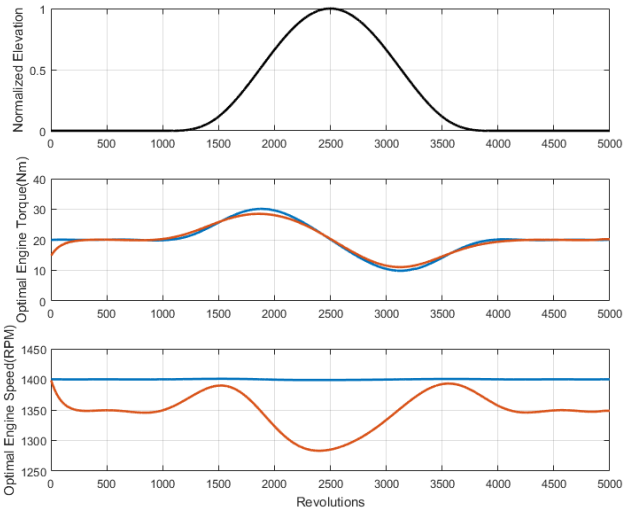

Figure A.1: Sine+

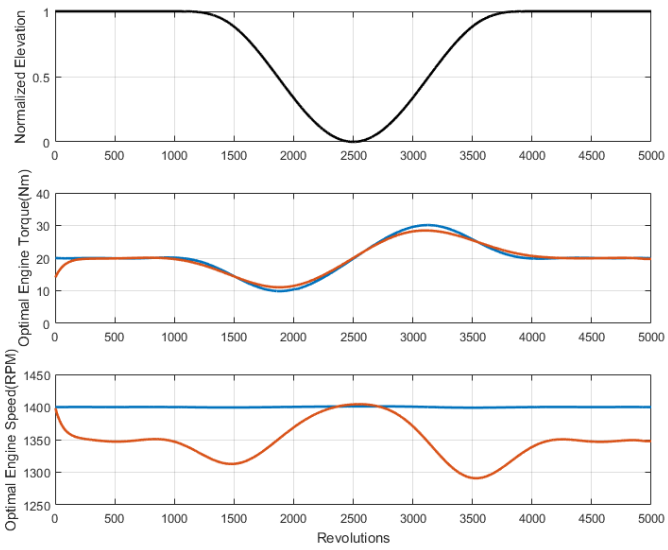

Figure A.2: Sine-

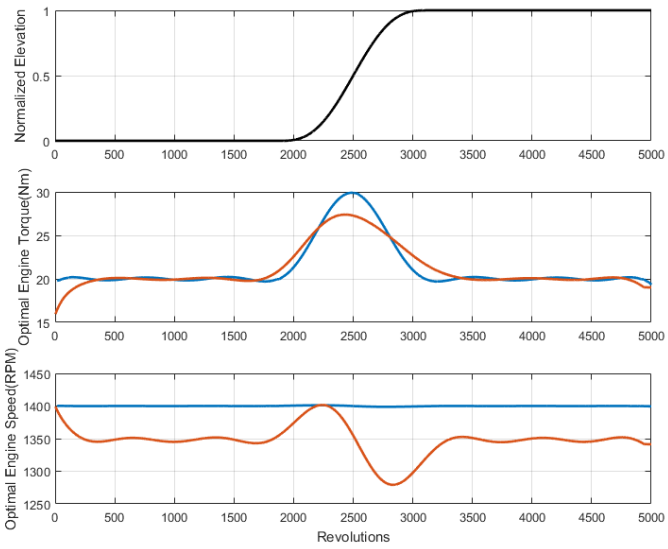

Figure A.3: Cosine+

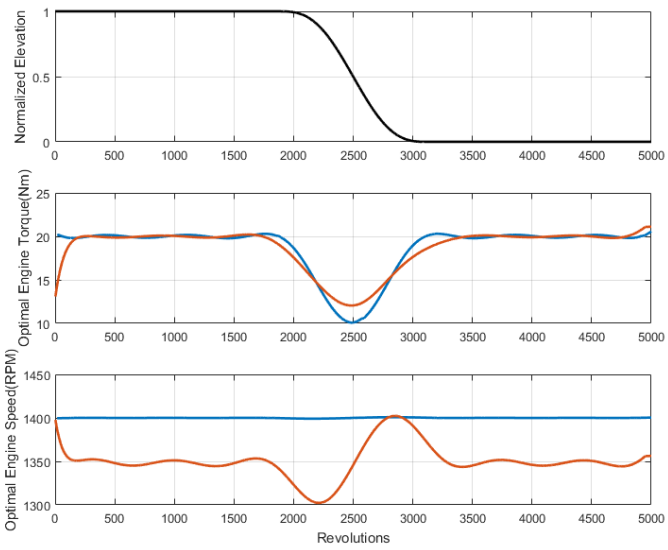

Figure A.4: Cosine-

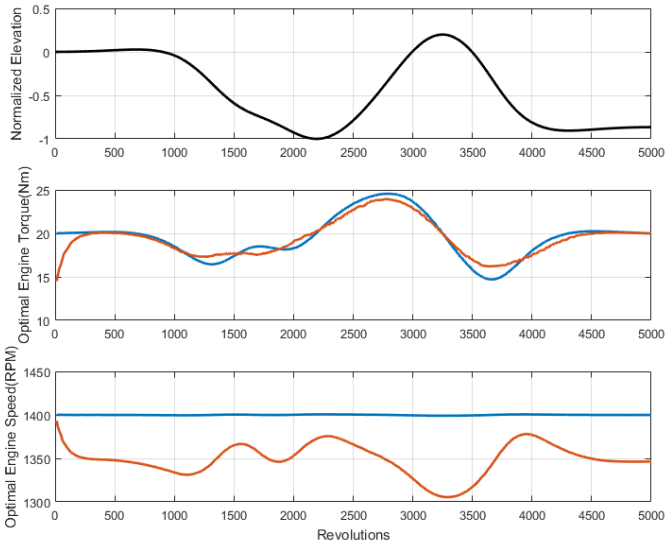

Figure A.5: Complex Spline

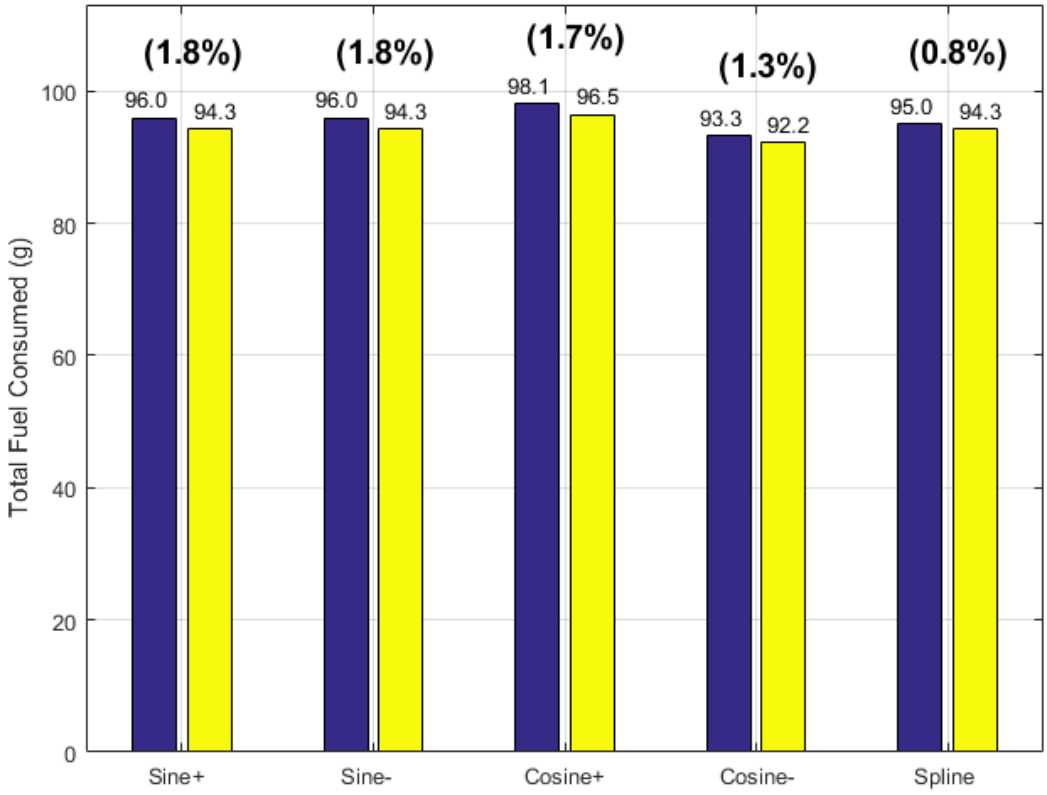

Figure A.6: Total Simulated Fuel Consumed during Low Speed/Low Load Trials

A.1.2 Low Speed, High Load

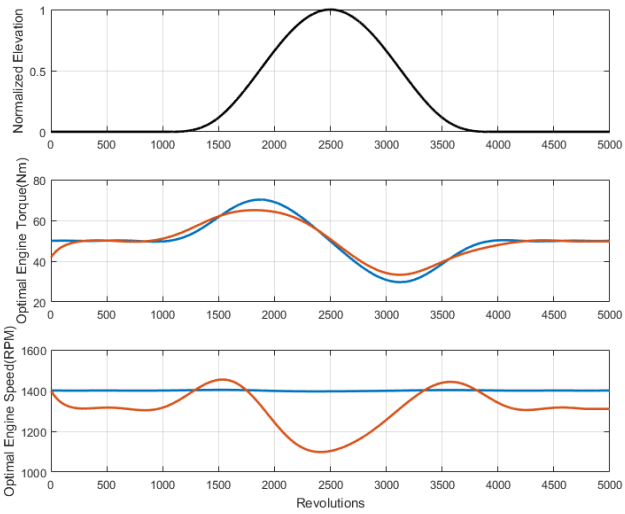

Figure A.7: Sine+

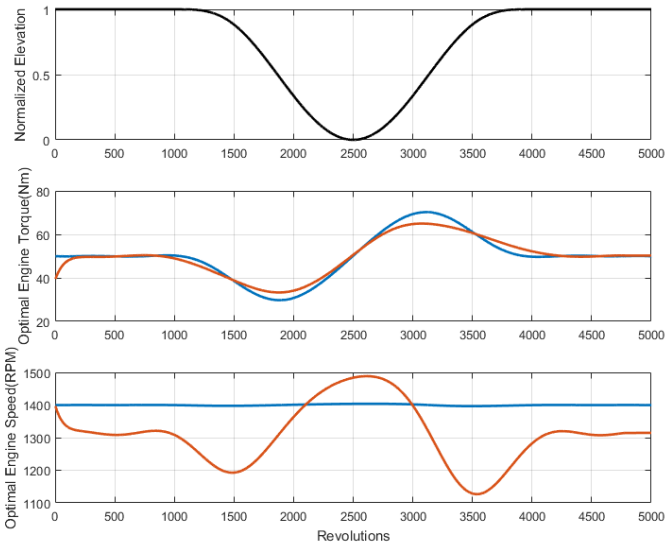

Figure A.8: Sine-

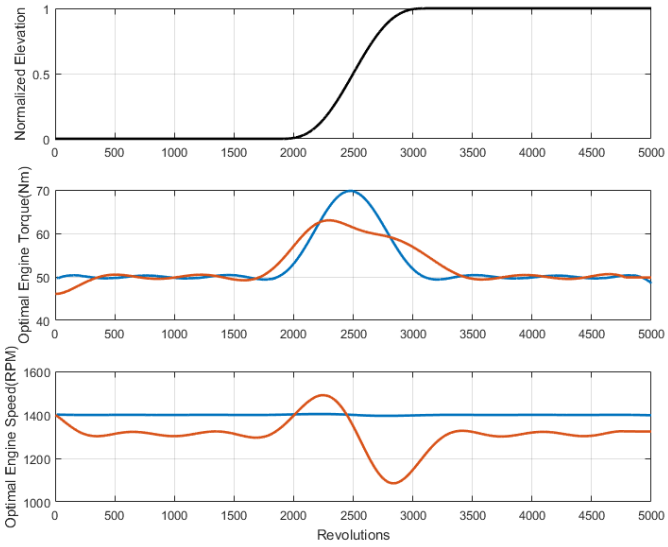

Figure A.9: Cosine+

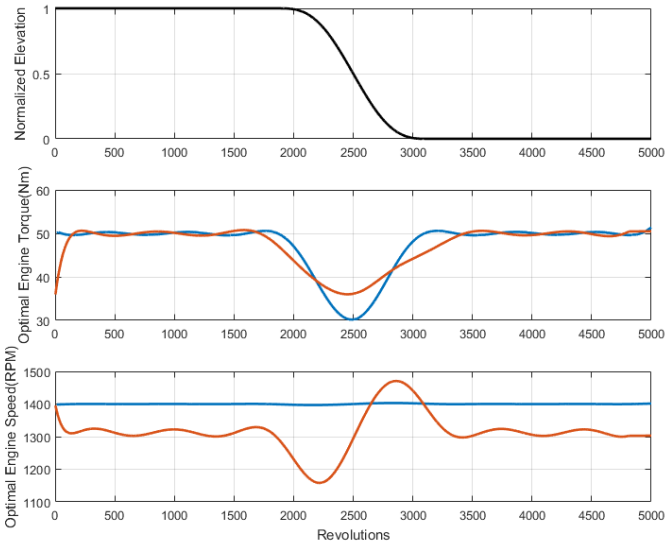

Figure A.10: Cosine-

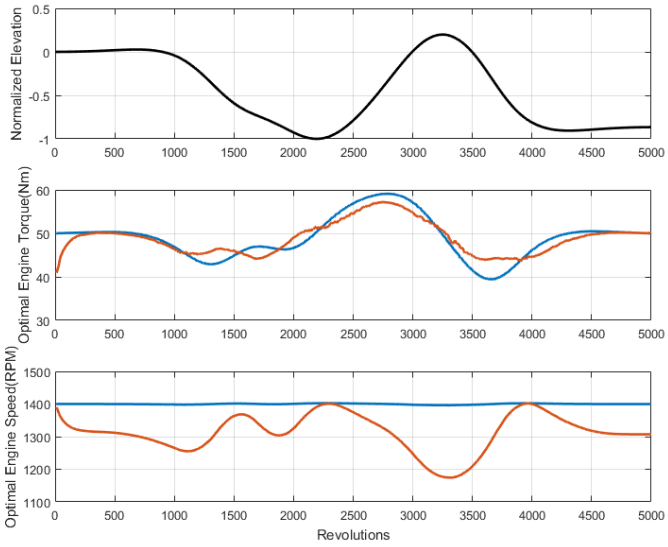

Figure A.11: Complex Spline

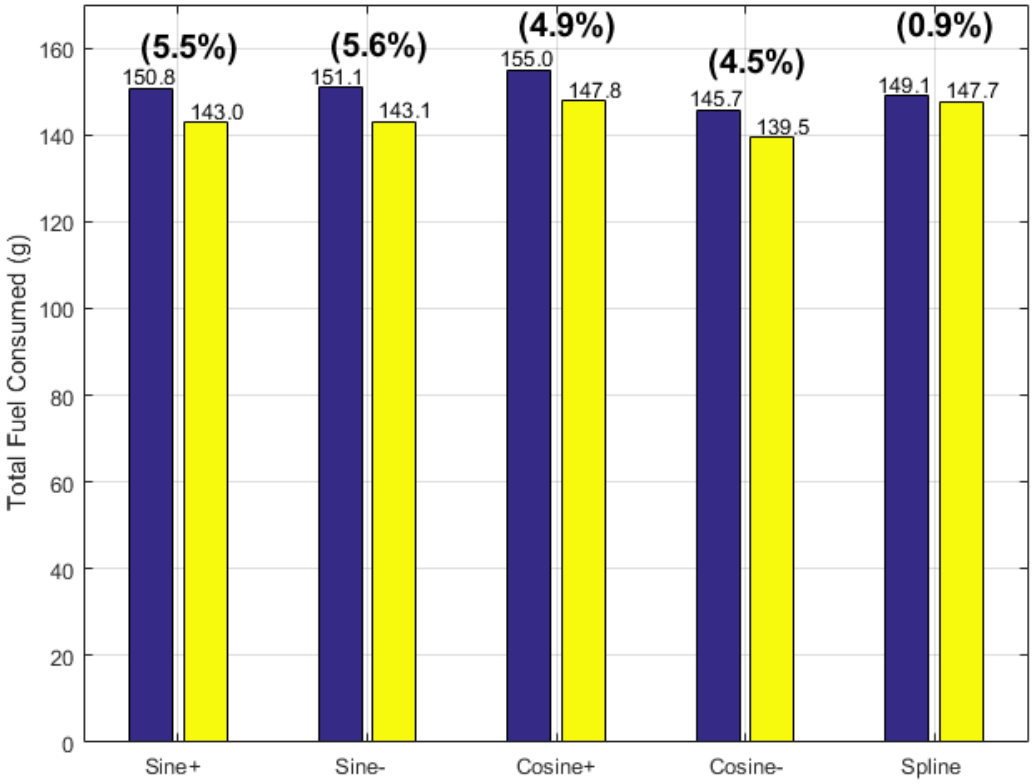

Figure A.12: Total Simulated Fuel Consumed during Low Speed/High Load Trials

A.1.3 High Speed, Low Load

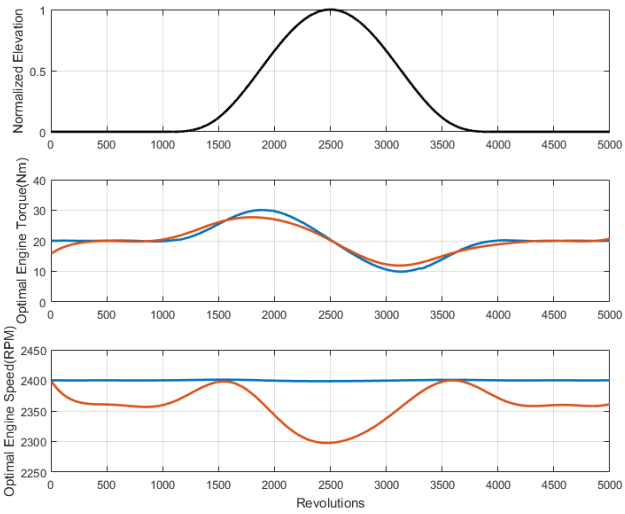

Figure A.13: Sine+

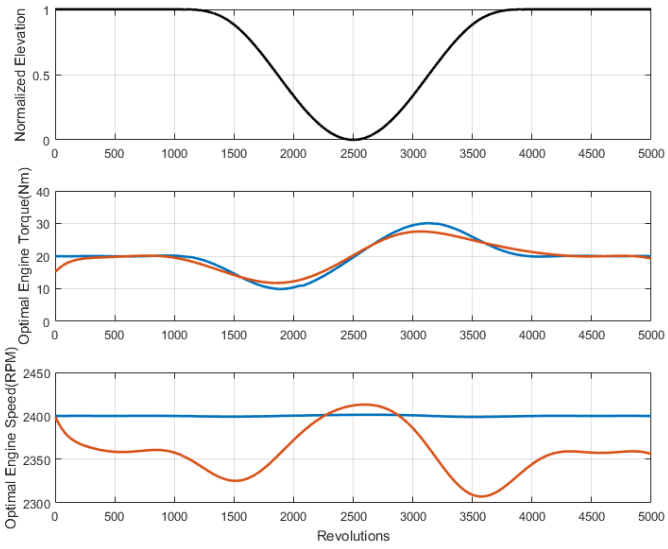

Figure A.14: Sine-

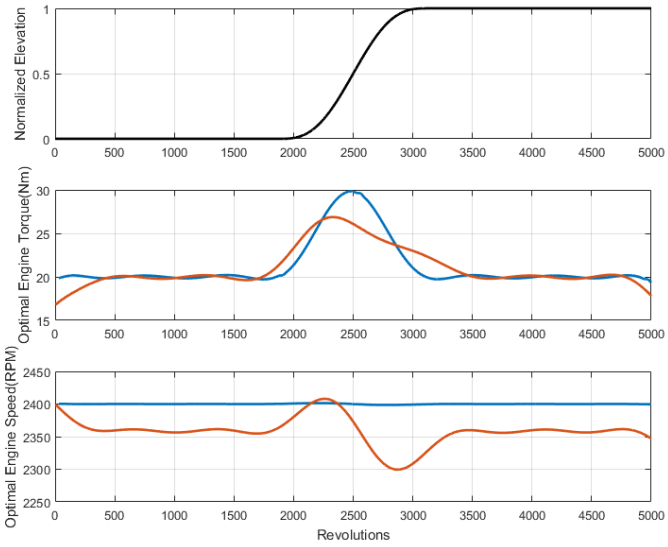

Figure A.15: Cosine+

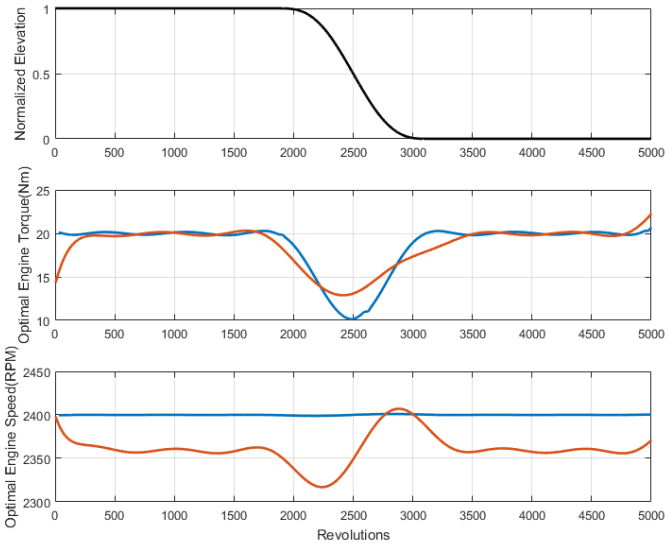

Figure A.16: Cosine-

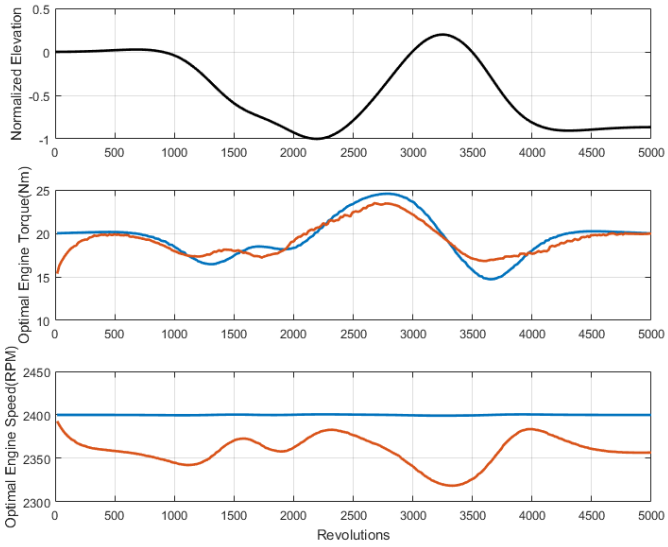

Figure A.17: Complex Spline

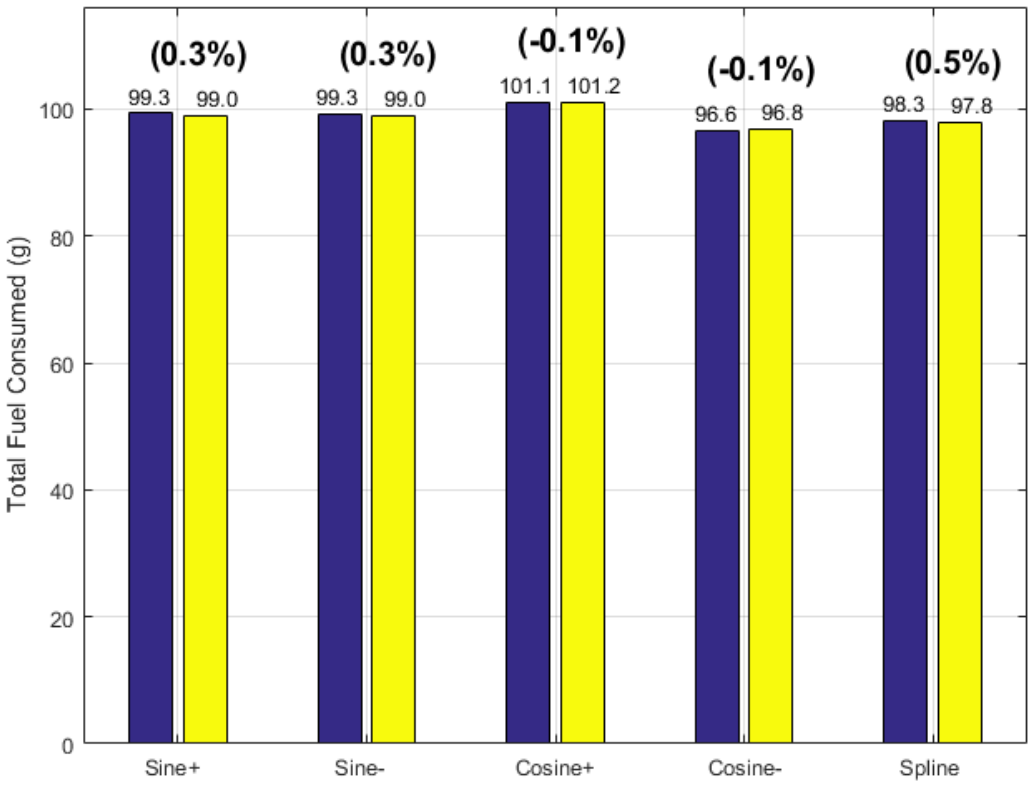

Figure A.18: Total Simulated Fuel Consumed during High Speed/Low Load Trials

A.1.4 High Speed, High Load

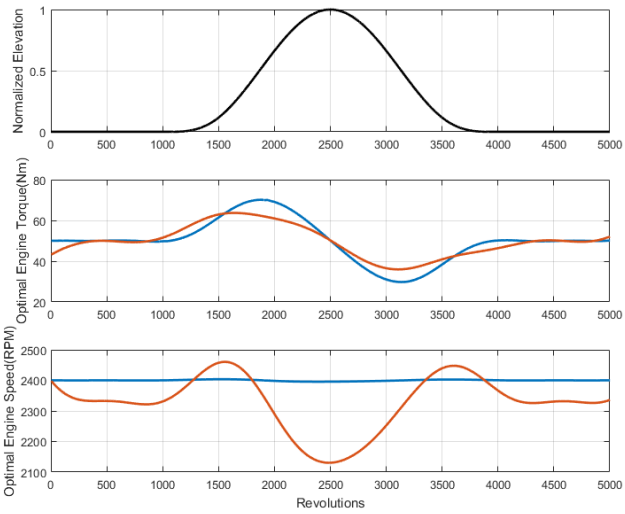

Figure A.19: Sine+

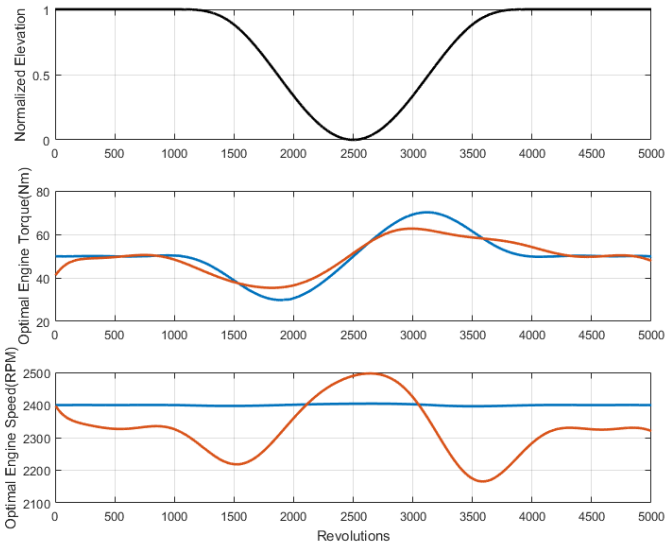

Figure A.20: Sine-

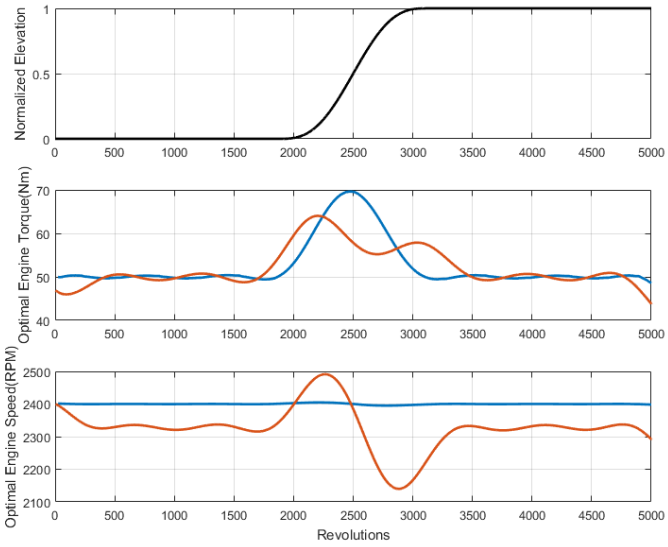

Figure A.21: Cosine+

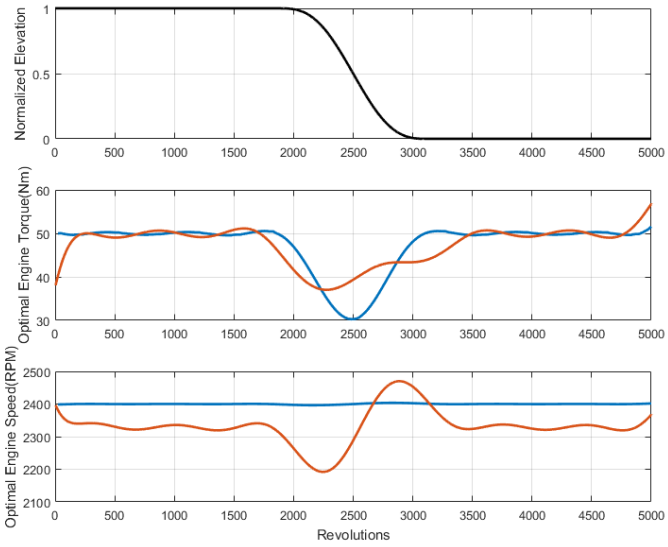

Figure A.22: Cosine-

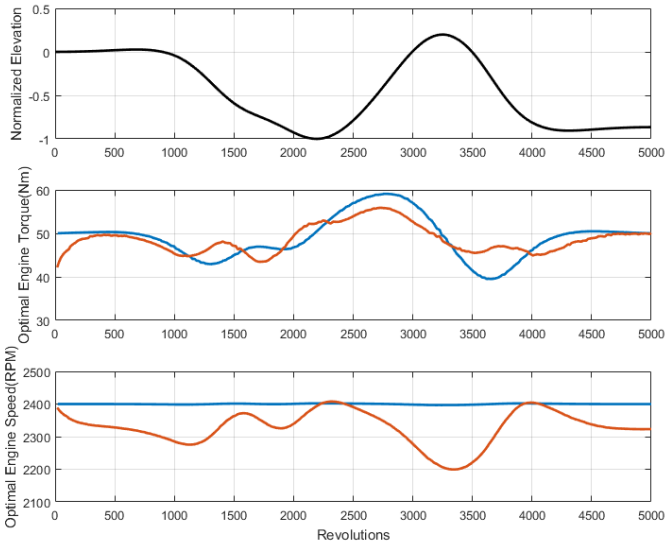

Figure A.23: Complex Spline

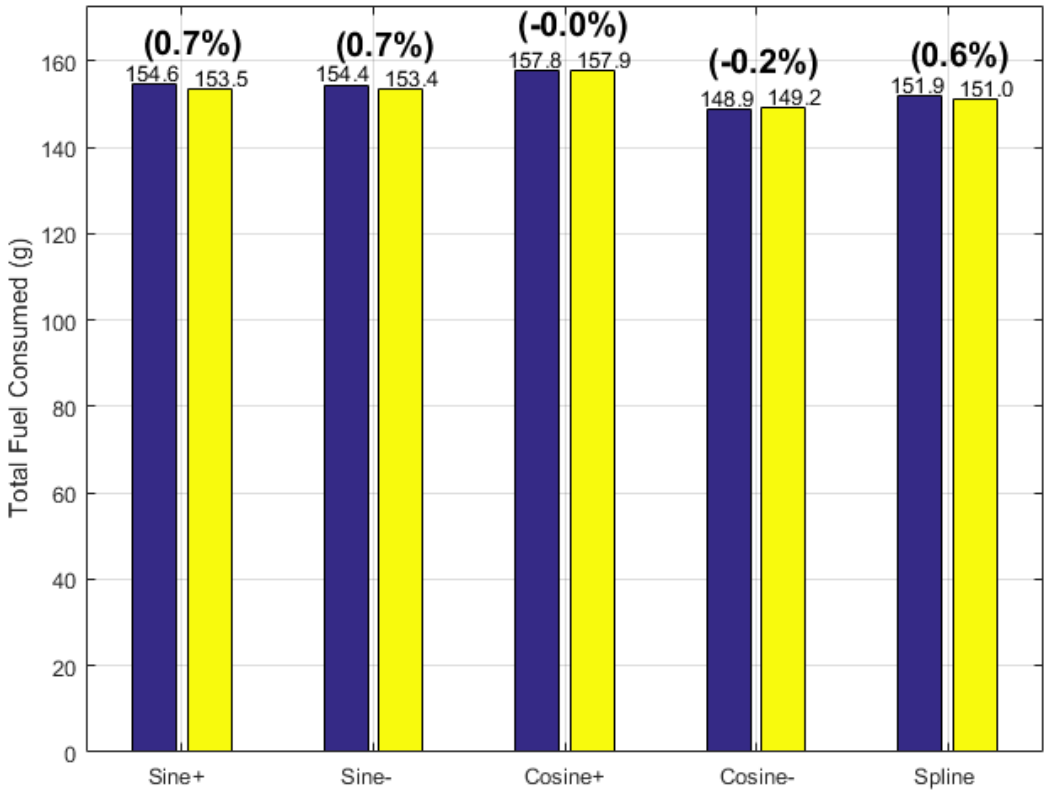

Figure A.24: Total Simulated Fuel Consumed during High Speed/High Load Trials

A.1.5 Totals

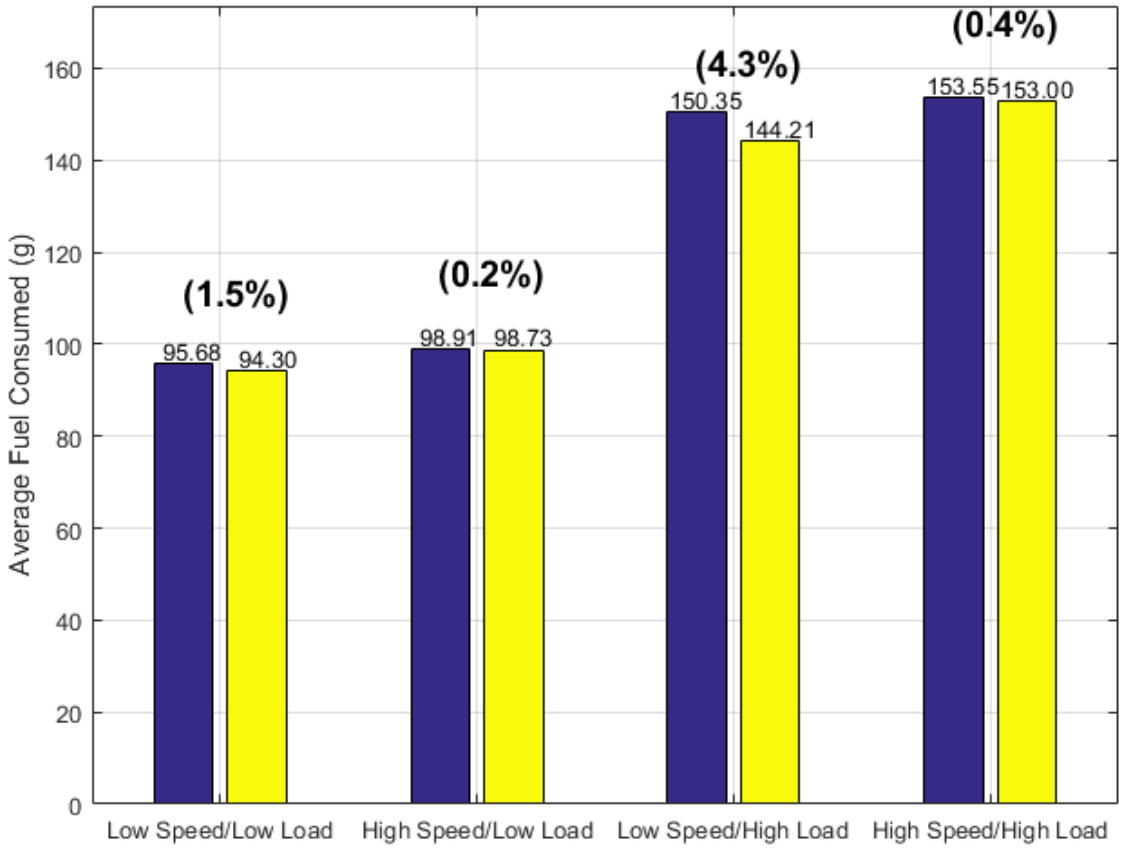

Figure A.25: Average Total Fuel Consumed for each Speed/Load Category

A.2 Simulation Vs. Experimental Results

In the following figures displaying simulation vs experimental optimal trajectories, blue curves represent optimal simulations while orange curves represent the optimal trajectories derived during physical experiments. Blue Bar graphs represent simulated cruise control, teal bar graphs represent simulated efficiency trials, green bar graphs represent experimental cruise control, and yellow bar graphs represent experimental efficiency trials.

A.2.1 Low Speed, Low Load

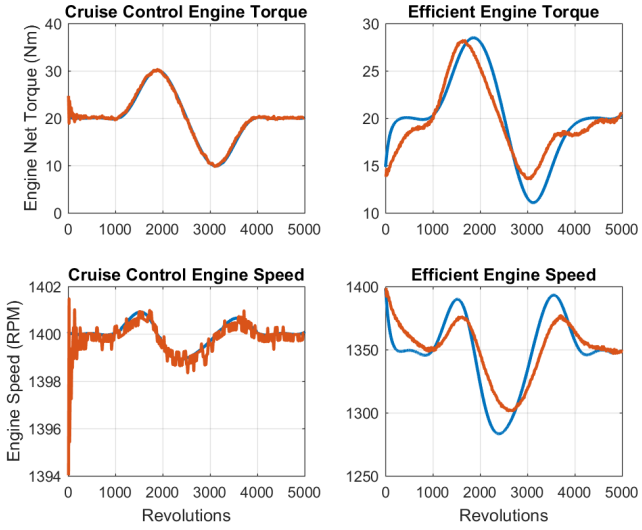

Figure A.26: Sine+

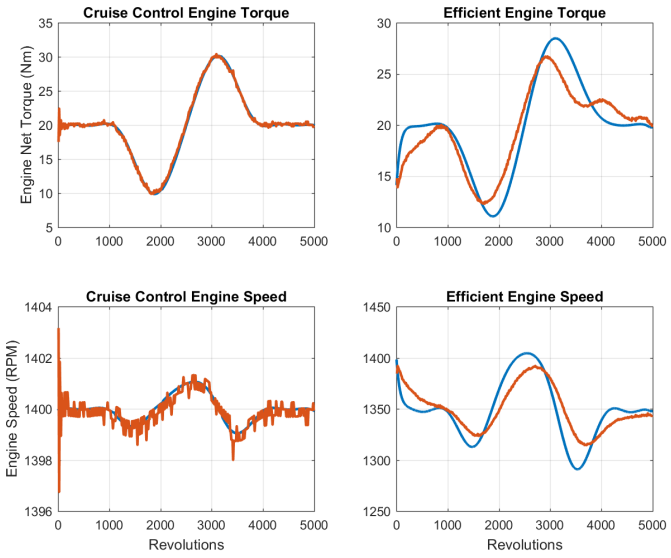

Figure A.27: Sine-

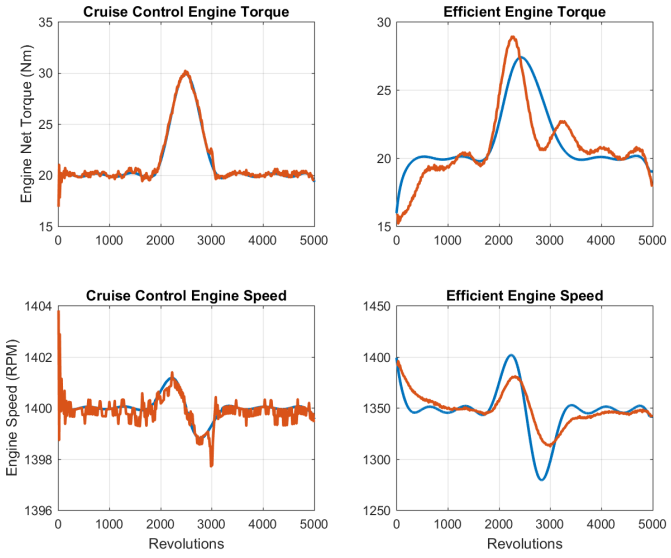

Figure A.28: Cosine+

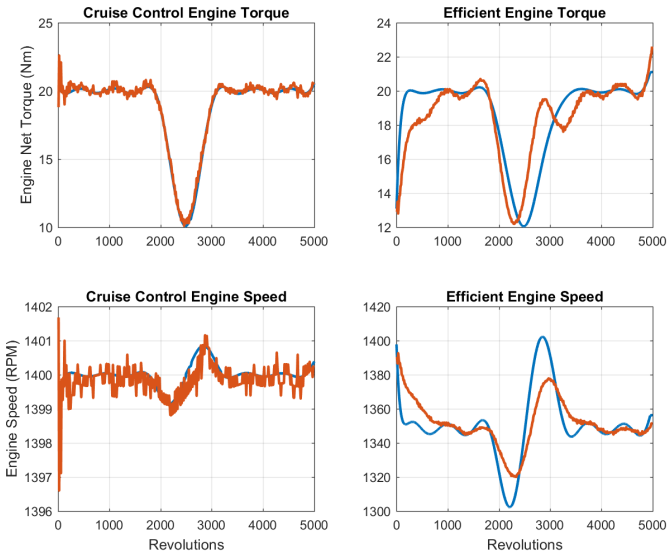

Figure A.29: Cosine-

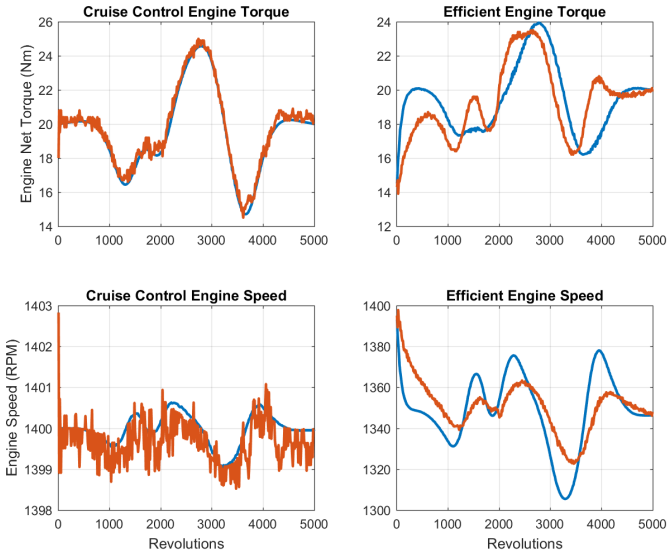

Figure A.30: Complex Spline

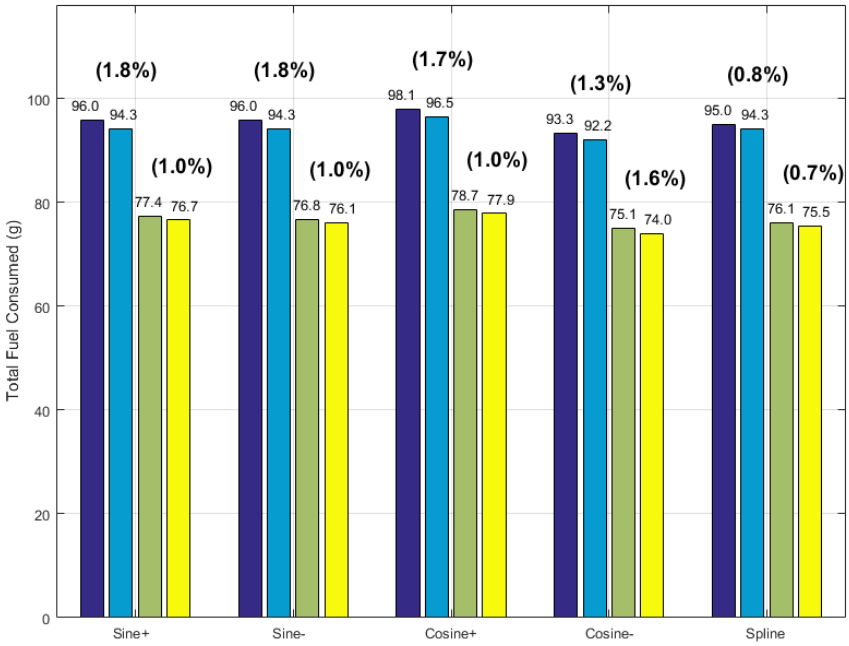

Figure A.31: Total Simulated vs. Experimental Fuel Consumed during Low Speed/Low Load Trials

A.2.2 Low Speed, High Load

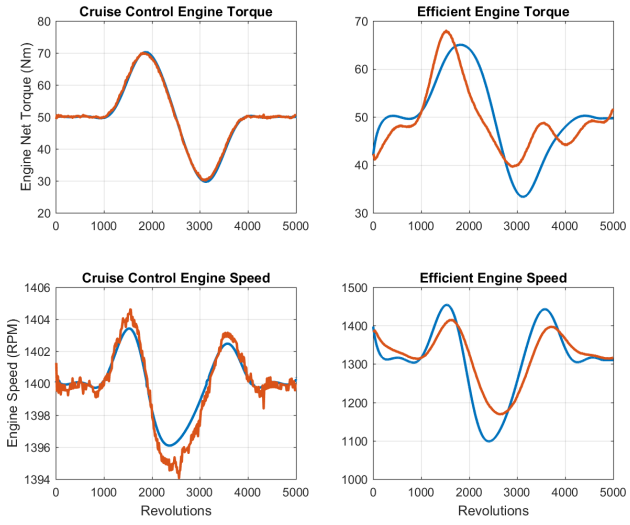

Figure A.32: Sine+

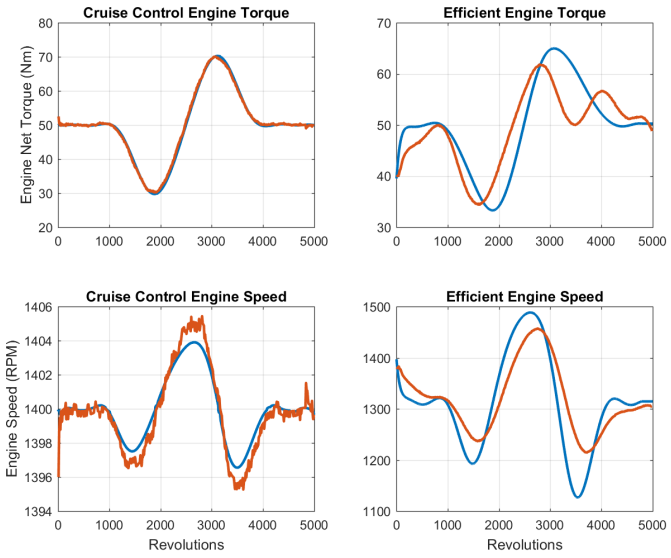

Figure A.33: Sine-

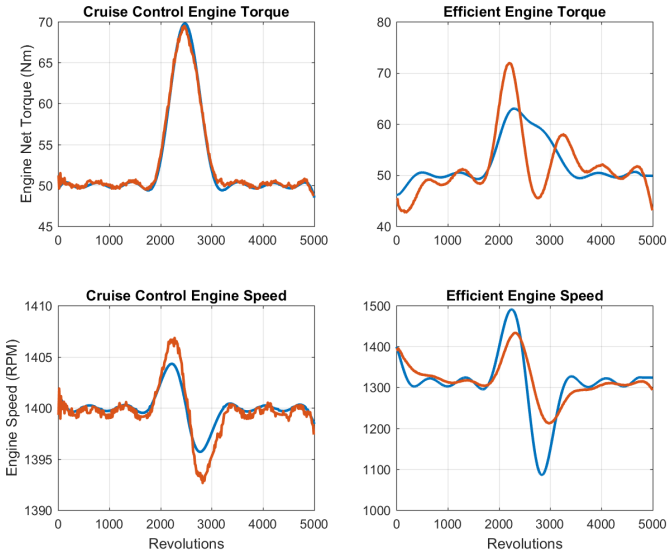

Figure A.34: Cosine+

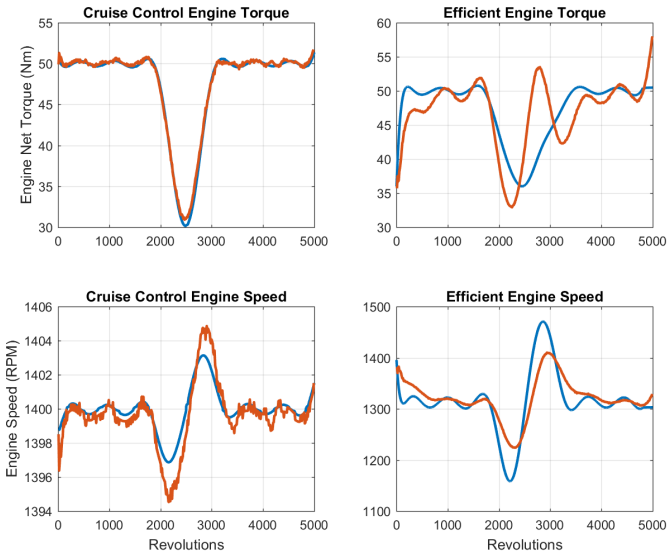

Figure A.35: Cosine-

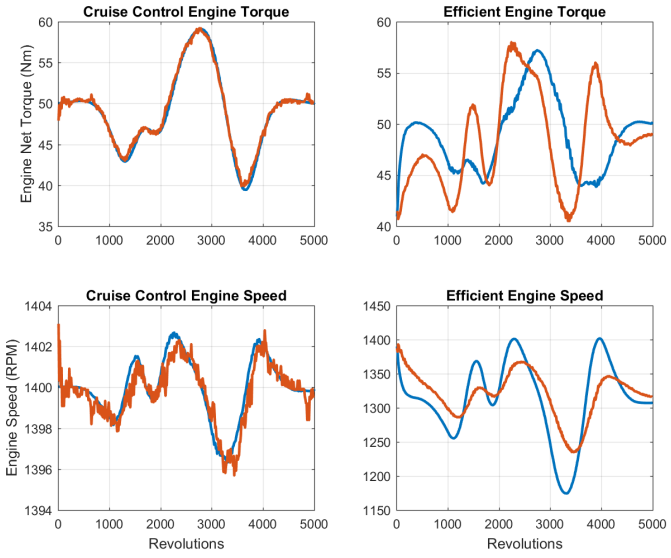

Figure A.36: Complex Spline

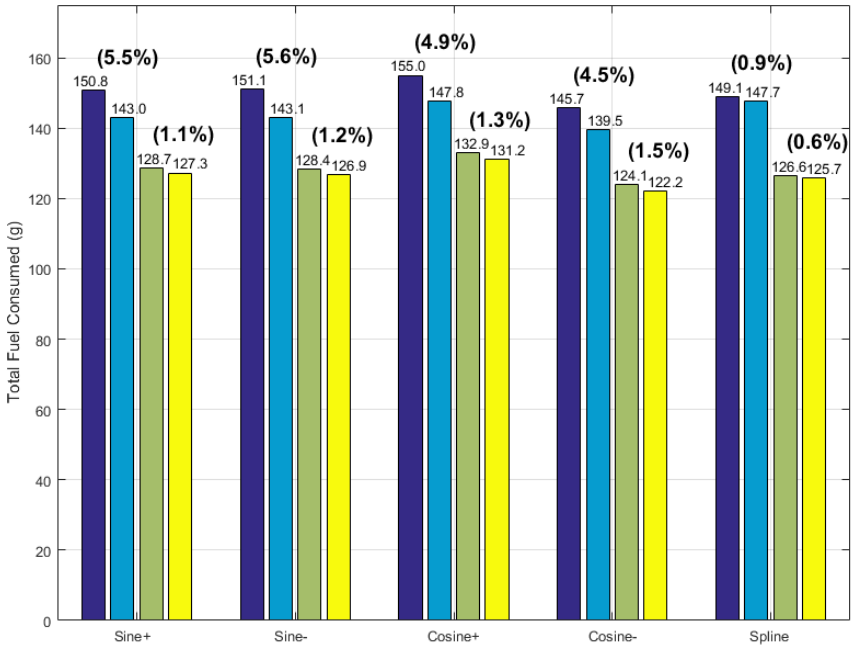

Figure A.37: Total Simulated vs. Experimental Fuel Consumed during Low Speed/High Load Trials

A.2.3 High Speed, Low Load

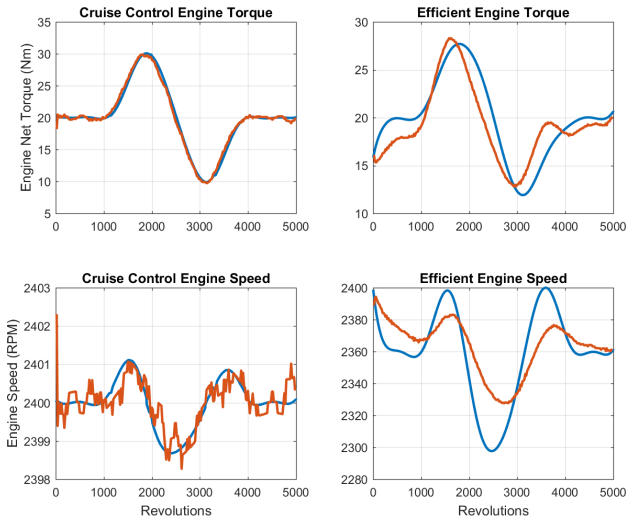

Figure A.38: Sine+

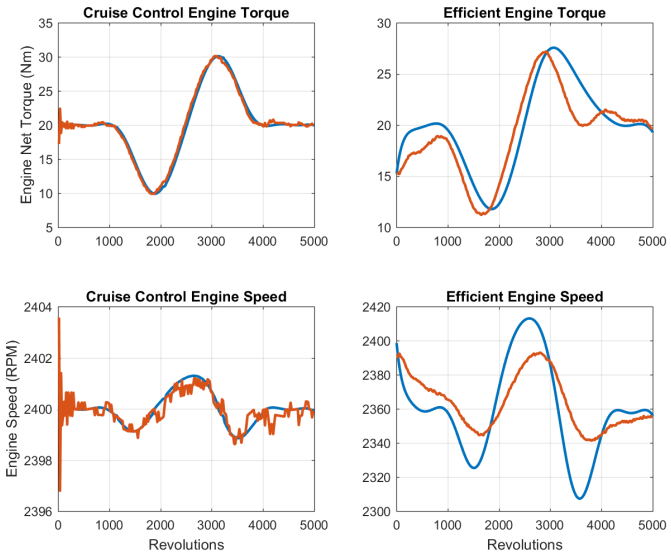

Figure A.39: Sine-

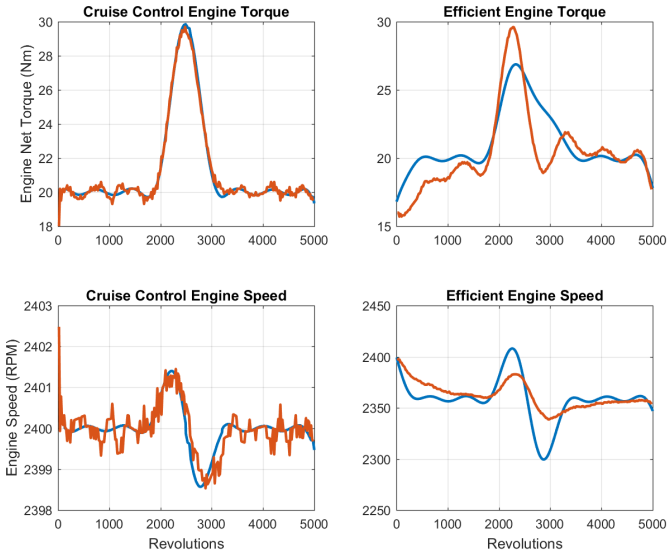

Figure A.40: Cosine+

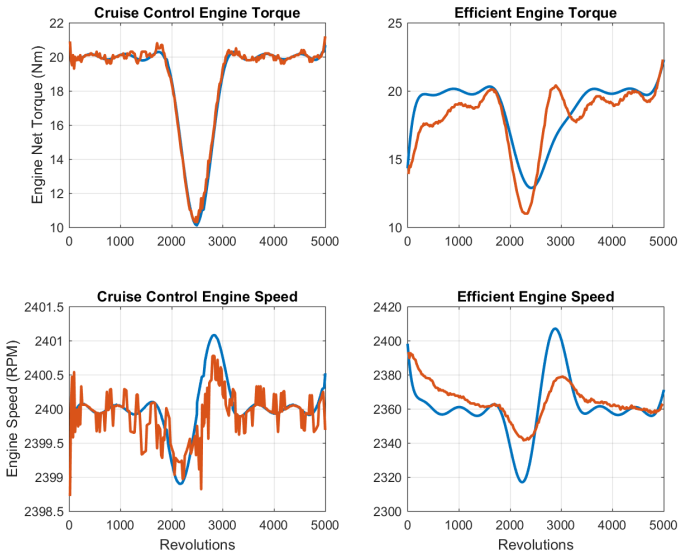

Figure A.41: Cosine-

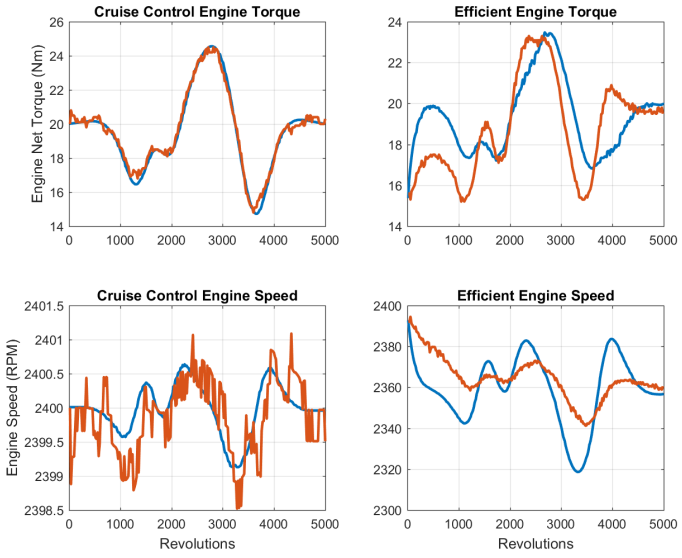

Figure A.42: Complex Spline

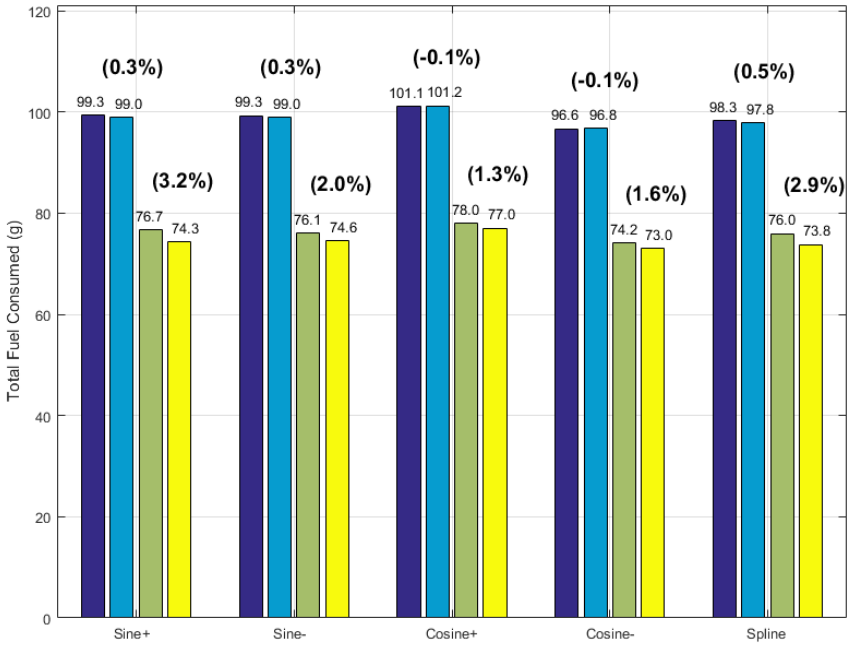

Figure A.43: Total Simulated vs. Experimental Fuel Consumed during High Speed/Low Load Trials

A.2.4 High Speed, High Load

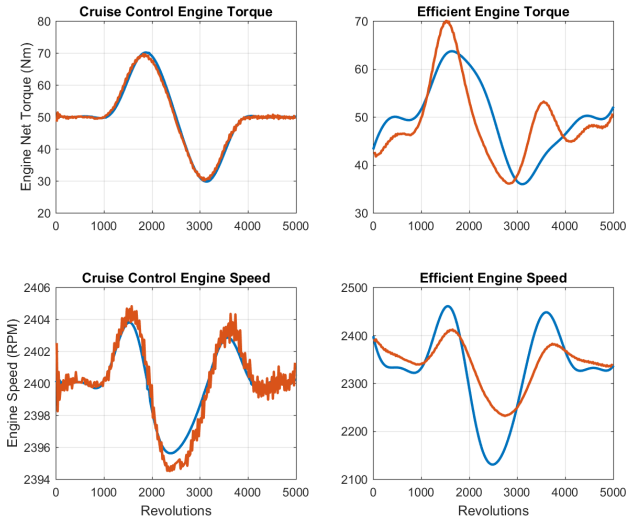

Figure A.44: Sine+

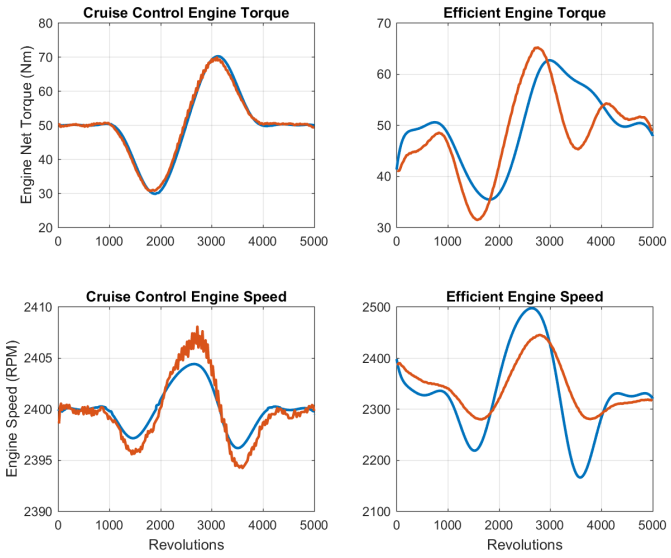

Figure A.45: Sine-

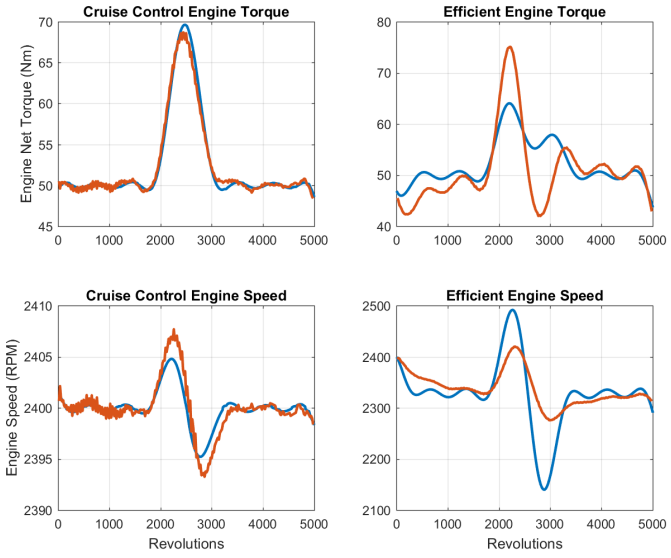

Figure A.46: Cosine+

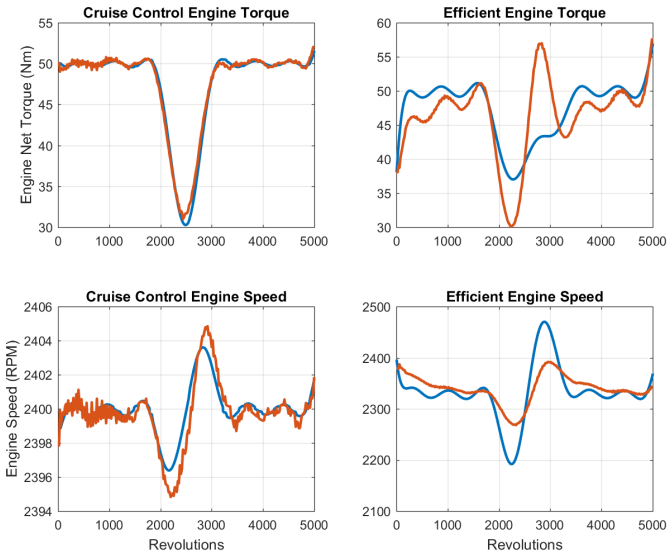

Figure A.47: Cosine-

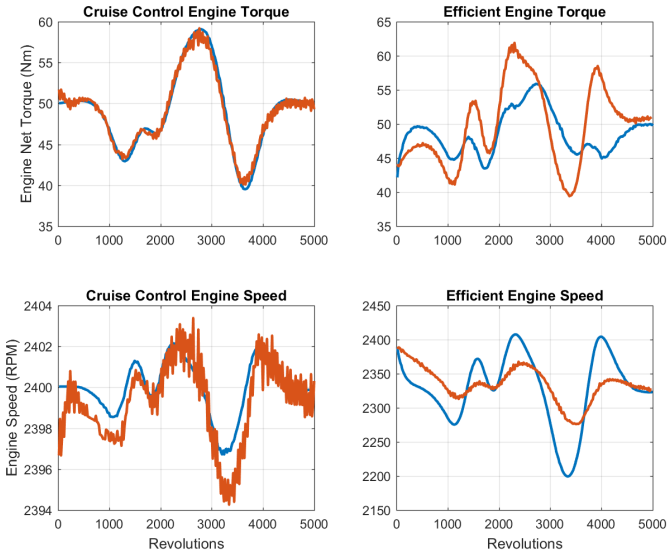

Figure A.48: Complex Spline

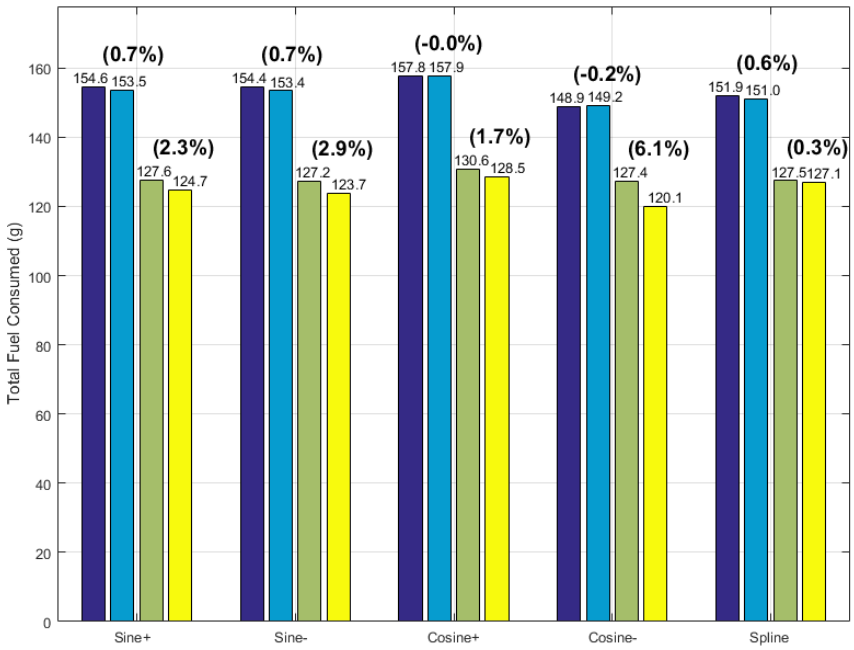

Figure A.49: Total Simulated vs. Experimental Fuel Consumed during High Speed/High Load Trials

A.2.5 Totals

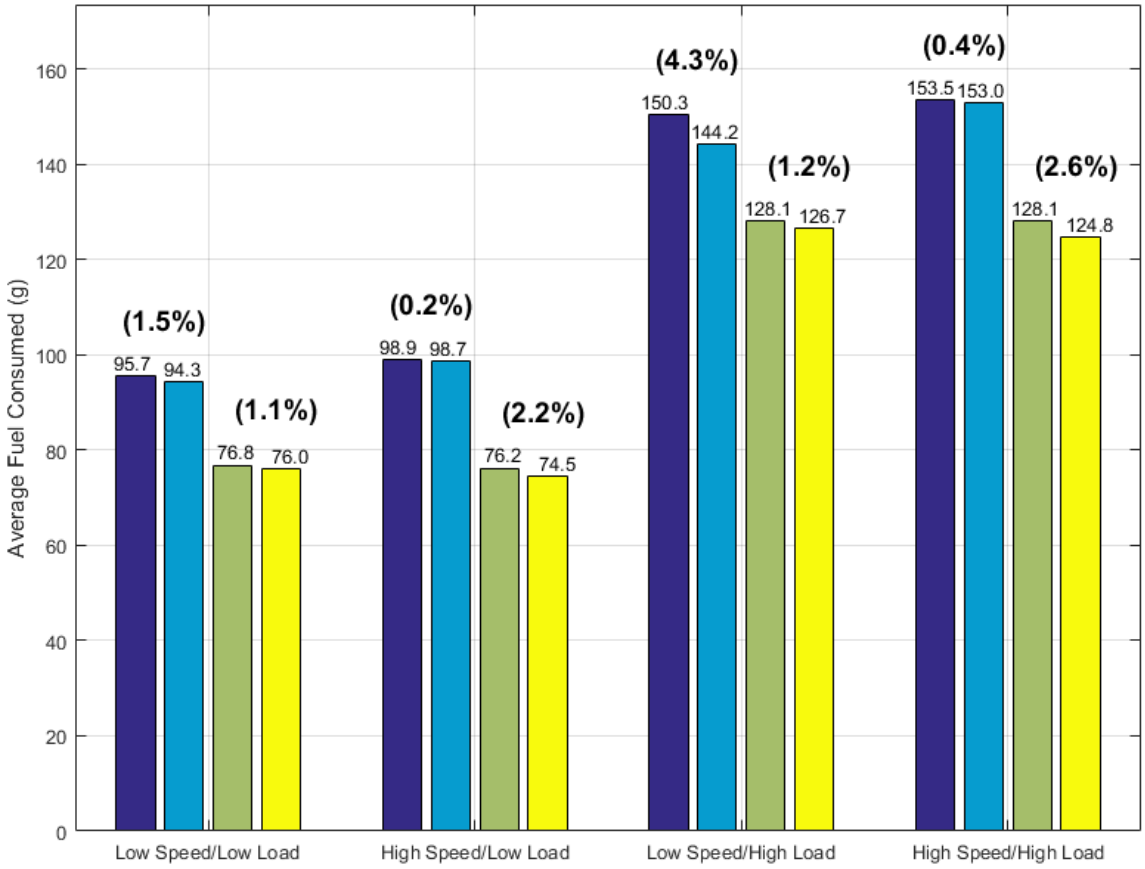

Figure A.50: Average Total Fuel Consumed for each Speed/Load Category

A.3 Experimental Results

In the following figures displaying experimental results, blue curves represent optimal simulations while orange curves represent the optimal trajectories derived during physical experiments. Blue Bar graphs represent total fuel consumed during cruise control trials, yellow bar graphs represent total fuel consumed during efficiency trials, red bar graphs represent average fuel mileage during cruise control trials, and green bar graphs represent average fuel mileage during efficiency trials.

A.3.1 Low Speed, Low Load

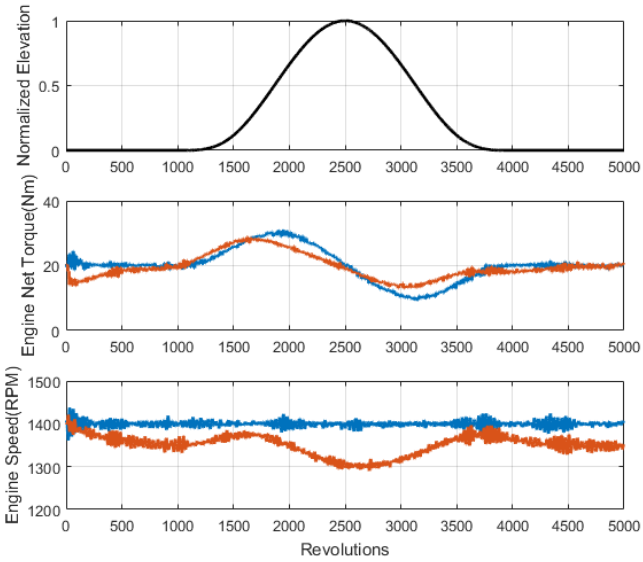

Figure A.51: Sine+

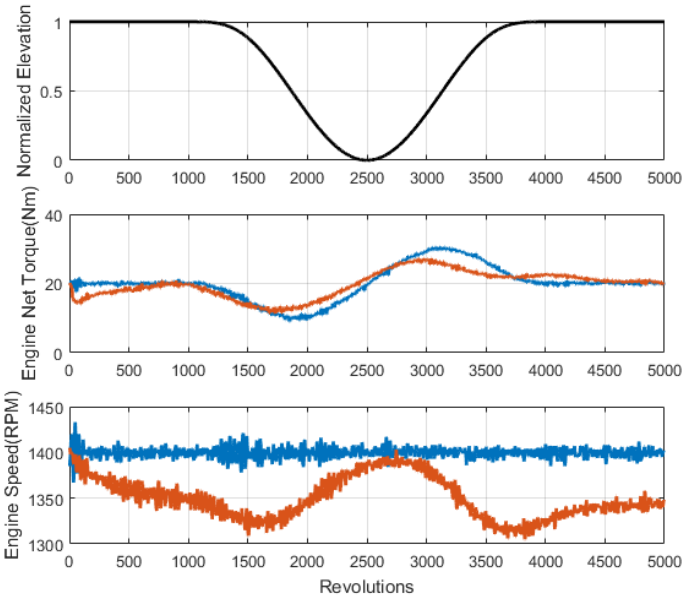

Figure A.52: Sine-

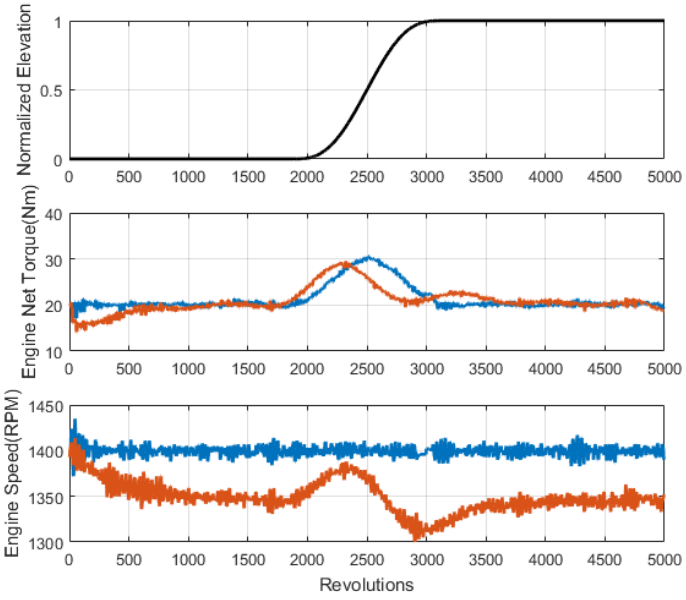

Figure A.53: Cosine+

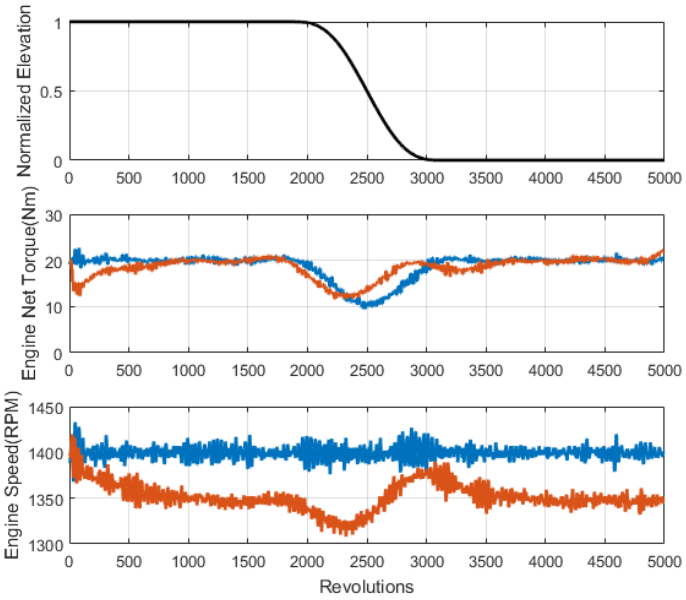

Figure A.54: Cosine-

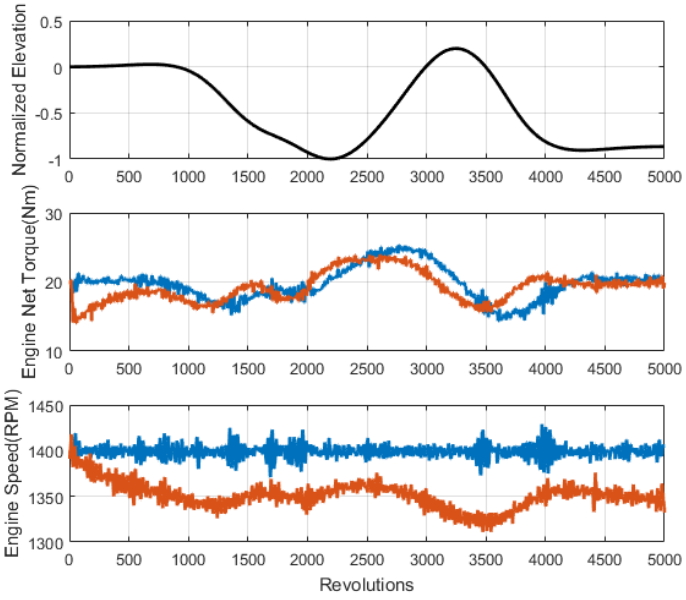

Figure A.55: Complex Spline

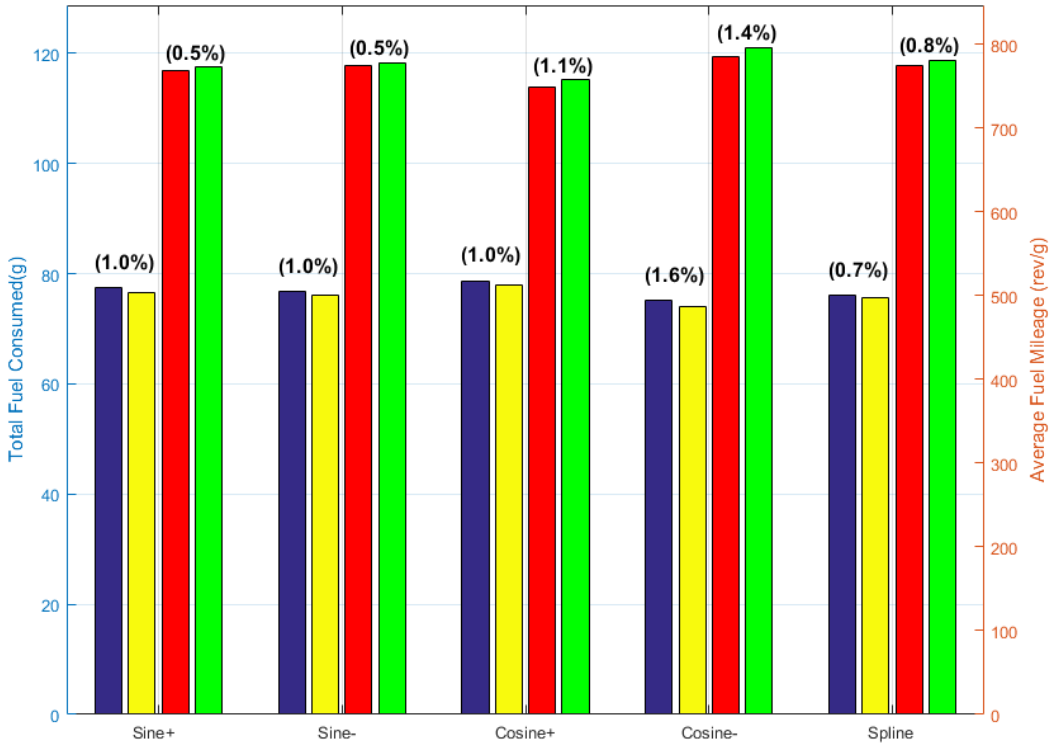

Figure A.56: Total Fuel Consumed and Average Fuel Mileage during Low Speed/Low Load Trials

A.3.2 Low Speed, High Load

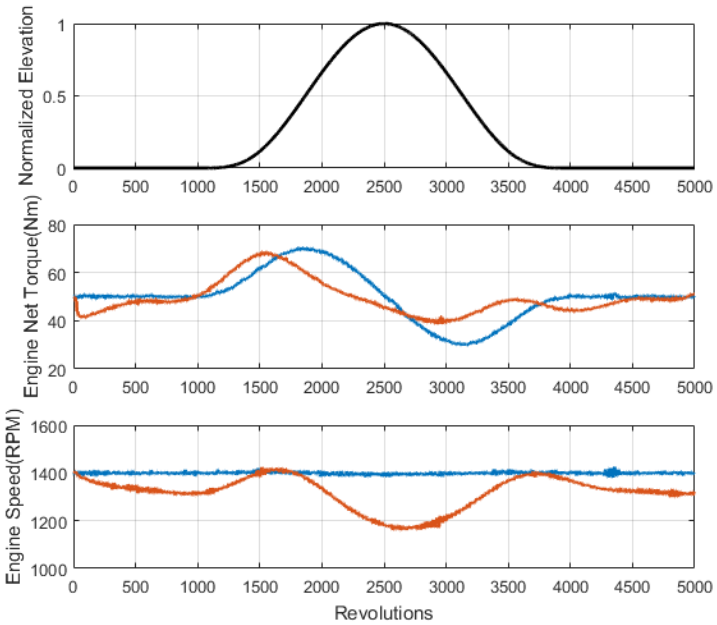

Figure A.57: Sine+

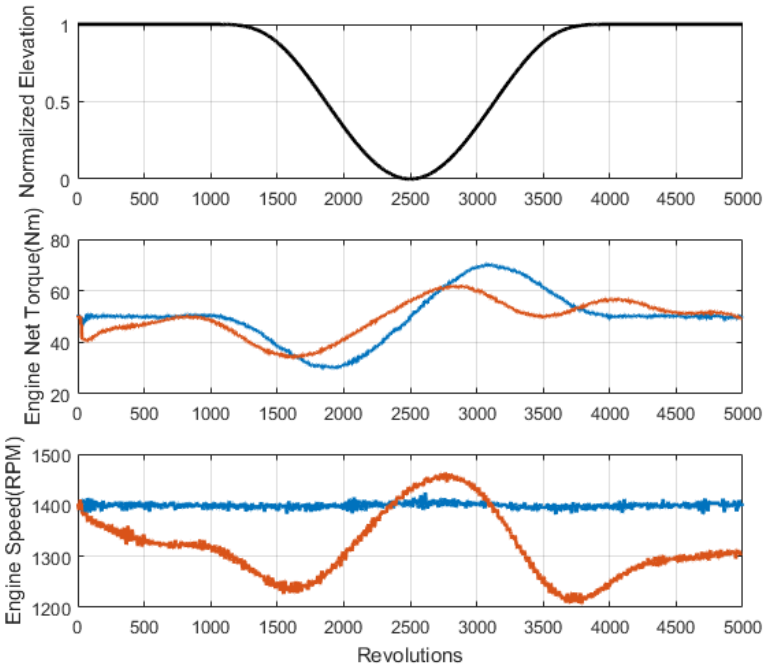

Figure A.58: Sine-

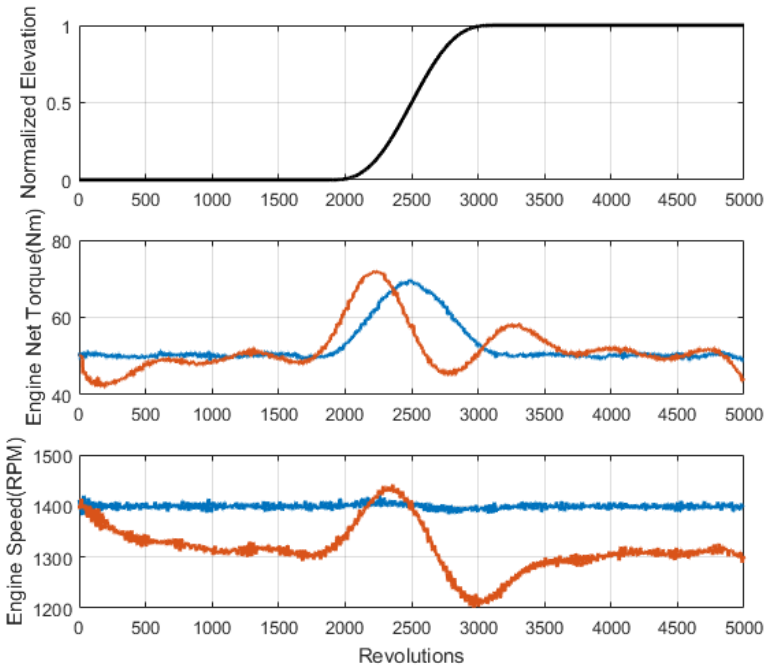

Figure A.59: Cosine+

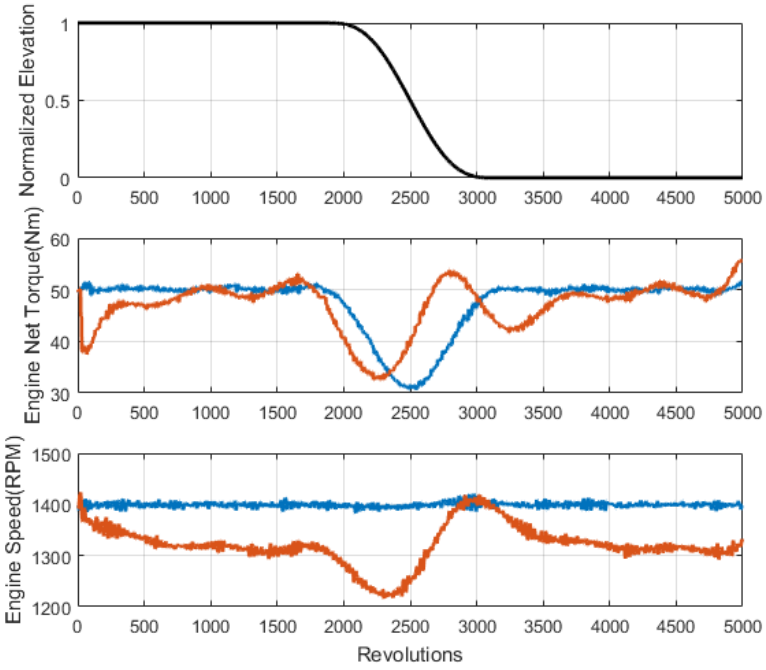

Figure A.60: Cosine-

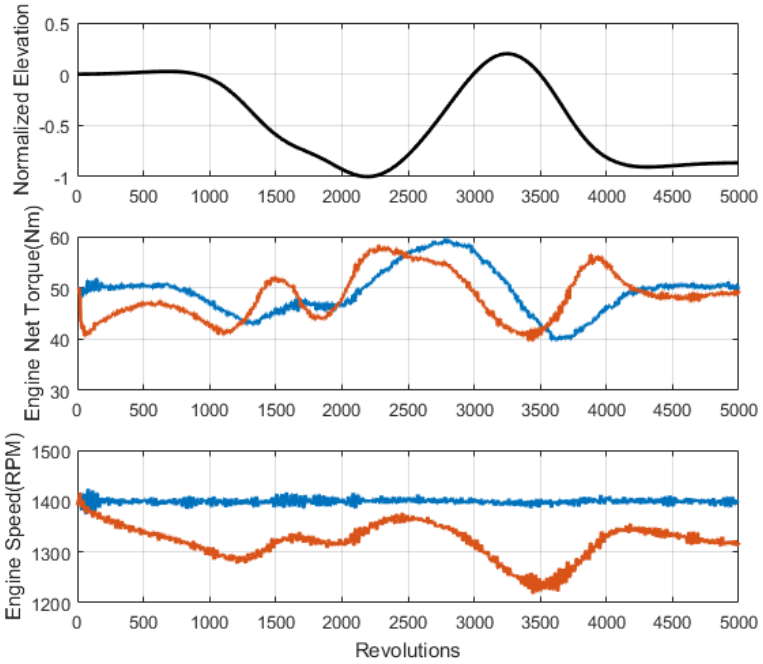

Figure A.61: Complex Spline

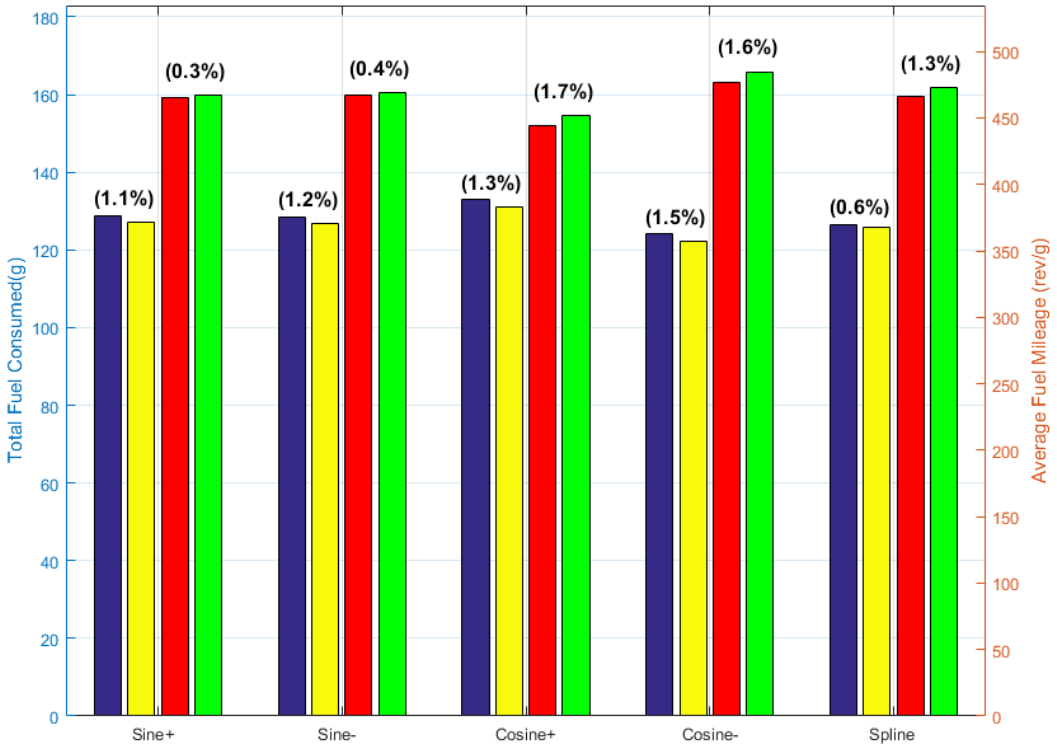

Figure A.62: Total Fuel Consumed and Average Fuel Mileage during Low Speed/High Load Trials

A.3.3 High Speed, Low Load

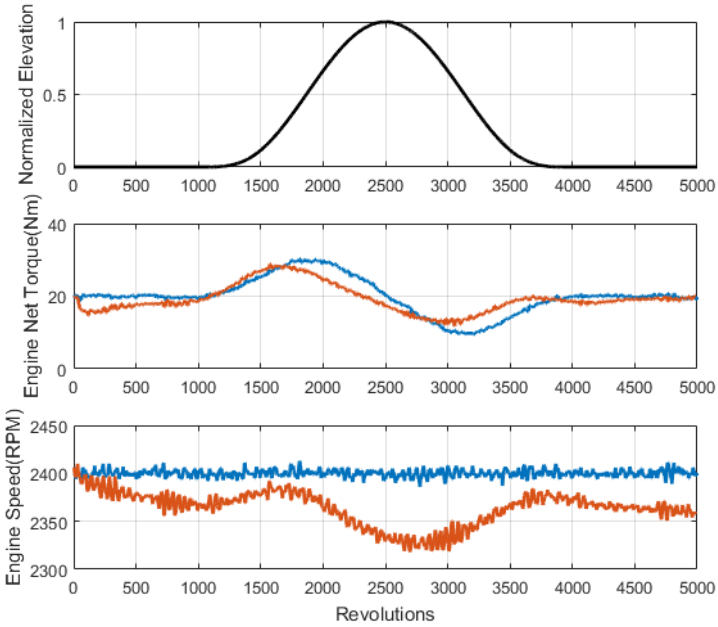

Figure A.63: Sine+

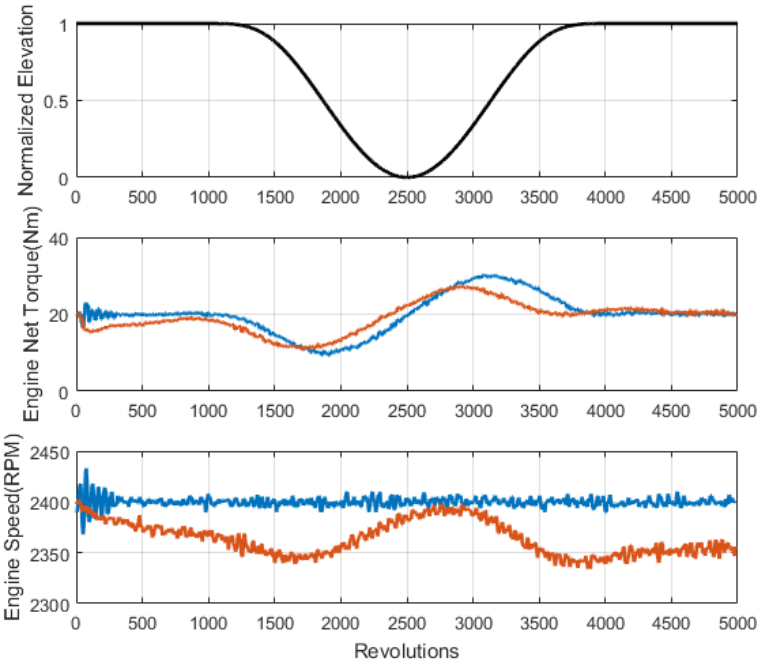

Figure A.64: Sine-

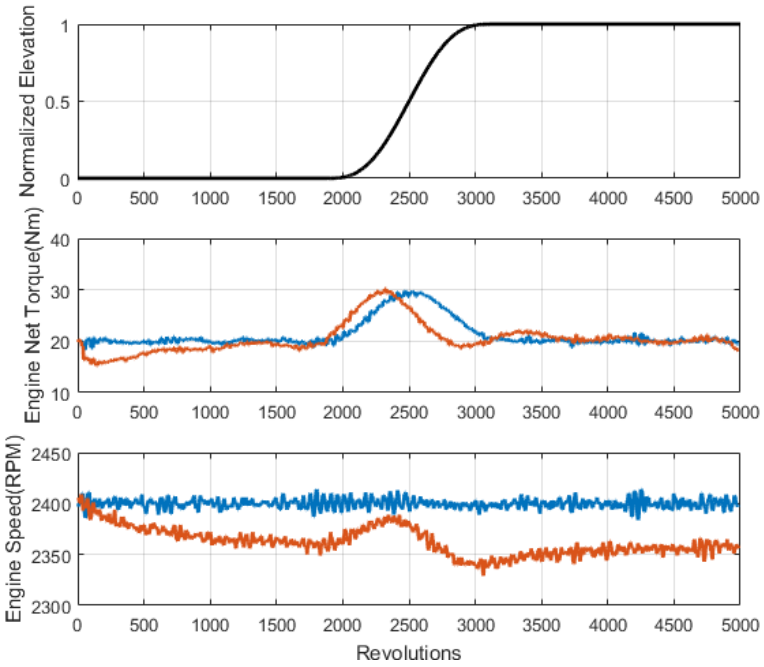

Figure A.65: Cosine+

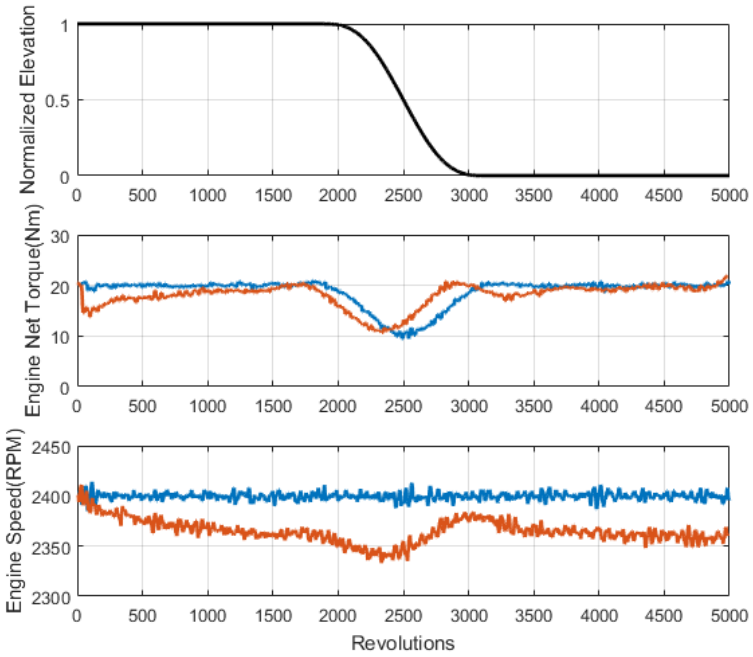

Figure A.66: Cosine-

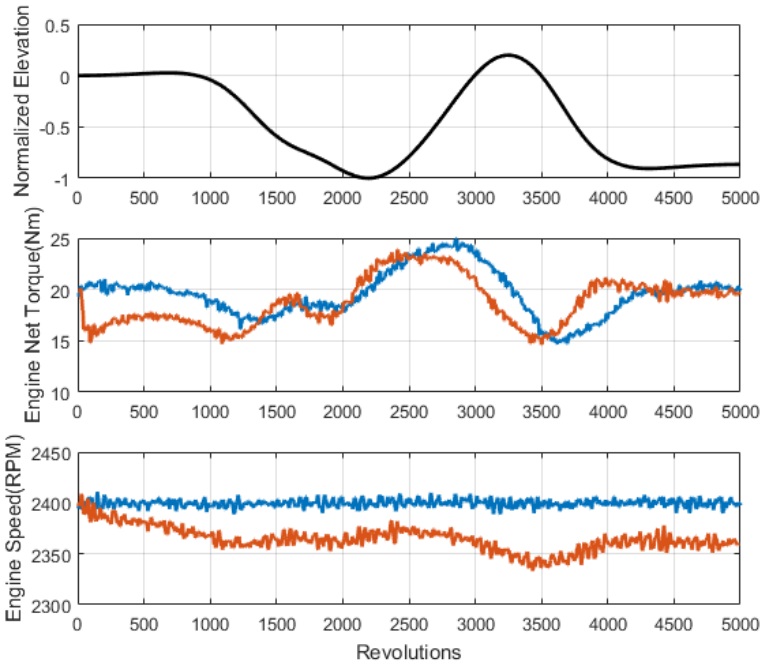

Figure A.67: Complex Spline

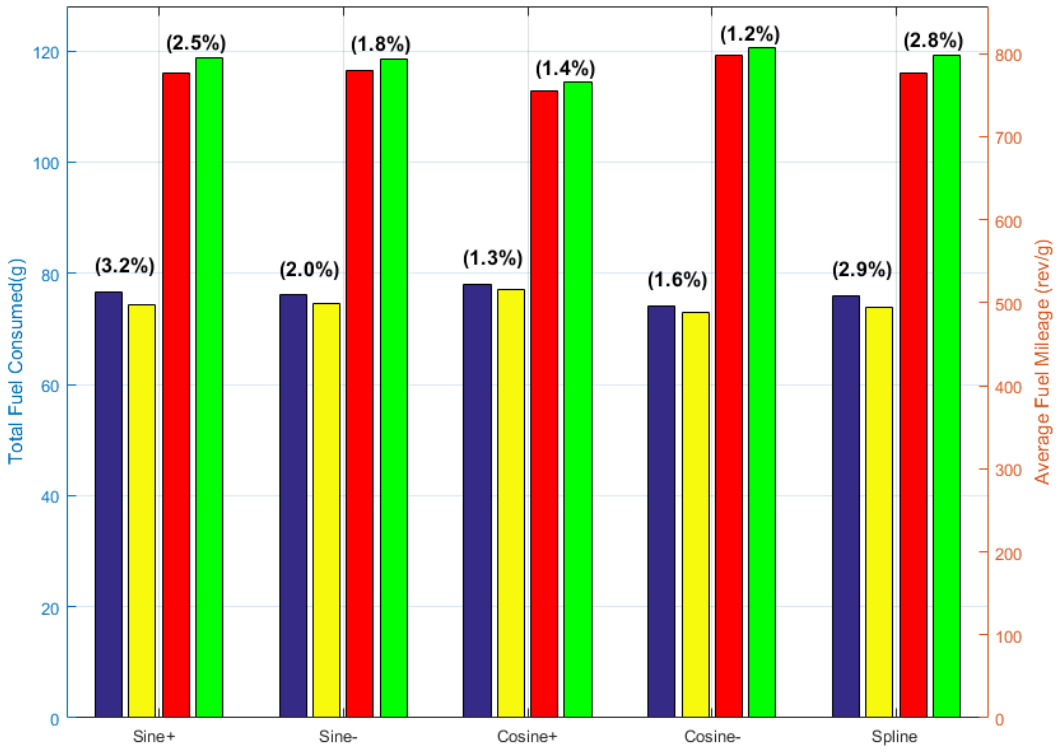

Figure A.68: Total Fuel Consumed and Average Fuel Mileage during High Speed/Low Load Trials

A.3.4 High Speed, High Load

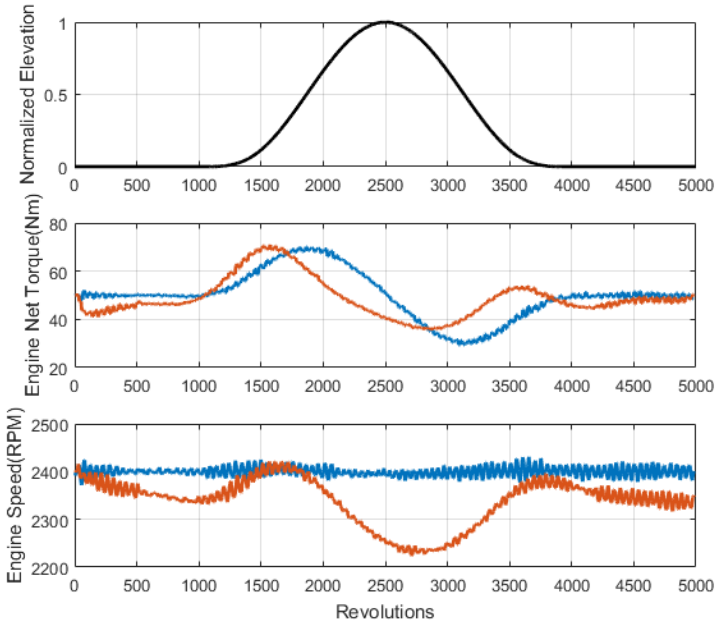

Figure A.69: Sine+

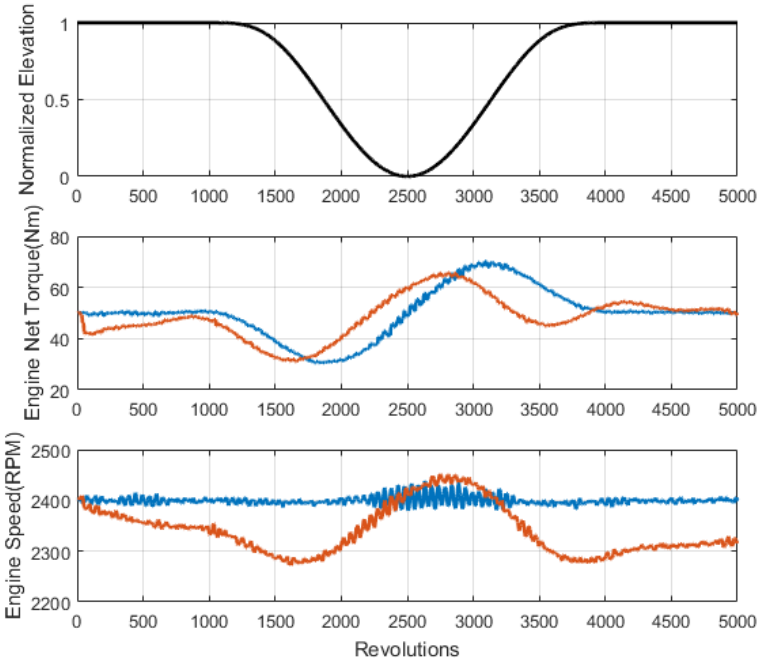

Figure A.70: Sine-

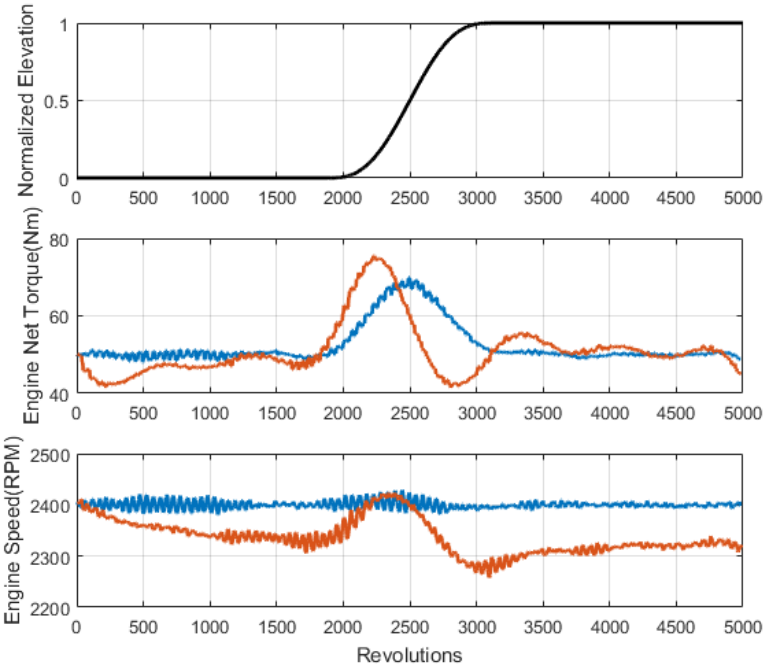

Figure A.71: Cosine+

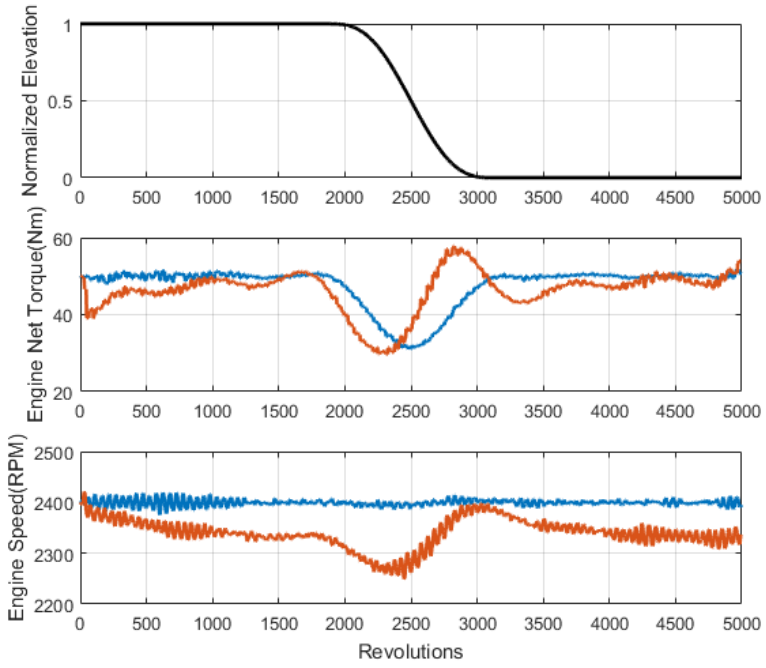

Figure A.72: Cosine-

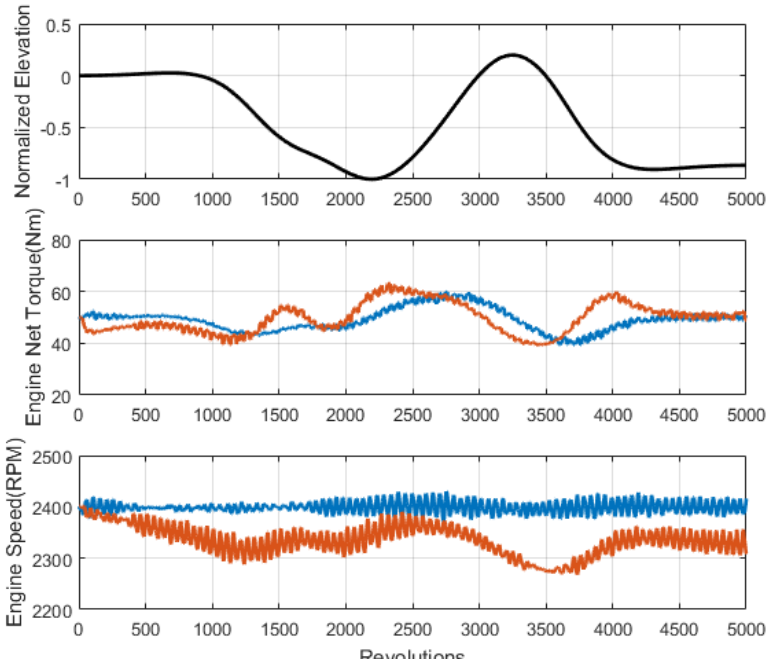

Figure A.73: Complex Spline

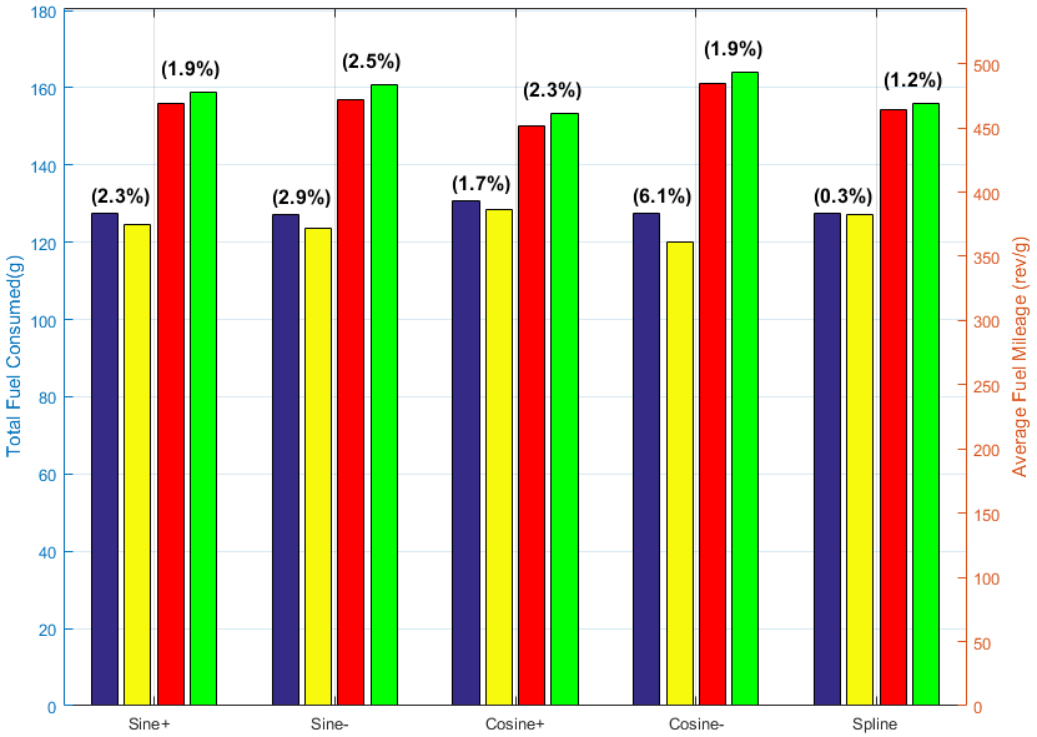

Figure A.74: Total Fuel Consumed and Average Fuel Mileage during High Speed/High Load Trials

A.3.5 Totals

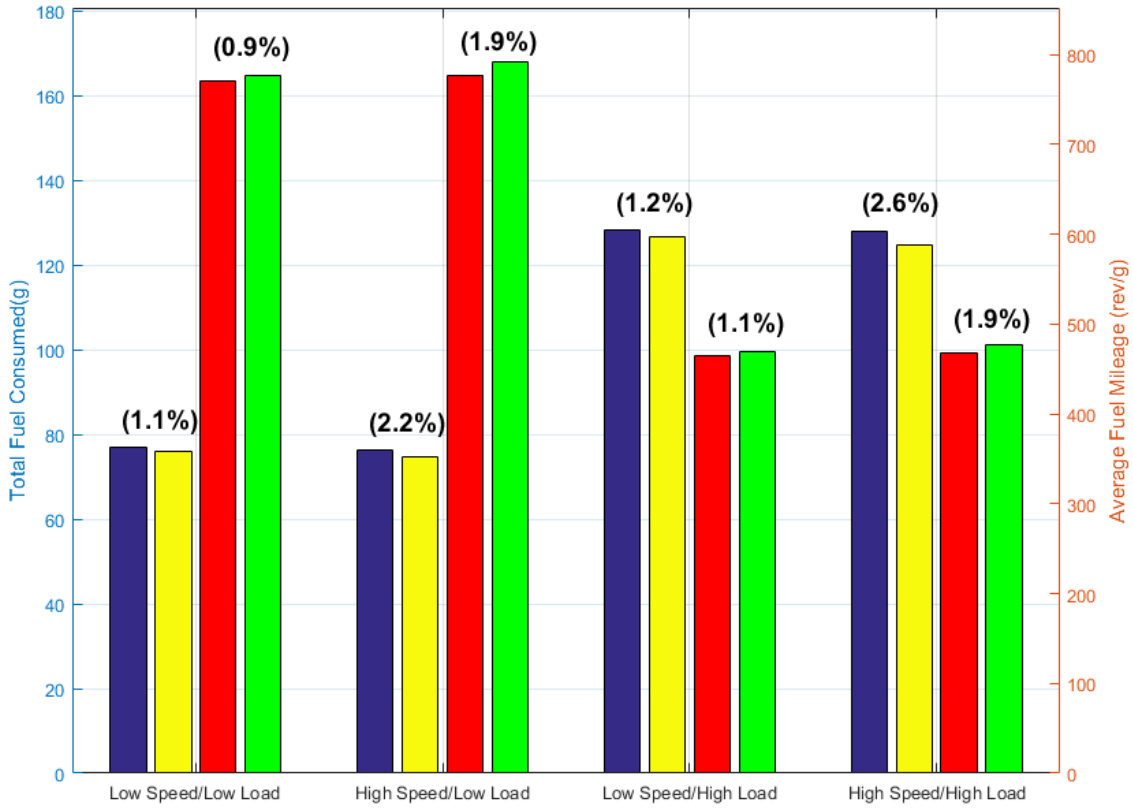

Figure A.75: Total Fuel Consumed and Average Fuel Mileage for each Speed/Load Category